



**GDAŃSK UNIVERSITY
OF TECHNOLOGY**

Faculty of Electronics,
Telecommunications and
Informatics

Załącznik nr 1/2
do Zarządzenia Rektora PG nr 5/2015 z 10 lutego 2015 r.



The author of the PhD dissertation: Monika Kosowska
Scientific discipline: Automation, electronic and electrical engineering

DOCTORAL DISSERTATION

Title of PhD dissertation: Tuning of the finesse coefficient of optoelectronic devices.

Title of PhD dissertation (in Polish): Dostosowywanie współczynnika finezji urządzeń optoelektronicznych.

Supervisor

signature

Małgorzata Szczerska, PhD, DSc EE

Gdańsk, 2021



**GDAŃSK UNIVERSITY
OF TECHNOLOGY**

Faculty of Electronics,
Telecommunications and
Informatics



STATEMENT

The author of the PhD dissertation: Monika Kosowska

I, the undersigned, agree/~~do not agree~~* that my PhD dissertation entitled:
Tuning of the finesse coefficient of optoelectronic devices

may be used for scientific or didactic purposes.¹¹

Gdańsk,.....

.....
signature of the PhD student

Aware of criminal liability for violations of the Act of 4th February 1994 on Copyright and Related Rights (Journal of Laws 2006, No. 90, item 631) and disciplinary actions set out in the Law on Higher Education (Journal of Laws 2012, item 572 with later amendments),²² as well as civil liability, I declare, that the submitted PhD dissertation is my own work.

I declare, that the submitted PhD dissertation is my own work performed under and in cooperation with the supervision of Małgorzata Szczerska, PhD, DSc EE.

This submitted PhD dissertation has never before been the basis of an official procedure associated with the awarding of a PhD degree.

All the information contained in the above thesis which is derived from written and electronic sources is documented in a list of relevant literature in accordance with art. 34 of the Copyright and Related Rights Act.

I confirm that this PhD dissertation is identical to the attached electronic version.

Gdańsk,.....

.....
signature of the PhD student

I, the undersigned, agree/~~do not agree~~* to include an electronic version of the above PhD dissertation in the open, institutional, digital repository of Gdańsk University of Technology, Pomeranian Digital Library, and for it to be submitted to the processes of verification and protection against misappropriation of authorship.

Gdańsk,.....

.....
signature of the PhD student

*) delete where appropriate.

¹ Decree of Rector of Gdansk University of Technology No. 34/2009 of 9th November 2009, TUG archive instruction addendum No. 8.

² Act of 27th July 2005, Law on Higher Education: Chapter 7, Criminal responsibility of PhD students, Article 226.



ABSTRACT

Optoelectronic devices attracted considerable attention in many branches of science and technology, which can be attributed to their unique properties. Many of them use optical cavities which parameters can be adopted to specific requirements. This thesis investigates the introduction of diamond structures (nitrogen-doped diamond film, boron-doped diamond film, undoped diamond sheet) to optical cavities to tune their finesse coefficient. Moreover, their application enabled development of a system for optical monitoring of electrochemical reactions. A detailed review of the state-of-the-art presents techniques of cavities tuning in optoelectronic devices, diamond applications in optoelectronics and current solutions combining optical and electrochemical measurement techniques in one system is presented. The work includes mathematical investigation, description of the construction of cavities and measurement setup, as well as results of experimental measurements. Applications of optical cavities tuned by the use of diamond structures are presented on the example of fiber-optic sensors: for measurements of distance and liquids refractive index, and for construction of a hybrid optoelectrochemical system.

STRESZCZENIE

Urządzenia optoelektroniczne cieszą się dużym zainteresowaniem w wielu dziedzinach nauki i techniki, co można przypisać ich unikalnym właściwościom. Wiele z nich wykorzystuje w swej konstrukcji wnęki optyczne, których parametry można dostosować do określonych wymagań. Rozprawa dotyczy zastosowania struktur diamentowych (warstw diamentowych domieszkowanych azotem, borem oraz niedomieszkowanych folii) we wnękach do strojenia ich współczynnika finezji oraz opracowania systemu do optycznego monitorowania reakcji elektrochemicznych. Przedstawiono szczegółowy przegląd aktualnego stanu wiedzy w zakresie technik strojenia wnęk optycznych w urządzeniach optoelektronicznych, zastosowań diamentu w optoelektronice oraz obecnych rozwiązań łączących optyczne i elektrochemiczne techniki pomiarowe. Praca obejmuje modelowanie matematyczne, opis konstrukcji wnęk optycznych i systemu pomiarowego oraz wyniki pomiarów eksperymentalnych. Przedstawiono także przykładowe zastosowania strojenia wnęk ze strukturami diamentowymi na przykładzie czujników światłowodowych: do pomiaru odległości i współczynnika załamania cieczy oraz hybrydowego systemu optoelektrochemicznego.

TABLE OF CONTENTS

Table of contents	4
List of important symbols and abbreviations	5
1. Introduction and theses.....	7
2. State of the art: tuning of the cavities of optoelectronic devices	11
3. Mathematical investigation of the optical cavity finesse coefficient.....	17
4. Experimental verification of the mathematical results in a measurement system.....	29
4.1 Tuning of the finesse coefficient with nitrogen-doped diamond film.....	31
4.2 Tuning of the finesse coefficient with boron-doped diamond film.....	33
4.3 Tuning of the finesse coefficient with nanocrystalline diamond sheet.....	35
5. Applications of the optical cavity tuning method.....	39
5.1 Application of cavity tuning in fiber-optic sensors of distance and refractive index	39
5.2 Cavity tuning in opto-electrochemical measurement system	42
5.3 The cavity tuning method for protecting the fiber-optic measurement head	46
6. Summary and conclusions	51
6.1 Author's scientific achievements.....	53
6.2 Planned further research	54
7. List of published papers.....	57
8. References	59

LIST OF IMPORTANT SYMBOLS AND ABBREVIATIONS

ALD	–	Atomic Layer Deposition
BDD	–	Boron-Doped Diamond
c	–	Light velocity in vacuum ($c = 2,998 \cdot 10^8$ km/s)
CVD	–	Chemical Vapor Deposition
δ	–	Phase difference between the interfering beams
F	–	Finesse coefficient
\mathcal{F}	–	Finesse
FIB	–	Focused Ion Beam
FSR	–	Free Spectral Range
FWHM	–	Full-width at Half Maximum
I	–	Intensity of the measured optical signal
I_i	–	Incident light intensity
I_{\max}	–	Maximum light intensity
I_{\min}	–	Minimum light intensity
I_r	–	Reflected light intensity
I_t	–	Transmitted light intensity
L	–	Cavity length
λ	–	Wavelength
n	–	Refractive index
MW PA CVD	–	Microwave Plasma Assisted Chemical Vapor Deposition
NDD	–	Nitrogen-Doped Diamond
NDS	–	Nanocrystalline Diamond Sheet



OSA	–	Optical Spectrum Analyzer
P	–	Optical power
R	–	Reflectivity
R^2	–	Correlation coefficient
S	–	Sensitivity
SEM	–	Scanning Electron Microscopy
SLD	–	Superluminescent Diode
T	–	Transmission
V	–	Visibility
ZnO	–	Zinc Oxide

1. INTRODUCTION AND THESES

The growing interest in applying optical methods is related to the many benefits they offer. Optical techniques assure fast operation and allow real-time monitoring of the investigated object [1]. They can operate in a contactless mode and due to their non-destructive working manner, they do not damage the tested samples [2,3]. This can be crucial for measurements where direct contact of the probe may alter or damage the sample. Moreover, they exhibit a great potential for coupling with other methods, giving multi-mode systems capable of providing more comprehensive results [4–6].

Many optoelectronic systems utilize optical cavities (also called resonant cavities [7]), built of the specific arrangement of reflective surfaces, forming a variety of possible applications, from lasers and filters constructions to advanced biomedical sensing. There are many types of optical resonant cavities where light is guided in a closed path. They can be designed as linear or ring resonators, they may also include bulk optical elements or waveguides, using optical fibers or integrated optics. A wide range of construction designs and materials options allows for optimization of the cavity construction to the desired application.

The construction that offers open access to the cavity and allows many ways of its tailoring is a Fabry-Perot cavity. The reasoning behind its the popularity lies in its robustness [8], simplified fabrication process [9] and cost reduction [10] while maintaining high measurement resolution [11] and sensitivity [12]. It consists of two parallel reflective surfaces with a gap in between, where the light forms a standing wave for specific resonance frequencies [13] - this cavity design is investigated in detail within this dissertation. A Fabry-Perot cavity is one of the most popular constructions appearing in optoelectronics where any perturbations inside – for example changes in the refractive index of the medium fulfilling the cavity or geometrical length of the cavity - impacts the acquired signal.

The key parameter describing a cavity is its finesse F . It is the ratio of the separation between neighboring maxima (also called the free spectral range - FSR) and the full-width at half maximum (FWHM), presented in Figure 1.1.

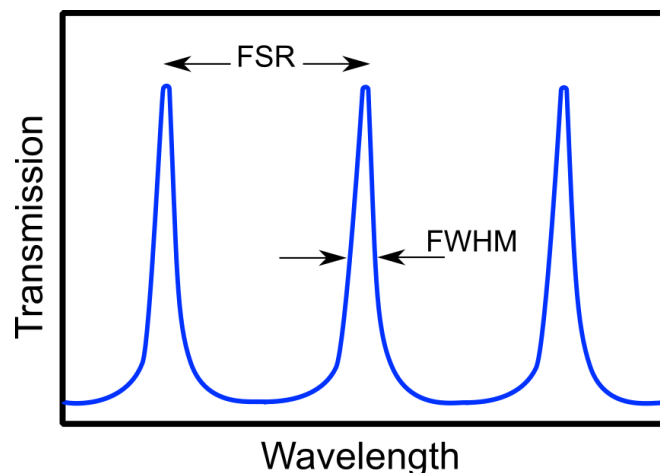


Figure 1.1. Full spectral range (FSR) and full-width at half maximum (FWHM).

The finesse can be tailored depending on our needs, e.g. low finesse cavities work well for filtering while high finesse cavities serve for precise spectroscopy. Several factors impact the finesse coefficient value: reflectance of the mirrors, roughness of the surfaces creating the cavity, coating nonuniformities, scattering (defects after polishing or dust particles) and losses (caused by e.g. non-parallelism between the surfaces, divergence of the incident light) [13]. As such, it is clear that the choice of materials and manufacturing process impacting mirror properties, and as consequence cavity properties, is crucial to improve the performance of the developed optoelectronics devices. Therefore, several strategies for tuning the finesse of optoelectronic devices can be distinguished.

The properties of diamond structures reported in the literature, as well as the need for tunable cavities allow the assumption that the parameters of the optical cavity can be modified by the introduction of diamond structures to its construction. Moreover, the solution will give the possibility of developing a robust optoelectrochemical setup by coupling the Fabry-Perot interferometer and electrochemical system through the diamond film. Hence, the following theses were established:

- T1: Finesse coefficient of a Fabry-Perot cavity can be tailored by the use of diamond structures.
- T2: Application of diamond structures enables construction of opto-electrochemical system for optical investigation of electrochemical processes.

The full development process of fiber-optic cavities applying diamond structures is presented: from the mathematical investigation of the cavity, through diamond materials characterization, construction, to measurements verifying proper devices operation in proposed potential applications. The following goals were established as research plan steps to prove the dissertation theses:

- Conducting a mathematical investigation of diamond structures' impact on the cavity finesse.
- Design and construction of the Fabry-Perot cavities utilizing diamond films and sheets to tune their finesse. Assembling of the measurement setup for exploring the cavities' properties.
- Development of potential applications of the proposed solution, focusing on an optoelectrochemical setup for monitoring of electrochemical processes. Testing and verification of the developed devices.

The development of an optoelectrochemical system is described, as well as example measurements conducted for reversible electrochemical reactions and obtained measurement results. The results of the research have been presented in 6 scientific articles published in recognized international journals – in each of them as a first author.

Chapter 1 introduces the optoelectronic devices using optical cavities with a brief description of finesse coefficient, highlighting their importance in technology and showing the need for further development through tailoring their properties e.g. by using new materials for their construction. The goals and theses of this dissertation were established. Chapter 2 describes in detail the current state-of-the-art in terms of the tuning of the cavities of the optoelectronic devices. The review presents reported methods and examples of their applications. Since their tailoring can be achieved by employing new materials, the unabated trend of using a diamond in optoelectronics is presented. The current solutions for linking optics with electrochemistry create a background for the optoelectrochemical setup developed within this study. Chapter 3 shows the mathematical investigation of the Fabry-Perot cavities modified with diamond structures and their comparison with conventional cavities using silver mirrors; a setup for assessment of the designed cavities is described. Chapter 4 focuses on the physical realization of the cavities: their

construction with the utilization of nitrogen-doped diamond films, boron-doped diamond films, undoped diamond sheets. Direct comparison of mathematical and experimental studies is presented. In Chapter 5, three applications are presented: fiber-optic Fabry-Perot sensors, the nanocrystalline diamond sheet as a protective coating for fiber end-faces, and a hybrid optoelectrochemical setup, being a culmination of the research cycle: the tunable Fabry-Perot interferometer and electrochemical system were linked into one setup with the use of diamond film. The dissertation is concluded in Chapter 6 where all achievements of this study are briefly concluded, as well as presentation of the further plans. Chapter 7 includes a list of selected published articles thematically related to the presented research, while the bibliography can be found in Chapter 8. The work ends with full-text scientific papers along with co-authors' contribution statements.

2. STATE OF THE ART: TUNING OF THE CAVITIES OF OPTOELECTRONIC DEVICES

Optical techniques like interferometry [14], spectroscopy [15,16], quantum electrodynamics [17] and other [18] are widely applying optical cavities. Such cavities attracted significant attention in many branches of science and technology, especially in sensing, which can be attributed to their properties. Such cavities are used in telecommunications for Wavelength Division Multiplexing (WDM), they create resonant cavities of lasers [19–21], tunable lasers [22,23], laser diodes [24,25], color displays [26,27], they are also applied as filters [28,29] and selective filters [30,31], resonant cavities can be met in refractometers [32], spectrometers [33], antennas [34,35]. They are also used in metrology, sensing [36–38] and biosensing [39–41] solutions. As such, tailoring and adjusting parameters of the cavities to meet certain requirements is highly desirable.

The great popularity of the cavities in optoelectronics leads to the need of improving their parameters to fit the intended application. Hence, several strategies for creating tunable optical cavities can be described. Curwen et al. reported on a wavelength-size laser cavity with a movable end mirror [42]. Varying cavity length changes the wavelength of the laser. The crucial elements are patterned metasurface that consists of an array of subwavelength metal-metal waveguides (fixed mirror) and a polarizer attached to piezoelectric actuators (moving mirror). This approach allows dynamic tuning of the cavity where the phase response of the metasurface is the main limitation. The complicated procedure of metasurface fabrication (including obtaining layer thickness of Å order) is another drawback of this solution. Chen et al. proposed a microelectromechanical gap-adjustable Fabry-Perot cavity using a graphene-bonded fiber device serving as a microheater [43]. Current application results in the temperature increase, which in return causes fiber deformation. The solution requires the preparation and transfer of graphene and gold electrodes onto the fiber end-face.

Sikdar and Kornyshev presented an electro-tunable Fabry-Perot cavity based on mirror-on-mirror metamaterials [44]. The cavity consisted of two reflective surfaces made of self-assembling nanoparticle monolayers deposited on electrodes. The cavity was filled with an aqueous solution. The mirrors' reflectivity can be electrically adjusted thanks to the variation of the electrode potentials. Voltage-controlled alterations impact the inter-nanoparticle separation in the

monolayers. This design enables continuous *in situ* tuning of the multiple transmission peaks in a relatively cheap and energy-efficient way. The main disadvantage of this solution is the need for an aqueous electrolyte that excludes its integration with electronics. Another drawback is a potential need for additional coatings for mirrors in direct contact with the electrolytic solution. Although electrical tuning is fast and continuous, the tuning range is relatively small, and the manufacturing procedures can be costly. Fuscaldo et al. proposed a voltage-controlled dynamic tuning of the Fabry-Perot cavity, shown on an example of an antenna [45]. The authors investigated a construction using nematic liquid crystals and thin films of alumina layered alternately on the grounded substrate. Changes in applied voltage resulted in changing dielectric properties of the crystals. Those alterations caused changes in the propagation wavenumber of the modes enabling beam adjustments at a fixed frequency. The main advantage of the solution assures the finest performance and dynamic cavity tailoring, but the fabrication procedure is complicated, as several layers of the nematic liquid crystal have to be used.

T. Ding describes a method based on a plasmon-assisted laser printing technique [46]. The cavity was prepared from metal-polymer insulator-metal structures. The polymer is degradable and prone to photothermal effect and multiphoton ablation: the material changes as a response to laser illumination. The incident laser beam induces degradation of the polymer medium fulfilling the cavity. Tuning is therefore dependent on the material thickness and power of the laser. The cavity parameters are monitored using reflection spectra to continuously control the process. The laser printing solution can be used to tune the cavities in a continuous, fast and location selective manner. However, the polymer is not re-usable: after setting it to a certain state there is no possibility of turning the settings back. In extreme cases, the metallic mirrors can collapse uncontrollably changing the cavity size.

The approaches reported by Braakman and Blake [47] as well as by Alligood DePrince et al. [48] shows tuning of the Fabry-Perot cavity by application of wire-grid polarizers as mirrors for far-infrared spectroscopic techniques. The optimization of the cavity was achieved by changing the ratio of wire spacing to its diameter, as well as using metallic material with low resistivity. The obtained results present a promising solution for far-infrared spectroscopy, however, its full potential and outstanding performance are limited by currently available optical elements. The manufacturing cost and dimensions of such a device are too high to justify its implementation.

The introduction of new materials into the cavity to tune its properties on example of the Fabry-Perot resonator is a promising strategy. Mitra et al. [49] reported a Fabry-Perot microcavity with a gold nanoparticle placed in between silver mirrors. The interaction between them resulted in a redshift of the cavity modes. The discrete nanoparticles introduced in the construction allow selective tailoring of the cavity which can be exploited for micromechanical and optical sensing. Nonetheless, proper introduction of the nanoparticles and centering them in the light path can be challenging. Hirsch et al. presented a Fabry-Perot cavity tuning through the placement of a birefringent material inside it [50]. The investigation included high and low finesse interferometers. The study concludes with the possibility of doubling the number of maxima in the desired spectral range, which can be used for reducing the bandwidth of the light source applied in the sensor's construction or reducing the cavity length with nearly the same interference pattern for bigger cavities in standard interferometers. The solution requires material of the highest quality and proper positioning of the material to achieve the desired effect. Isaacs et al. report on liquid crystal Fabry-Perot tunable filters [51]. The use of liquid crystals assures continuous tailoring with a wide dynamic range and low power consumption. The drawback of this solution is the difficulty of proper ITO (Indium Tin Oxide) layer positioning.

The approach with the use of various materials in cavity construction is a promising strategy, considering the constant development of material engineering that offers a wealth of structures with tailored properties and ease of their application. Moreover, with a proven procedure of required material deposition, this solution assures simple and robust tuning of the cavity through elements replacement depending on the needs. The material that is investigated within this study is diamond due to its outstanding properties and enduring popularity among optoelectronic solutions. Diamond can be applied for the construction of lasers [52] or detectors [53–55]. The diamond structure can be used in the production of membranes, as presented on the example of a miniature fiber-optic sensor of pressure [56]. Recent materials science achievement allows fabrication of elastic diamond microarrays, which controllable strains could influence their properties, opening new possibilities in photonics and electronics [57].

The great potential of using diamonds in sensing encourages the development of materials for components construction to improve their metrological parameters. The material influence on the resulting element gives a wide field to tailor device to very specific applications. For example, using biocompatible materials opens a way to biomedical measurements with no risk of poisoning



the biological sample or destroying the sensor parts in contact with it [58]. While applying mechanically and chemically resistive materials, we can significantly increase the lifespan and extend the possibilities of the usage of such sensors on measurements in harsh environmental conditions [59]. Those benefits can be provided by the use of synthetic diamond structures, known for their properties [60]. Synthetic diamond structures have remarkable optical [66], mechanical and thermal [67], and chemical [63] properties which distinguish them among others materials. Synthesized diamond has the biggest band gap (5.45 eV) among elemental semiconductors and is one of the biggest among all conductors [64]. It is chemically stable, very hard (Vickers hardness 10 000 kg/mm²) and resistant to mechanical and chemical damage [65,66]. It has a broad electrochemical window (from -1.25 V to +2.3 V) [67], a low coefficient of thermal extension and high thermal conductivity [68]. It is transparent in a broad wavelengths range and it is characterized by a very high (for semiconductor material) refractive index ($n = 2.41 @ 500 \text{ nm}$) [69]. Moreover, it is biocompatible [70]. The properties of the diamond can be also tuned i.e. by changing parameters of the CVD (Chemical Vapor Deposition) process e.g. temperature, time, working gas mixture composition.

Incorporation of dopant elements into diamond results in different properties the material achieves. boron-doped diamond (BDD) and nitrogen-doped diamond (NDD) structures are frequently used as electrodes in electrochemical systems. Electrochemistry (EC) allows for the detection of small concentrations of tracked substances and the degradation of hazardous chemicals. EC setups can be designed as mobile systems with electrodes selected to meet given requirements.

For example, NDDs were applied for electrochemical reduction of toxic nitrobenzene [71]. The electrode exhibited more negative hydrogen evolution potential leading to high energy efficiency. The authors showed that the NDD electrode had higher electrocatalytic activity and selectivity in the reduction of nitrobenzene to aniline than a graphite electrode. A diamond film with incorporated nitrogen allows for the detection of toxic heavy metal ions [72] and bioanalytes like dopamine [73]. The nitrogen incorporation level has a tremendous impact on the electrochemical properties of the resulting film and its surface morphology translating to the electrode performance [74]. Further investigations led to the fabrication of an ultra-microelectrode array for detection of dopamine [75] and electrodes for *in situ* detection of dopamine in presence of interfering substances - ascorbic acid and uric acid [76]. Despite the

great potential of the NDD structures, their reported applications are scarce in the literature as the BDD remain dominant.

The boron-doped diamond films are also well-known in electrochemistry, eagerly applied as working electrodes, because they assure high response reproducibility, wide electrochemical potential window, stable and low values of background current (enhancing the signal to noise ratio), chemical inertness, long-time response stability, and biocompatibility [77]. BDDs are used in the construction of e.g. biosensors dedicated for detection of various compounds such as antibiotics or DNA [78–81], they can be also used in wastewater treatment [82] and degradation of dangerous chemical compounds[83,84], as well as tracking of hazardous materials [85].

Since the electrochemical measurement methods assure high sensitivity and selectivity, while the measurement systems remains relatively simple and cheap to implement, an opportunity arises to couple such a system with other modalities. The development of one setup combining the optical sensing method with electrochemistry may give promising results like obtaining more information because of the synergy between two techniques, and giving a new insight on the investigated processes, as well as saving time and resources by performing simultaneous measurements in two domains. Different approaches to combining these methods have been proposed in the literature. An optoelectrochemical sensor joining fluorescence and electrochemical impedance spectroscopies applying modified graphene served for monitoring insulin level [86]. Dual detection of heavy metals via electrochemical impedance spectroscopy and Raman spectroscopy was reported [87]. Liu et. al presented an optoelectrochemical setup using internal reflection ellipsometry and an electrochemical setup for sub-surface electrochemical processes monitoring [88]. Cobet et al. proposed an ellipsometric spectroelectrochemical system for *in situ* investigations of polymer doping [89]. Sobaszek et al. described a system for *in situ* Mach-Zehnder interferometric monitoring of electropolymerization at boron-doped diamond electrodes [90]; a spectral shift occurred due to the electrode surface modification with melamine. Janczuk-Richet et al. constructed a setup for electrochemical reactions investigations using fiber Bragg gratings coated with ITO (indium tin oxide) [91,92]. ITO served as a working electrode in an electrochemical system and as a sensitivity enhancing coating of Bragg gratings to refractive index changes in the optical subsystem.

According to the best author's knowledge, a solution on combining the tunable Fabry-Perot cavity with an electrochemical setup has not been reported yet. This dissertation presents a unique hybrid system with a tailored optical cavity working as a Fabry-Perot interferometer applying diamond structures and an electrochemical setup. This way, real-time optical monitoring of electrochemical reactions is possible in a simple and robust way, with the opportunity to miniaturize it.

3. MATHEMATICAL INVESTIGATION OF THE OPTICAL CAVITY FINESSE COEFFICIENT

Optical cavities are widely in optoelectronics. They can be used for developing tunable passband filters with a tailored transmission of selected wavelengths. Using the cavities in the interferometers, any perturbations influencing the phase difference between the interfering beams inside the will impact the recorded signal, which is used in sensors of displacement, stress, pressure, refractive index, pH and many others. In lasers, the mirrors creating the resonant cavity assure proper conditions for lasing to occur. By adjusting the reflectivity of the mirrors, optimization of the Fabry-Perot based laser diodes output power is achieved. Such cavity can also be found in optical amplifiers, where relatively weak reflections are below the laser threshold, while increasing the amplifier gain.

The mathematical investigation of the finesse coefficient of the optical cavity allows to indicate the factors that determine its value and how to tune it to meet given requirements and improve the performance of the developed optoelectronic devices. The calculated and plotted modeling results allow prediction of the optical signals that can be registered under certain measurement conditions (e.g. with the use of a light source working at selected central wavelength, cavity length, mirror material creating the cavity). The theoretical results enable their direct comparison with the experimental results and confirm their agreement. In this study, the investigation is conducted on the example of a Fabry-Perot cavity. It is constructed of two parallel, partially reflecting surfaces, separated from each other with a small gap between them as shown in Figure 3.1.

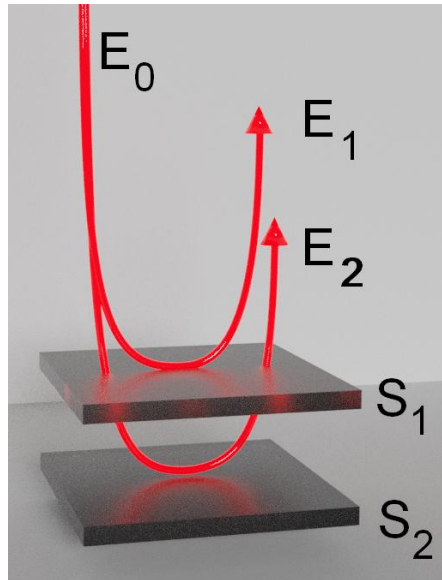


Figure 3.1. Fabry-Perot cavity formed between two partially reflective surfaces, red arrows symbolize the light reflections. E_0 – amplitude of electric vector of the incident beam, E_1 , E_2 – amplitudes of electric vectors of waves reflected from reflective surfaces S_1 and S_2 , respectively.

The air-gap Fabry-Perot cavity provides advantages: it has adjustable cavity length and provides easy access e.g. for analytes. It can be tailored by developing curved mirrors, using techniques such as focused-ion-beam (FIB) milling [93] or laser ablation [94]. A popular strategy is to fabricate the mirrors on the end-face of a single-mode optical fiber [94,95], giving more robust constructions.

The partially reflecting surfaces S_1 and S_2 characterized by reflectances of R_1 and R_2 and the separation of length L create a cavity where the light forms of a standing wave for specific resonance frequencies [13]. The light entering the cavity through the first surface S_1 is partially reflected and partially transmitted through it. The transmitted light, propagating inside the cavity is then partially reflected from the surface S_2 and partially transmitted. The reflected light undergoes further partial reflections and transmissions as shown in 42.

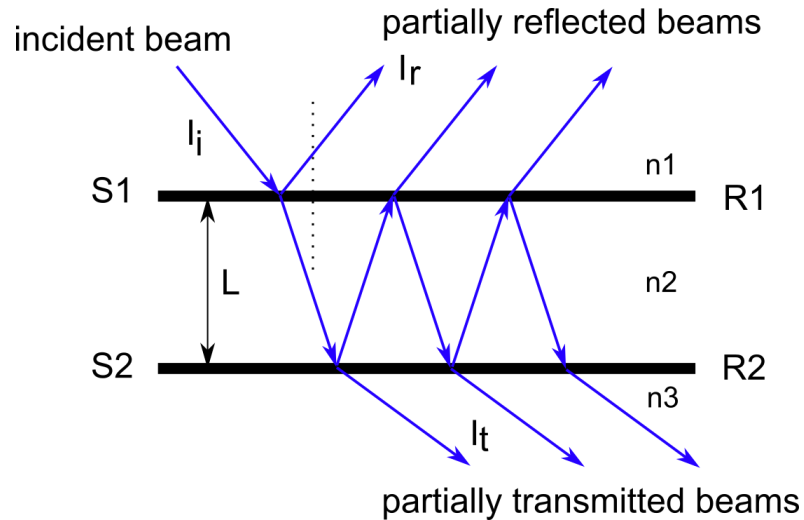


Figure 3.2. Schema of the Fabry-Perot cavity. $S1, S2$ – partially reflective surfaces, L – cavity length, I_i – intensity of the incident beam, I_r – intensity of the reflected beam, I_t – intensity of the transmitted beam, n_1, n_2, n_3 – refractive indices of the materials creating interfaces, $R1$ – reflectivity of the surface $S1$, $R2$ – reflectivity of the surface $S2$.

Plane waves for the planar Fabry-Perot cavity are assumed. The intensity I of the measured signal can be expressed as:

$$I = I_1 + I_2 + 2\sqrt{I_1 I_2} \cos \delta \quad (4.1)$$

where: I – intensity of the measured optical signal, I_1, I_2 – intensity of the interfering beams, δ – phase difference between interfering beams.

When a plane wave incidents the planar-mirror cavity, multiple partial reflections and transmissions occur. The interference between the beams depends on their optical path difference δ – only certain frequencies are supported (constructive interference) and others are canceled (destructive interference). The achieved transmission and reflection characteristics of a Fabry-Perot interferometer show resonances whose position is dependent on the optical path length of the cavity [96]. The phase difference between two beams is described by:

$$\delta = 2\pi \frac{2nL}{\lambda} \quad (4.2)$$

where: n – refractive index of the medium inside the cavity, L – cavity length, λ – wavelength.

The factor that greatly influences the cavity properties is the reflectivity of its mirrors. The reflectivity R of the surfaces creating the cavity can be expressed as follows [97]:

$$R = \left(\frac{n_1 - n_2}{n_1 + n_2} \right)^2 \quad (4.3)$$

where: R – reflectivity, n_1, n_2 – refractive indices of the materials creating the interfaces.

The intensity of the reflected light is expressed by [97]:

$$I_r = \frac{(2 - 2\cos\delta)R}{1 + R^2 - 2R\cos\delta} I_i = \frac{4R\sin^2 \frac{\delta}{2}}{(1 - R)^2 + 4R\sin^2 \frac{\delta}{2}} I_i \quad (4.4)$$

where: R – reflectivity, δ – phase difference, I_i – incident light intensity.

The corresponding intensity of the transmitted light I_t is [97]:

$$I_t = \frac{T^2}{1 + R^2 - 2R\cos\delta} I_i = \frac{T^2}{(1 - R)^2 + 4R\sin^2 \frac{\delta}{2}} I_i = \frac{(1 - R)^2}{(1 - R)^2 + 4R\sin^2 \frac{\delta}{2}} I_i \quad (4.5)$$

where: R – reflectivity, T – transmission, δ – phase difference between interfering beams, I_i – incident light intensity.

These expressions are known as Airy's formulas. By using the relation $R + T = 1$ (assuming no losses) and introducing the finesse coefficient F we can express the Airy formulas as [97]:

$$\frac{I_r}{I_i} = \frac{F\sin^2 \frac{\delta}{2}}{1 + \sin^2 \frac{\delta}{2}} \quad (4.6)$$

$$\frac{I_t}{I_i} = \frac{1}{1 + F\sin^2 \frac{\delta}{2}} \quad (4.7)$$

where F is defined as:

$$F = \frac{4\sqrt{R_1 R_2}}{(1 - \sqrt{R_1 R_2})^2}, \text{ when } R_1 = R_2 \text{ then } F = \frac{4R}{(1 - R)^2} \quad (4.8)$$

R_1 and R_2 describe the reflectivity of the mirrors. The finesse coefficient F is therefore a function of reflectivity as shown in Figure 3.3.

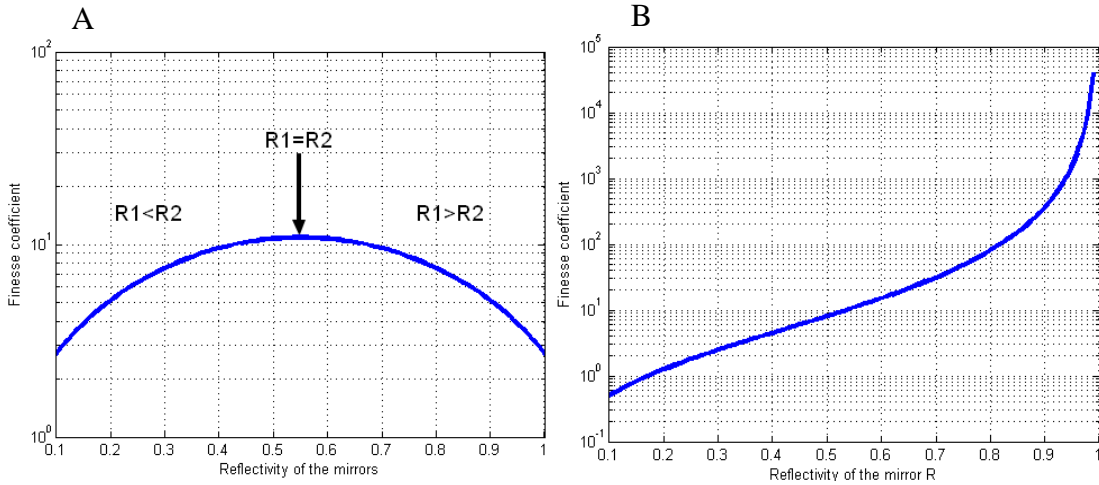


Figure 3.3. Finesse coefficient in a function of reflectivity for A) asymmetrical cavity $R_1 \neq R_2$, B) symmetrical cavity where $R_1 = R_2$.

For an asymmetrical cavity, the bigger the reflectivity difference between the mirrors creating the cavity, the smaller the finesse coefficient value. The maximum value is achieved for two mirrors characterized by the same reflectivity value resulting in a symmetrical cavity. In this case, reflectivity changing from 0 to 1 for both reflective surfaces results in finesse coefficient increase.

With the increase of R , the minima of the transmitted light characteristics decrease, resulting in narrower peaks. The transmittance and reflectance characteristics are presented in 05. The sharpness of the obtained fringes can be described by their full width at half maximum (FWHM). The separation between adjacent fringes is called free spectral range. The ratio of the FSR and the FWHM is called the finesse F [97]:

$$F = \frac{\text{FSR}}{\text{FWHM}} = \frac{2\pi}{\text{FWHM}} = \frac{\pi\sqrt{F}}{2} \quad (4.9)$$

where: FSR – free spectral range, FWHM – full width at half maximum.

The value of FSR and FWHM ratio - the finesse - depends on the reflectivities of the reflective surfaces used for the construction of the cavity [98]. The cavities built with high reflecting mirrors assure high values of the finesse resulting in narrower transmittance peaks in comparison to mirrors with lower reflectivity.

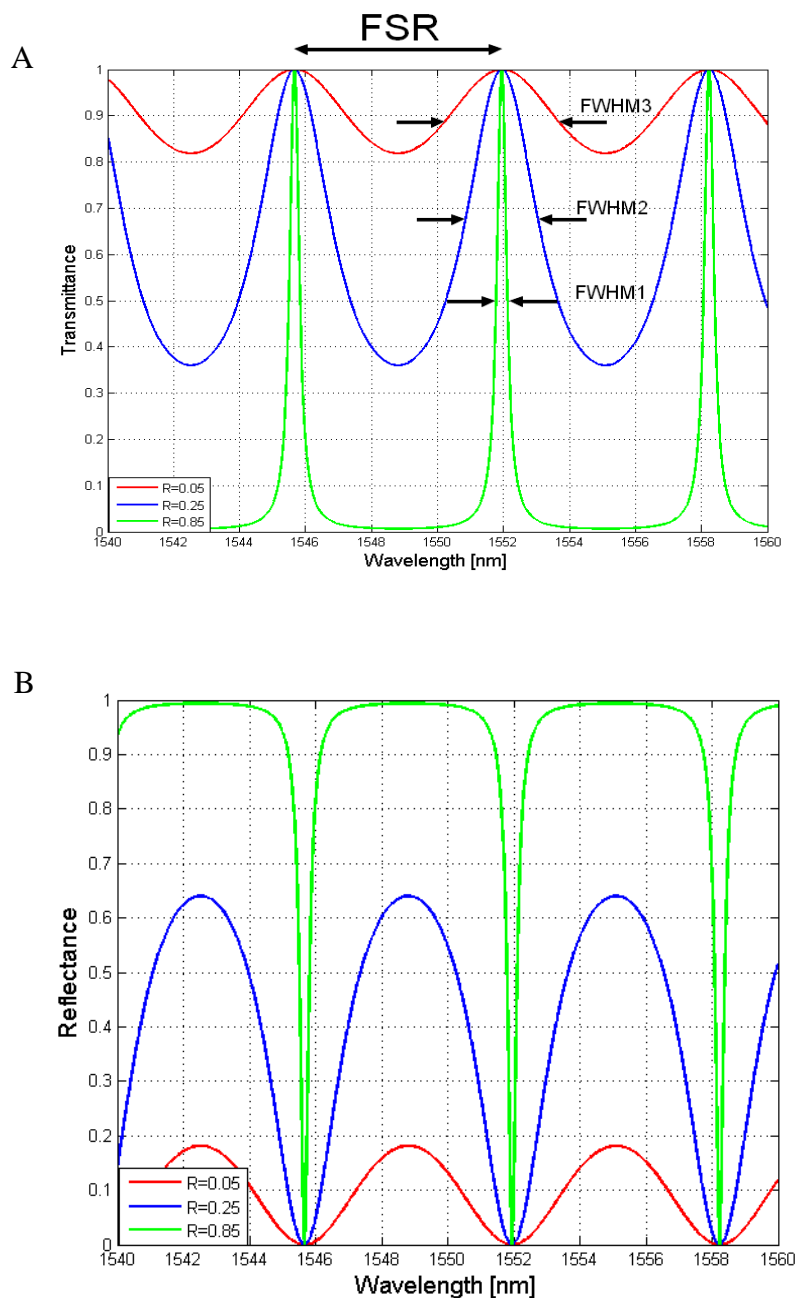


Figure 3.4. a) Transmittance and b) reflectance characteristics for selected modeled R values. FSR – free spectral range, FWHM – Full width at half maximum. FWHM1 = 0,25 nm, FWHM2 = 2,5 nm FWHM3 = 3,8 nm.

The transfer function of a multi-beam interferometer can be approximated with a two-beam interferometer in case of low values of R resulting in low-finesse coefficient F. Such simplification is possible because higher-order reflections do not significantly contribute to the resulting spectrum, and hence can be neglected [99]. The equation for the reflected and transmitted light can be simplified to:

$$I_R = F \sin^2 \left(\frac{\delta}{2} \right) = \frac{F}{2} (1 - \cos(\delta)) \quad (4.10)$$

$$I_T = 1 - F \sin^2 \left(\frac{\delta}{2} \right) = 1 - \frac{F}{2} (1 - \cos(\delta)) \quad (4.11)$$

Based on the recorded interference signal, fringe contrast value, also known as visibility can be calculated. The visibility changes from zero to unity, where unity indicates a perfect fringe contrast [97].

$$V = \frac{I_{max} - I_{min}}{I_{max} + I_{min}} \quad (4.12)$$

where: V – visibility, I_{max} – maximum light intensity, I_{min} – minimum light intensity.

Visibility is one of the most important parameters describing an interferometer. Its high value indicates a high signal-to-noise ratio and allows for more accurate measurements. Low visibility leads to the inability of resolving spectral interference fringes and limits the maximum cavity length for which measurements can be taken.

In this study, the mathematical investigation of the Fabry-Perot cavity with an external cavity working in a reflective mode is presented. The influence of different mirrors (made of silver, boron-doped diamond film, nitrogen-doped diamond film) and an additional layer of the nanocrystalline diamond sheet attached over the fiber end-face on the finesse coefficient is investigated. The plots below show results of theoretical modeling of the cavities built of a fiber end-face and the investigated mirrors, with the air fulfilling the gap between them.

The first investigated cavity construction was utilizing the nitrogen-doped diamond film working as an external mirror as shown in Figure 3.5. The cavity interfaces were created at the boundaries of the optical fiber end-face/air and air/nitrogen doped diamond film surface.

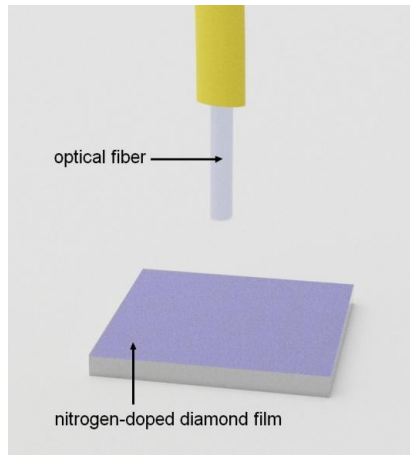


Figure 3.5. Cavity construction utilizing nitrogen-doped diamond film.

The transmittance characteristics were then plotted along with the results obtained for the conventional cavity applying silver mirror in place of nitrogen-doped diamond film as a reference.

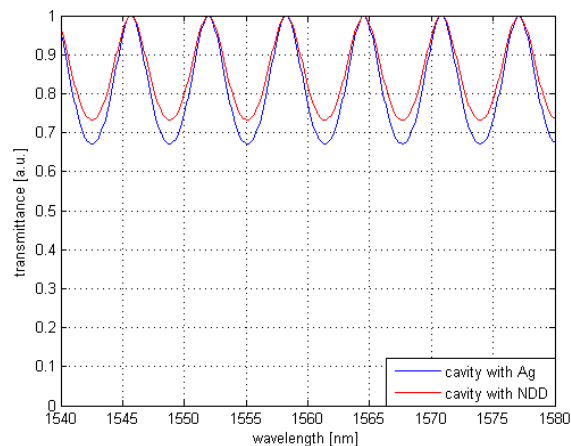


Figure 3.6. Transmittance characteristics for a nitrogen-doped diamond film and a silver mirror.

The calculated characteristics show that the introduction of the nitrogen-doped diamond film slightly increases the FWHM value which results in lower finesse coefficient. The transmittance minimum value is greater than that of a cavity with silver meaning that the

reflectivity of the diamond structure is lower. The calculation results show that with NDD films we can decrease the finesse coefficient value of the cavity.

The next investigated cavity was applying the boron-doped diamond film as presented in Figure 3.5. The cavity interfaces were formed at: fiber end-face/air and air/boron doped diamond film surface boundaries.

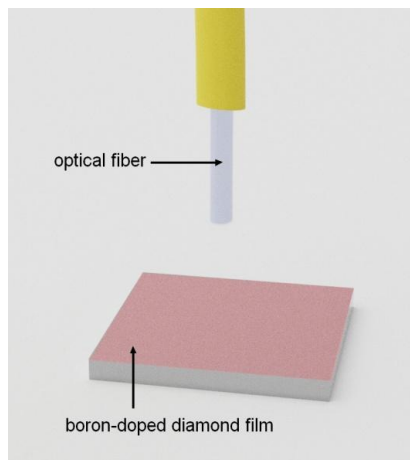


Figure 3.7. Cavity construction utilizing boron-doped diamond film.

The transmittance characteristics were calculated and plotted with the results achieved for the silver reference.

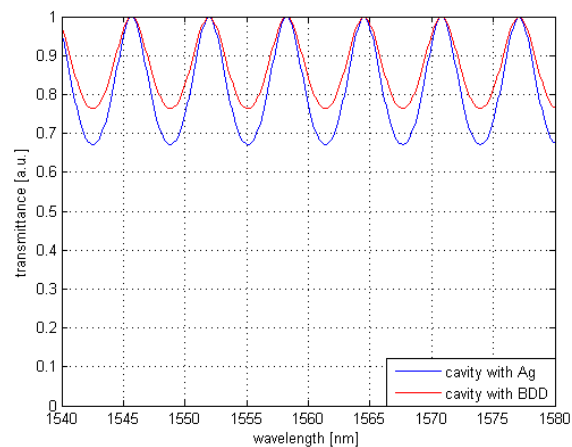


Figure 3.8. Transmittance characteristics for a boron-doped diamond film and a silver mirror.

Similar behavior to the NDD film is observed, as the FWHM value increases lowering the finesse coefficient value. The reflectivity of the BDD contributes to the increase of the minimal transmittance value. The results for NDD and BDD have the same character due to the similar

surface morphology of the structures. Changes observed in the characteristics are dependent on their reflectivity. The refractive indices of the diamond films can be tailored during the CVD process via e.g. dopant element and its level selection which directly translated to the parameters of the cavity applying them.

The possibility of the cavity modification with the diamond structures is not only limited to the external mirror. Attachment of a nanocrystalline diamond sheet allows changing the parameters of the first interface as shown in Figure 3.9.

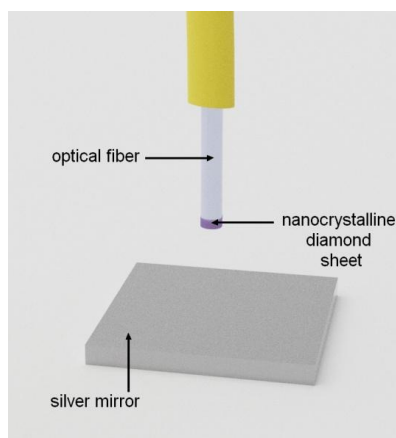


Figure 3.9. Cavity construction utilizing nanocrystalline diamond sheet.

Such configuration is possible due to low adhesion of the NDS to the substrate which allows its delamination and transfer onto the desired surface. The transmittance characteristics obtained for this configuration are shown in Figure 3.10.

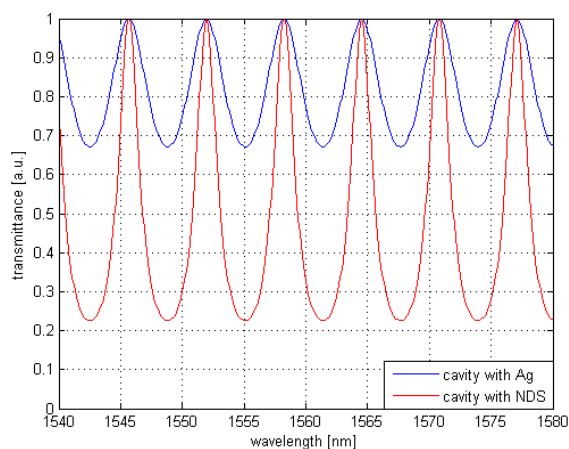


Figure 3.10. Transmittance characteristics for a nanocrystalline diamond sheet and silver mirror.

A significant signal change was obtained. The introduction of the NDS into the cavity resulted in lowering the FWHM value leading to the narrower peaks and higher finesse coefficient value. By using diamond structures in the cavity construction, its finesse parameter can be changed. In the case of BDD film working as a reflective surface, the minima of the characteristics have higher values, resulting in a lower finesse coefficient. The same phenomenon is observed for NDD films. The reason behind it lies in their lower reflectivity values in comparison to standard silver mirrors. However, around 10% reduction is rewarded with other benefits: better wear resistance, biocompatibility, and as shown later, significant reduction of required sample volume. Application of NDS and silver mirror allows increasing the finesse coefficient while introducing protection from potential mechanical and chemical damage of the fiber end-face. The values describing obtained characteristics are shown in Table 1.

Table 1. Parameters of the transmittance characteristics of the investigated cavities.

Parameter	NDD	BDD	NDS
Finesse coefficient	0.3094	0.3653	4.4383
Minimal value	0.7637	0.7324	0.2253
FWHM	3 nm	3.5 nm	2.5 nm

The obtained values of the finesse coefficient differ depending on the diamond structure type introduced into the cavity. The highest finesse coefficient value was achieved for the cavity using a silver mirror and a nanocrystalline diamond sheet, while boron-doped diamond film showed the lowest value, yet comparable with nitrogen-doped diamond film and silver results. Close values obtained for A and B result from similar surface morphology and characteristic of the material. However, since nitrogen-doped diamond has a higher refractive index which results in higher surface reflectivity, the final finesse value is greater for the cavity with this sample. The cavities with NDD and BDD have finesse coefficient values of ~30% lower than those for silver mirror. The low-thickness and high refractive index of the nanocrystalline diamond sheet allowed obtaining the highest finesse coefficient of the cavity. The conducted research has shown that the finesse coefficient of the cavities can be tuned with diamond structures. Both cavity interfaces can be modified: the first surface creating the cavity can be tailored with nanocrystalline diamond sheet attached over it, while the second surface can be tuned by doped diamond films. Depending on the deposition process parameters, we can adjust structure properties to obtain needed finesse coefficient values.





4. EXPERIMENTAL VERIFICATION OF THE MATHEMATICAL RESULTS IN A MEASUREMENT SYSTEM

This chapter describes the experimental verification of the results of the mathematical investigation. A measurement setup for cavity tuning assessment was designed, built and the measurements were performed. The setup allows for easy tuning of the finesse coefficient by an open-access cavity allowing mirrors exchange.

The measurement setup consists of the broadband light source operating at the central wavelength of: 1550 nm (SLD-1550-12-, FiberLabs Inc., Fujimi, Japan), 1560 nm (S1550-G-I-10, Superlum, Ireland), 1310 nm (SLD-1310-18-W, Fiber Labs Inc., Japan) and 1290 nm (S-1290-G-I-20, Superlum, Ireland), optical spectrum analyzer (Ando AQ6319, Yokogawa, Japan) for signal acquisition and a 2x1 fiber coupler with standard single-mode optical fibers connecting elements. A micromechanical setup allows for parallel positioning of the fiber above the external mirror, assuring its stability. A micromechanical screw enables changing the cavity length with an increment of 10 μm . The measurement setup is shown in Figure 4.1

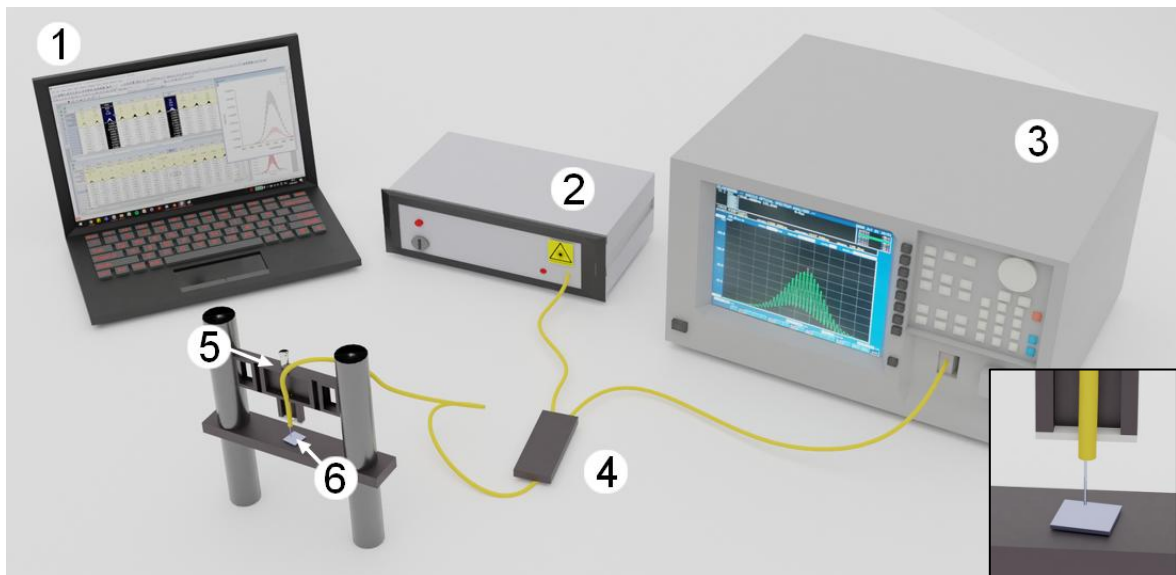


Figure 4.1. Measurement setup for the cavity parameters assessment. 1 – PC, 2 – light source, 3 – optical spectrum analyzer, 4 – 2x1 fiber coupler, 5 – micromechanical setup, 6 – cavity. Inset shows a zoom onto the cavity.

The incident beam guided by the fiber reaches the fiber tip and partially reflects on the first boundary. Part of the beam is guided through the cavity and then reflects from the second

boundary. The reflected beams interfere with each other and the resulting signal is registered by the optical spectrum analyzer.

The interfering beams are reflected back to the optical spectrum analyzer acquiring the created signal. The recorded spectra are then analyzed and plotted on the PC, sample interferogram can be seen in Figure 4.2.

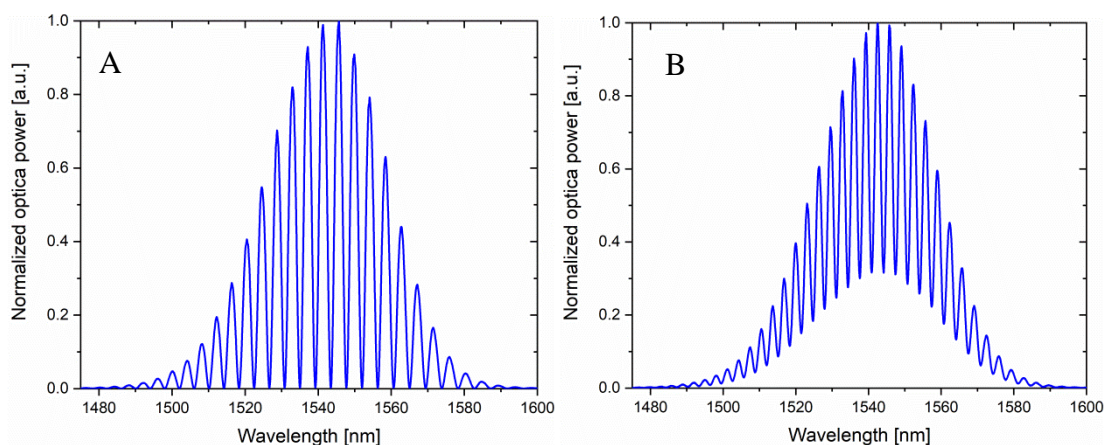


Figure 4.2. Representative optical spectra for the refractive index of A) $n=1$ and B) $n= 1.35$ recorded for a cavity length of $280 \mu\text{m}$ with silver mirror, the light source of central wavelength 1550 nm was used.

The signal modulation is dependent on the cavity length and refractive index of the medium inside the cavity. The above example shows changes in signal modulation and visibility values due to the change of refractive index. The analysis of the spectrum e.g. by investigating changes in spectral separation between neighboring maxima gives information about the measurand value.

The crucial aspect of this research is the surface morphology of the diamond structures. It was investigated using a Dual-beam system Helios 600 (FEI, Hillsboro, Oregon, USA) with SEM voltage-current of 2 kV and 0.17 nA and Ga FIB with voltage-current of 30 kV . A representative surface imaging is shown in Figure 4.3.

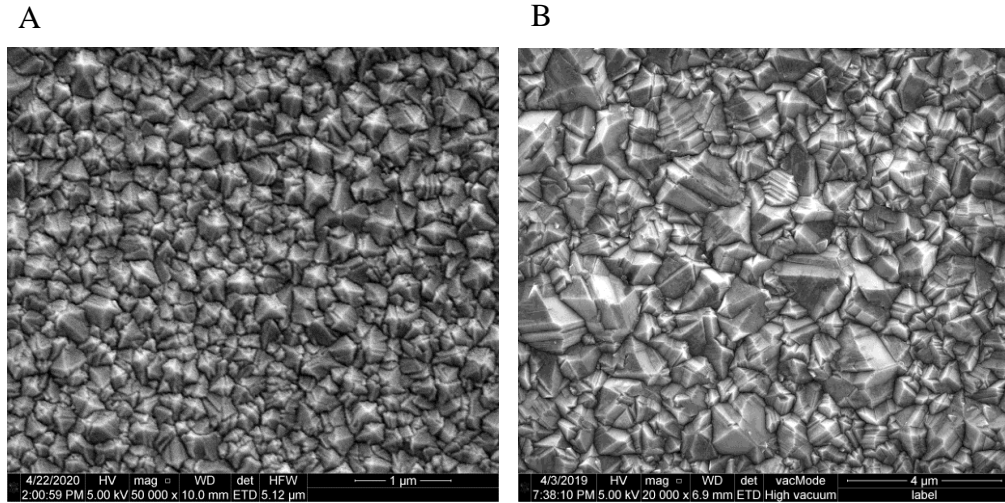


Figure 4.3. Representative SEM images of (a) nanocrystalline diamond sheet, magnification 50 000x (b) boron-doped diamond film, magnification 20 000x.

The crystallites are uniform in terms of their dimensions and distribution over the substrate surface for both diamond structures. There are no visible defects in the structures, nor cracks or other abnormalities impacting their continuity. The structures are made of equally distributed crystallites. The surface is continuous, homogenous without any visible defects hence, can be applied in the next step of the study. It is worth noting that the dimensions of the high quality nanocrystalline diamond sheet are large enough to cover an end-face of a standard fiber core.

4.1 Tuning of the finesse coefficient with nitrogen-doped diamond film

As a first step, tuning of the Fabry-Perot interferometer cavity with nitrogen-doped diamond films performing as passive optical elements was performed. Several samples differing in the nitrogen incorporation level (0%, 1%, 3%, 5%) were tested as mirrors. The diamond structures were deposited on silicon substrates in a Microwave Plasma Assisted Chemical Vapor Deposition System. The growth parameters (Table 4.1) were the same for each sample, excluding the nitrogen concentration in the working gas mixture.

Table 4.1. Growth conditions of nitrogen incorporated diamond films grown using CH₄, H₂, and N₂ plasma.

Sample	CH ₄ concentration	H ₂ concentration	N ₂ concentration	Pressure (Torr)	Microwave power (W)	Temperature (°C)	Thickness (nm)
NiD-0	3%	97%	0%	30	3000	675	500
NiD-1	3%	96%	1%	30	3000	700	500
NiD-3	3%	94%	3%	30	3000	720	500
NiD-5	3%	92%	5%	30	3000	750	500

Series of distance measurements were performed in the range of 0-100 μm with a step of 10 μm for all diamond samples and a silver mirror for reference. The air was filling the cavities during the whole measurement procedure.

Visible changes in the optical properties of the reflective surfaces result from different refractive indices caused by various nitrogen incorporation which entails a change of surface reflectivity. The refractive index of a nitrogen-doped diamond sample decreases with the increase of nitrogen level. The contrast values of the signals obtained for each construction are shown in Table 4.2.

Table 4.2. Comparison of visibility values for representative cavity lengths on nitrogen incorporated diamond films and silver.

Cavity length [μm]	Visibility			
	Ag	NDD-1	NDD-3	NDD-5
40	75.1 %	99.9 %	99.8 %	94.0 %
60	76.0 %	99.9 %	99.9 %	97.3 %
80	77.0 %	99.5 %	98.6 %	99.2 %
100	81.1%	97.6 %	97.0 %	99.9 %

The reflection coefficient of the mirror has the greatest impact on visibility as it determines the intensity level of the reflected signal. It was shown that the cavity tailored with NDD usage offers higher visibility values for smaller cavities in comparison to a silver mirror. Different growth conditions of the NDD directly translate to the reflectivity of the mirrors and the cavity finesse coefficient value metrological parameters of sensors applying them.

The model's quality and ability to describe the Fabry-Perot cavity can be evaluated by a direct comparison of modeled spectra with the experimental results. The light source used in both, theoretical and experimental investigations, was operating at 1550 nm and the Fabry-Perot

cavity was filled with air ($n = 1$). For each measured spectrum, the Gaussian light source characteristics were filtered out.

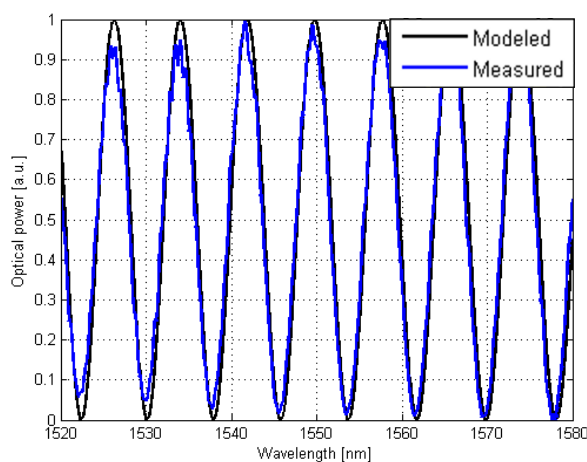


Figure 4.4. Comparison between the modeled and the measured spectra after removing the Gaussian characteristics. The cavities were fulfilled with air ($n=1$). nitrogen-doped diamond film $d=150 \mu\text{m}$

The calculated signal is in accordance with the theoretical one, proving the correctness of the mathematical investigation. The spectral distribution of signals maxima are in agreement overlapping each other. Slight differences in shape of the maxima can be explained by assuming an ideal source characteristics in case of the modeled results. Slight mismatches in terms of the intensity can be attributed to the optical spectrum analyzer sampling process.

4.2 Tuning of the finesse coefficient with boron-doped diamond film

This approach was used to investigate cavity tuning with a boron-doped diamond film and to directly compare it with a nitrogen-doped diamond film. The distance measurements were performed for two light sources: with a central wavelength of 1290 nm and 1560 nm. Both diamond structures were deposited by MWPACVD method on the silica substrates. Obtained data allowed calculation of visibility values for various cavity lengths; selected ones are presented in Table 4.3.

Table 4.3. Comparison of visibility values for representative cavity lengths on nitrogen incorporated diamond films and silver.

NDD			
Wavelength - 1290 nm		Wavelength - 1560 nm	
Cavity length	Visibility	Cavity length	Visibility
60 μm	0.9917	90 μm	0.9939
120 μm	0.8394	190 μm	0.7905
BDD			
Wavelength - 1290 nm		Wavelength - 1560 nm	
Cavity length	Visibility	Cavity length	Visibility
80 μm	0.9915	110 μm	0.9950
160 μm	0.8239	200 μm	0.8727

The cavity parameters change while introducing different diamond materials. The boron-doped diamond film assures better visibility for greater cavity lengths while nitrogen-doped diamond films allow better contrast for smaller cavities: this way, exchanging the external mirror tailors the cavity parameters for specific needs dictated e.g. by the available amount of sample.

For mathematical investigation, the light source characteristics was modeled to fit the characteristics of the source used in experiment, working at a central wavelength equal to 1550 nm. The Fabry-Perot cavity was assumed to be filled with air ($n = 1$). The Gaussian light source characteristics were filtered out.

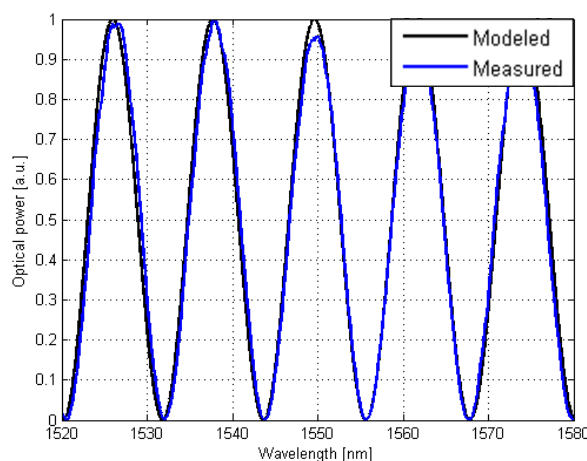


Figure 4.5. Comparison between the modeled and the measured spectra after removing the Gaussian characteristics. The cavities were fulfilled with air ($n=1$). b) boron-doped diamond film $d=100 \mu\text{m}$

The modeled optical signal overlaps nearly ideally with the experimental one. The number and positioning of the maxima are in accordance, showing that the applied model predicted the experimental signal correctly. A visibly smaller amplitude for the measurement results are most likely caused by the optical spectrum analyzer sampling process, leading to averaging of the acquired signal.

4.3 Tuning of the finesse coefficient with nanocrystalline diamond sheet

Tailoring of the first reflective interface of the cavity can be also achieved. In this study, a nanocrystalline diamond sheet (NDS) was applied in a Fabry-Perot cavity and its influence on the optical signal was investigated. The Fabry-Perot interferometer working in a reflective mode was applied, with a silver mirror as the second reflective surface. The planar cavity was formed between the fiber end-face cover with NDS and the silver. NDS attachment modifies the reflective properties and assures protection from damage caused by e.g. chemical factors. This approach shows a potential application for this kind of structure. To the best of the author's knowledge, only several research groups report on the diamond sheet applications, while the majority focuses on deposition process varieties and characterization of surface and resulting materials properties [100–103].

The nanocrystalline diamond sheet was deposited on a tantalum substrate in the MW PA CVD setup. Such substrate was selected to assure low adhesion of the growing structure to its surface, allowing easy delamination of free-standing diamond flakes. This significantly distinguishes the deposition process of the sheets from films, where achieving the highest possible adhesion of crystallites to the substrate is crucial. The flakes can be released by introducing external stress to the structure – detached flake can be then transferred to the desired surface and joined with it by the means of van der Waals forces. In this study, the diamond sheet was realized from the substrate with the stress induced by the scalpel. The flake was then transferred onto the single-mode standard optical fiber end-face.

The light source assumed for modeling was of a central wavelength of 1550 nm to suit the characteristics of the experimental setup. The Fabry-Perot cavity was assumed to be filled with air ($n = 1$). The Gaussian light characteristics were filtered out.



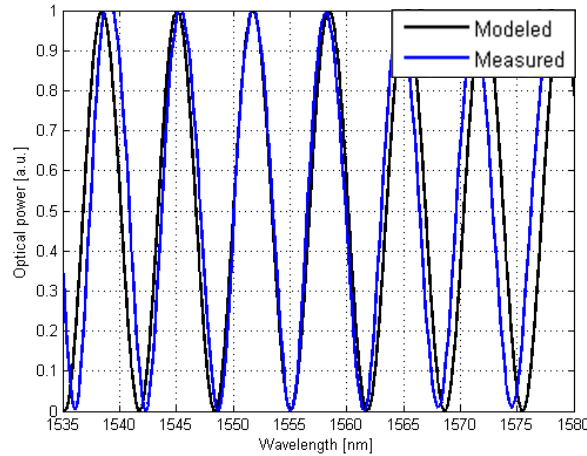


Figure 4.6. Comparison between the modeled and the measured spectra after removing the Gaussian characteristics. The cavities were fulfilled with air ($n=1$). nanocrystalline diamond sheet and silver mirror $d=180 \mu\text{m}$.

The experimental and theoretical characteristics are in agreement, showing the proper calculation process. Small mismatches in terms of the maxima positioning can be explained by non-ideal positioning of the measurement head during experiments.

In this chapter, three configurations of a Fabry-Perot cavity were presented. The results show that the diamond structures can be successfully adopted by a Fabry-Perot cavity for tailoring its properties. The developed cavities remain properly working, assuring satisfying measurement results. The transfer function of each presented configuration was different due to the different optical parameters of the diamond materials. The results of the experiments were compared to the transfer function calculated theoretically and presented in the next section. The adopted models are in agreement with the measured data. The fringe number and distribution are consistent in each case. Slight differences in amplitude values are caused by non-ideality of the real measurements resulting from e.g. a little misplacement of measurement head or light source instability.

Each of them assures tailoring of the metrological parameters of the sensors to specific needs while giving additional benefits like longer lifespan or sample volume reduction due to better signal visibility obtained for smaller cavity lengths. The mathematical investigation was confirmed by experimental measurements. The results presented in this section proved the first thesis: the finesse coefficient can be tailored with the use of diamond structures.

The detailed study on tuning the cavity with diamond structures can be found in the following articles. A physical realization of the measurement setup, conducted experiments, and data analysis for Fabry-Perot cavities applying diamond structures are presented. Their impact on the cavity properties is shown. The results of these studies were published in the articles:

[MK1] Kosowska, M.; Pawłowska, S.; Sankaran, K.J.; Majchrowicz, D.; Haenen, K.; Dholakia, K.; Szczerska, M. Incorporation of Nitrogen in Diamond Films – a New Way of Tuning Parameters for Optical Passive Elements. *Diamond and Related Materials* 2021, 111, 108221, doi:10.1016/j.diamond.2020.108221.

The investigation of the impact of selected nitrogen level incorporation (0%, 1%, 3%, 5%) in diamond films on an interferometric sensor of displacement is presented. The author's contributions were: conceptualization, methodology, analysis of optical data and writing selected parts of an original manuscript.

[MK2] Kosowska, M.; Majchrowicz, D.; Sankaran, K.J.; Ficek, M.; Haenen, K.; Szczerska, M. Doped Nanocrystalline Diamond Films as Reflective Layers for Fiber-Optic Sensors of Refractive Index of Liquids. *Materials* 2019, 12, 2124, doi:10.3390/ma12132124.

The application of nitrogen-doped diamond film and boron-doped diamond film as mirrors in a cavity of the refractive index of liquids in the range of 1.3-1.6 as well as comparison of both sensors parameters is provided. The author's contributions were: conceptualization, performing measurements, data analysis and writing selected parts of the manuscript.

[MK3] Kosowska, M.; Majchrowicz, D.; Ficek, M.; Wierzba, P.; Fleger, Y.; Fixler, D.; Szczerska, M. Nanocrystalline Diamond Sheets as Protective Coatings for Fiber-Optic Measurement Head. *Carbon* 2020, 156, 104–109, doi:10.1016/j.carbon.2019.09.042.

The first use of a new nanocrystalline diamond structure in a fiber-optic measurement head as a protective coating of the fiber end-face is described. Distance measurements and comparison of numerical modeling with experimental data are described. The author's contribution included conceiving and designing the experiments, developing a procedure of NDS transfer, performing measurements, data analysis and writing selected parts of the original manuscript. The conducted research aimed at proving the first established thesis: with the diamond structures we can directly tune the finesse coefficient of the Fabry-Perot cavity.





5. APPLICATIONS OF THE OPTICAL CAVITY TUNING METHOD

Previous chapters described laboratory models of sensors applying diamond structures in the construction of measurement heads. Such an approach allowed for tuning the finesse coefficient of the Fabry-Perot cavities. Those are increased wear-resistance due to extraordinary mechanical and chemical properties of diamond structures, better signal visibility for smaller cavity lengths resulting in a significant reduction in the sample volume required for performing measurements, and biocompatibility enabling measurements of biological samples without the risk of poisoning the sample or damaging elements with direct contact with it. Those advantages open up the field of many potential applications of the fiber-optic sensors and new materials combination, giving solutions with unique properties.

In this chapter, applications of diamond structures in fiber-optic sensors are proposed to prove the second thesis: diamond structures enable construction of an optoelectrochemical system for optical investigation of electrochemical processes. The first step aiming at the development of fiber-optic sensors of distance and refractive index of liquids is crucial for the validation of the proposed solution. While achieving correctly operating sensors utilizing diamond films, the coupling of such interferometer with an electrochemical system becomes possible. Moreover, tuning of the optical cavity with a nanocrystalline diamond sheet that also protects the fiber optic end-face was demonstrated.

5.1 Application of cavity tuning in fiber-optic sensors of distance and refractive index

The proposed application of the tunable cavities as a part of fiber-optic sensors for measurements of distance and refractive index was described in:

[MK2] Kosowska, M.; Majchrowicz, D.; Sankaran, K.J.; Ficek, M.; Haenen, K.; Szczerska, M. Doped Nanocrystalline Diamond Films as Reflective Layers for Fiber-Optic Sensors of Refractive Index of Liquids. *Materials* 2019, 12, 2124, doi:10.3390/ma12132124.

The nitrogen-doped diamond film and boron-doped diamond film served as external reflective surfaces while measuring distance and refractive index. The direct comparison of developed sensors parameters depending on the diamond structure and source wavelength is described. The author's contributions were: conceptualization, performing measurements, data analysis and writing selected parts of the manuscript.



The previous step proved that the nitrogen-doped diamond films can be successfully applied as reflective surfaces changing the metrological parameters of the fiber-optic cavities. This research extends the investigation on the use of NDD and BDD films as a part of interferometric fiber-optic sensors. The refractive index sensors applying boron-doped diamond mirrors were directly compared with those using nitrogen-doped diamond ones.

The measurement setup was build in the same configuration as presented in Section 4.1. The experiment was performed with the use of two light sources, working on the central wavelength of 1290 nm and 1550 nm, respectively (S-1290-G-I-20, and S1550-G-I-10, Superlum, Ireland).

The measurements were performed on liquids with known refractive indices in the range of 1.3-1.6. Such certified refractive index samples were purchased from Cargille® Lab. The experimental procedure is shown in Figure 5.1 below.

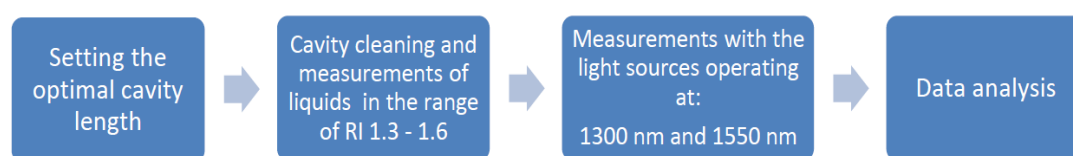


Figure 5.1. *The block diagram of the experiment.*

Firstly, the optimal cavity length ensuring the best signal visibility was determined in series of distance measurements and calculating the contrast value for each. Then the investigated liquid was introduced into the cavity and an optical spectrum was acquired. After the measurement, the sample was removed and the cavity was cleaned with isopropyl alcohol. The process was repeated for all refractive index liquids with both light sources for both diamond structures. The reference signal with air inside the cavity was taken every time after the cleaning to ensure the same measurement head positioning.

The refractive index change influenced the signal modulation. The spectral separation of the maxima in the recorded signals was used to plot the work characteristics of the sensors for a wavelength of 1290 nm (Figure 5.2).

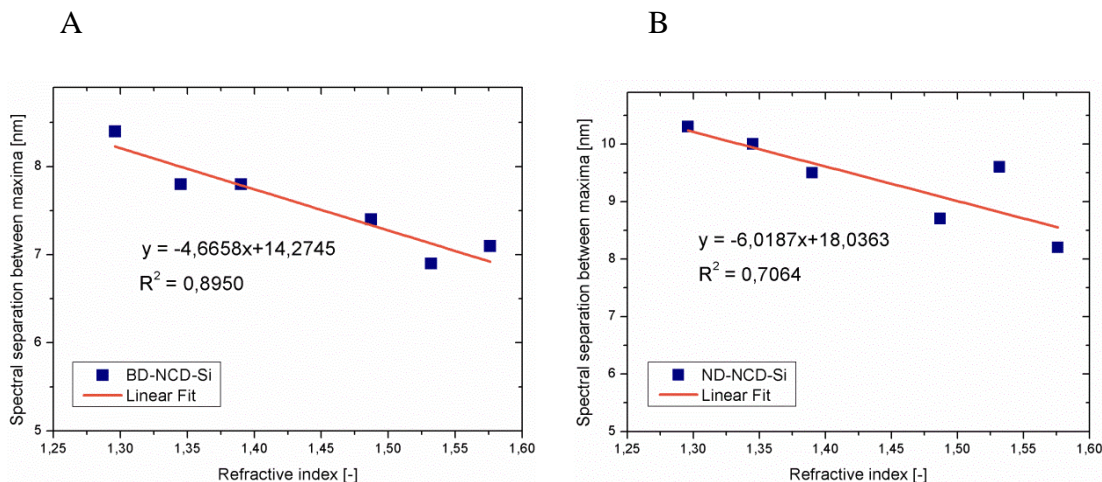


Figure 5.2. Measurements results: spectral separation between maxima as a function of refractive index for wavelength equal to 1290 nm (a) BDD, (b) NDD.

The values of correlation coefficient R^2 describing the quality of fitting of the mathematical model to the collected data and the sensitivity directly found from the slope of the linear characteristics are presented in Table 5.2.

Table 5.2. Correlation coefficient R^2 and sensitivity S values for sensors working at 1290 nm.

	BDD	NDD
R^2	0.8950	0.7064
S [nm/a.u.]	-4.6658	-6.0187

By analogy, the same steps were made for the results recorded with a 1550 nm light source. The work characteristics of the sensors were plotted based on the obtained signals as a spectral separation between maxima in the function of refractive index (Figure 5.3).

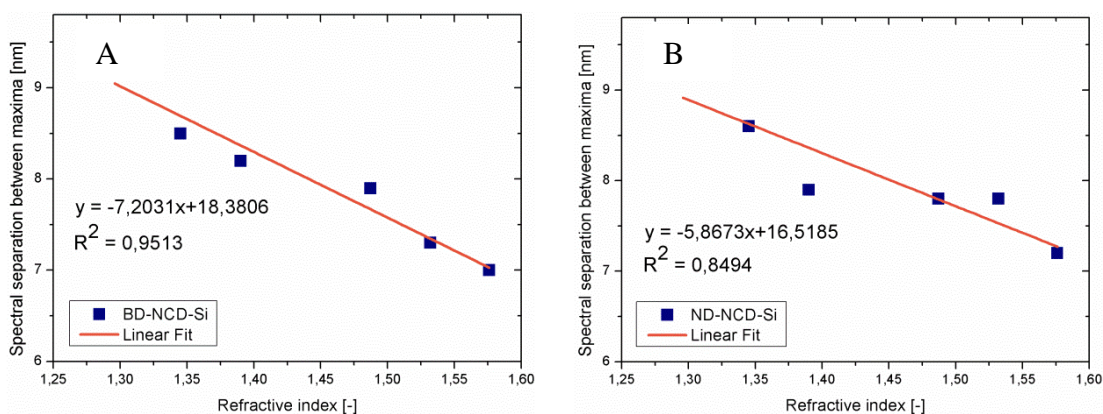


Figure 5.3. Measurements results: spectral separation between maxima as a function of refractive index for wavelength equal to 1550 nm (a) BDD, (b) NDD.

The parameters found from these functions are in Table 5.3.

Table 5.3. Correlation coefficient R^2 and sensitivity S values for sensors working at 1560 nm.

	BDD	NDD
R^2	0.9513	0.8494
S [nm/a.u.]	-7.2031	-5.8673

The results of this study show that both structures can be used as reflective layers, however, they provide different metrological parameters. The achieved values of R^2 show a high or very high negative correlation between refractive index and spectral separation of fringes in the measurement signal.

5.2 Cavity tuning in opto-electrochemical measurement system

Nowadays, electrochemistry is widely applied in science and industry, hence EC process control focused on monitoring of the reactions progress is needed. An optoelectrochemical setup allowing non-invasive optical monitoring of the reactions can fulfill this task. With such a system, additional measurements can be performed to investigate further correlations between low-coherence interferometry and electrochemistry while saving resources: sample (small volumes) and time (rapid monitoring and feedback). The developed setup enables control of the process and ensures that the substance quality remains the same for reversible EC processes. In case of irreversible EC processes the setup would give information about reactions, also these leading to the formation of new chemical compounds that have new properties, as this would manifest through the measured refractive index changes.

The results of the research carried out in the frame of this dissertation included the design and construction of a hybrid optoelectrochemical setup for monitoring of electrochemical reactions; its comprehensive description is presented in the following article:

publication [MK4] titled '*Low-coherence photonic method of electrochemical processes monitoring*', presents an optoelectrochemical system, applying a boron-doped diamond film, for optical monitoring of sample state during electrochemical processes through real-time refractive index measurements. The author's contribution includes conceiving, designing and performing the experiments, data analysis, graphical visualization and writing the original manuscript draft.

A system for simultaneous measurements of liquid samples by interferometric and electrochemical methods consisted of two main parts: a Fabry-Perot fiber-optic interferometer and a standard 3-electrode electrochemical cell, connected by a boron-doped diamond film. The optical part followed the general configuration and was built of a broadband light source (SLD-1550-13-, FiberLabs Inc., Fujimi, Japan), an optical spectrum analyzer (Ando AQ6319, Yokogawa, Japan), single-mode optical fibers and a 2x1 fiber coupler with a power split of 50:50. A stripped, cleaved and cleaned fiber end-face was used as an optical measurement head. The Fabry-Perot cavity was created at the boundaries of the fiber end-face/liquid sample and the liquid sample/BDD. The electrochemical setup consisted of a potentiostat-galvanostat (SP-240, BioLogic, Seyssinet-Pariset, France) and a three-electrode system. The setup is shown in Figure 5.4.

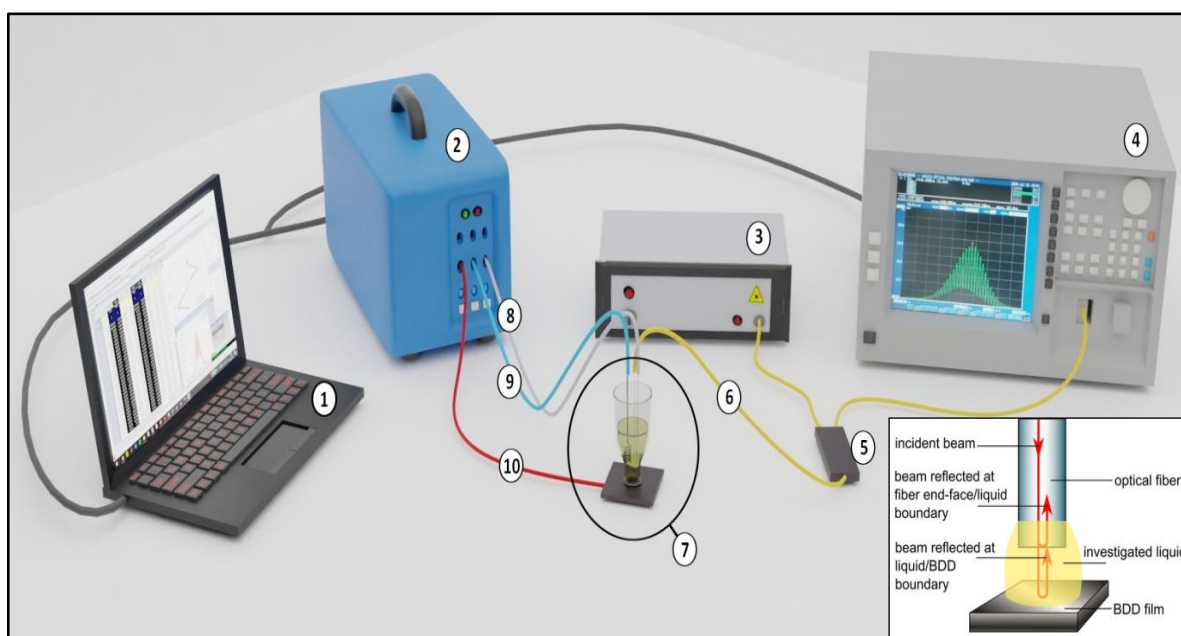


Figure 5.4. Measurement setup scheme (not to scale): 1 – PC for storing and processing measurement data, 2 – potentiostat-galvanostat, 3 – light source, 4 – optical spectrum analyzer (OSA), 5 – 2x1 fiber coupler, 6 – optical fiber, 7 – measurement head, 8 – connection to a reference electrode, 9 – connection to a counter electrode, 10 – connection to a working electrode. The inset figure shows a Fabry-Perot interferometer operation principle: reflected beams interfere with each other giving us a signal register by OSA.

The working electrode was made of a boron-doped diamond deposited on a silica substrate, a counter electrode of a platinum wire, and a reference electrode made of a silver wire with silver chloride deposited on its surface. An electrochemical cell was placed over a laser-cut gasket lying on the BDD surface. BDD is a crucial part of this setup, as it plays a dual role of a working electrode and a reflective surface. All electrodes were connected to the potentiostat

responsible for potential control and recording of the electrochemical curves. The active area of the working electrode was 0.2 cm^2 . The close-up of the hybrid measurement head is presented in Figure 5.5.

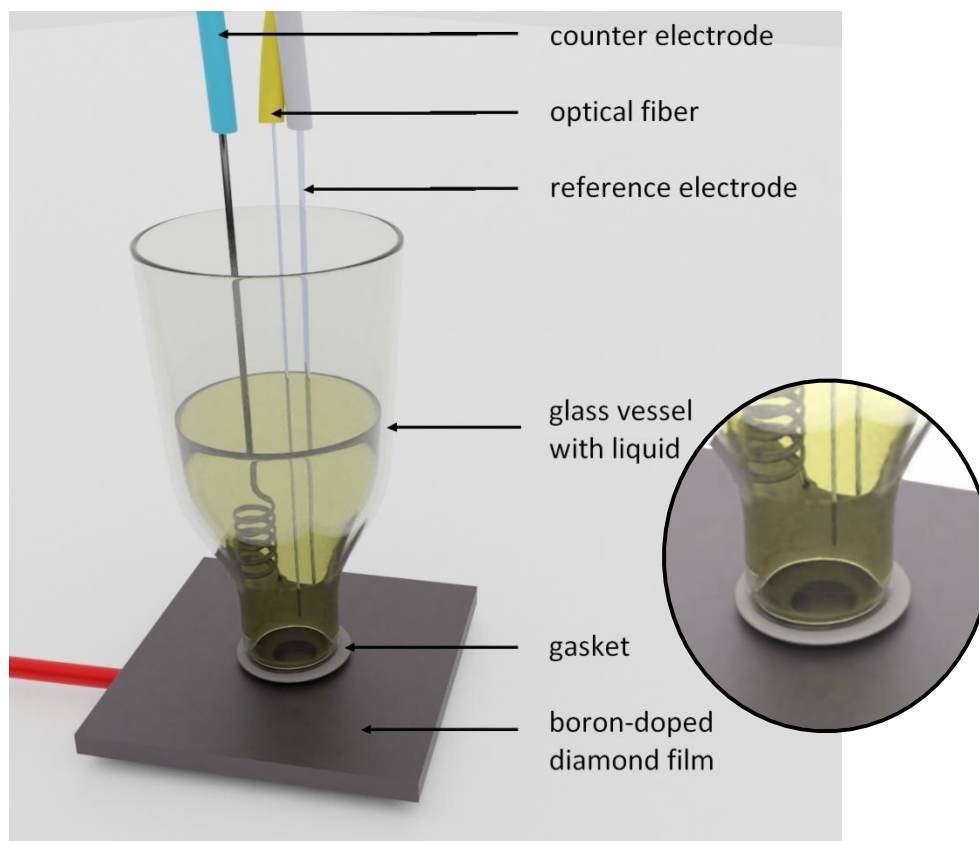


Figure 5.5. Measurement head scheme (not to scale). The counter, reference, and working electrodes are connected (blue, white, red wire, respectively) to the potentiostat-galvanostat, creating the electrochemical part of the measurement head. The optical fiber (yellow wire) is placed together with the electrodes in the glass vessel.

The electrodes and the optical fiber were mounted on the laboratory stand to immobilize them and assure proper placement over the whole experiment: parallelism of the fiber to the BDD surface and contactless arrangement of the electrodes. During the measurement, the length of the Fabry-Perot cavity remained constant, set to obtain the best visibility of the recorded signal.

Optical spectra were recorded during redox reactions by means of cyclic voltammetry (CV) at a scan rate of 10 mV/s using a solution of $2.5 \text{ mM K}_3[\text{Fe}(\text{CN})_6]$ in a $0.5 \text{ M Na}_2\text{SO}_4$. The registered voltammogram is consistent with a literature EC curve – clear oxidation (point A: peak anodic current, $E = 0.247 \text{ V}$, $I = 0.0195 \text{ mA}$) and reduction (point B: peak cathodic current

$E = -0.027 \text{ V}$, $I = -0.0194 \text{ mA}$) peaks correspond to the presence of $\text{Fe}(\text{CN})_6^{3-}$ and $\text{Fe}(\text{CN})_6^{4-}$ ions, respectively. During the electrochemical investigation, the optical signals were registered at starting and ending points (later referred to as before and after EC cycle) of each full CV cycle to assess the state of the sample (Figure 5.6).

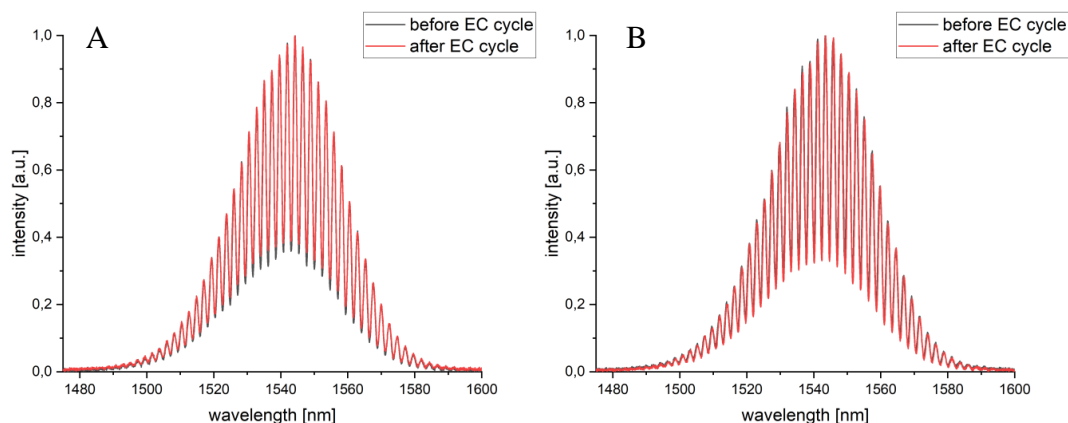


Figure 5.6. Optical spectra were obtained before and after the full electrochemical cycle. Spectra a) and b) show two out of five consecutive voltammetric cycles. Note the excellent overlap for the pairs, and the similarity of spectral pairs to each other across the longitudinal measurements, indicating that no significant perturbation appeared during measurements and the investigated sample was not damaged.

The measured spectra show no additional changes occurrence meaning that the refractive index of the sample did not change during the investigation. As the reversible process was performed, a nearly perfect overlap of signals before and after EC was expected. The results ensure that the sample was not damaged and the process was successful. For reversible reactions, the lowest measurement cost can be as liquid and the working electrode can be used many times, due to continuous quality control. It is not possible for irreversible EC processes where liquid properties change and the electrode surface can be covered with a newly formed chemical compound. In such case, its presence will be detected through the measured refractive index changes.

The achieved goal was to develop a system able to monitor liquid sample state during the electrochemical process by real-time refractive index measurements. It was accomplished through the application of a diamond structure as a linking element, proving the second thesis: application of diamond structures enables construction of optoelectrochemical system for optical investigation of electrochemical processes. Any perturbations in the refractive index value of a liquid can be detected and related to the EC process stage in a non-destructive way. This hybrid



sensor is distinguished from other projects by its quick operation, relatively low cost and simple configuration, robustness as well as the potential for miniaturization to achieve a lab-on-chip device. Such a system can be used in biomedical research or environmental analyzes, e.g. aimed at detecting and determining the level of a given substance in a liquid sample or to control the state of the working electrode/sample.

5.3 The cavity tuning method for protecting the fiber-optic measurement head

Due to the increasing popularity of fiber-optic sensors, researchers seek new materials to improve their performance and tailor their properties to specific needs. With the rapid development of materials science and nanotechnology, it is possible to build more elaborate measurement-head constructions with microstructured end-faces [104,105], embedded nanoparticles [106–109], or films [60,110,111]. One of the most common layers used in fiber-optic sensing is the thin zinc oxide (ZnO) layer. It is an n-type semiconductor known for a wide bandgap (approx. 3.3 eV) and high refractive index (1.929 at 1450 nm) [112,113], greater than that of silica. It assures the fiber-optic sensors measurement range extension because measurements of medium characterized by refractive index close to the refractive index of the fiber core are enabled in presence of a ZnO layer deposited over fiber end-face. The use of ZnO coating also improves the sensitivity of the sensor in comparison to solutions without it. Furthermore, numerous deposition methods (e.g. Atomic Layer Deposition [114], Chemical Vapor Deposition [115], sol-gel synthesis [116], magnetron sputtering [117], among others) are available for ZnO deposition to achieve properties and geometries tailored to given requirements. However, ZnO is susceptible to humidity reducing its sensitivity and stability [118], hence the need to secure it from environmental conditions.

Results of investigation of the nanocrystalline diamond sheet (NDS) playing the role of a ZnO coating protection were presented in the article:

publication [MK5] titled ‘Microscale diamond protection for a ZnO coated fiber-optic sensor’, describes the application of an undoped nanocrystalline diamond sheet as a protective layer for a ZnO-coated fiber-optic measurement head. The author’s contribution includes conceiving, designing and performing the experiments, optical data analysis, selected figures preparation and writing the original manuscript draft.



The measurement setup follows the general configuration of the Fabry-Perot fiber-optic sensor working in a reflective mode presented in detail in Chapter 4. The light source used was a superluminescent diode (SLD-1310-18-W, FiberLabs Inc., Japan) operating at the wavelength of 1310 nm. The measurement head was a fiber-optic end-face with a ZnO layer deposited by ALD and covered by a protective NDS. The procedure of NDS detachment from the substrate and its transfer onto the fiber covered with ZnO was described in Chapter 4. The measurement head can be seen in Figure 5.7.

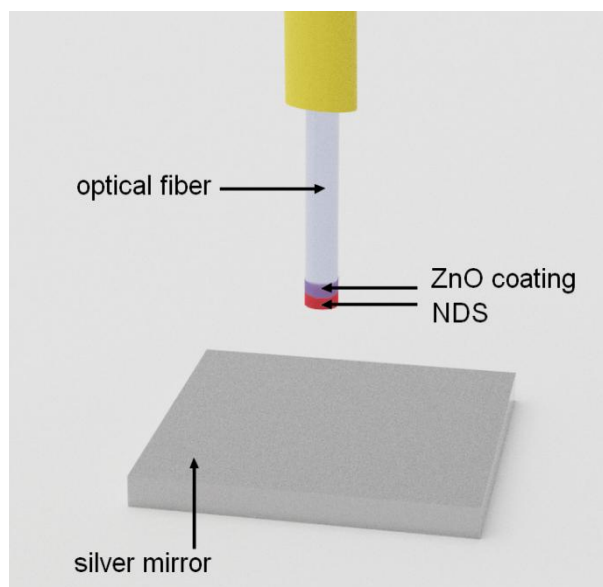


Figure 5.7. Cavity construction utilizing a ZnO coating deposited on the fiber end-face, nanocrystalline diamond sheet and a silver mirror.

The distance measurements were performed to assess the impact of the nanocrystalline diamond sheet on the resulting optical spectra. The series of measurements were carried out by increasing the cavity length up to 500 μm for two configurations: with a bare ZnO layer to obtain a reference, and with an NDS attached over the ZnO to evaluate its influence. An expected signal behavior appeared: the modulation changes with the change of the cavity length. The longer the cavity, the greater the number of maxima in the optical spectrum. The representative spectra for measurement head with bare ZnO and ZnO with NDS are shown in Figure 5.8



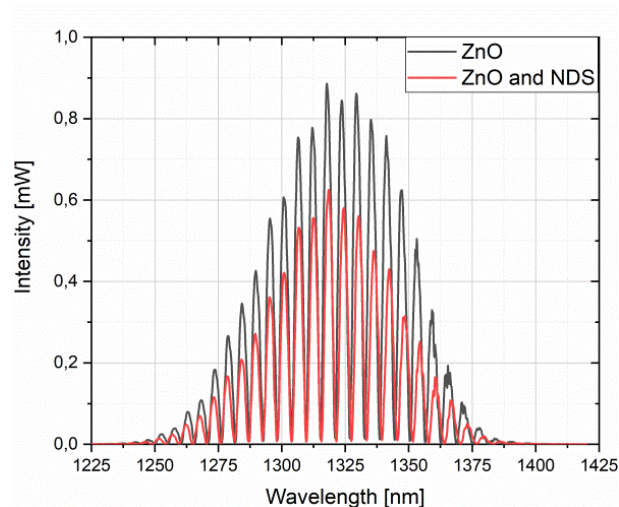


Figure 5.8. Representative signals were obtained for the measurement head with ZnO coating, and ZnO coating and nanocrystalline diamond sheet. The Fabry-Perot cavity length was set $70\ \mu\text{m}$, the light source operated at $1310\ \text{nm}$.

It can be noted that the intensity of the signal decreased by approx. 30% due to the application of the nanocrystalline diamond sheet. However, the spectrum modulation remains the same as the maxima distribution does not change and the perfect overlap is achieved. The visibility values of 0.7616 for bare ZnO and 0.8077 for ZnO and NDS were achieved proving that the sensor operates correctly with the diamond structure in its construction. This shows that the proposed solution can be successfully used in securing fiber end-faces covered with an additional layer. The trade-off between optical power decrease and gaining diamond protection from harsh environmental factors as well as prolonging its lifespan is acceptable. The sensing abilities of the sensor were maintained while introducing additional benefits to the device.

Up to date, only few reports describing nanocrystalline diamond sheets were published, focusing mainly on the growth process, properties characterizations and developing methods of effective sheet release and its transfer to the selected surface [119–121]. Propositions of its applications are rather rare. Bogdanowicz et. al described a comprehensive study of the NDS deposition, characterization of its properties and showed the development of a prototypical, low-temperature diamond-on-graphene transistor [122]. Seshan et al. presented the growth process and described a transfer method of the diamond sheets with the use of a visco-elastic stamp. The NDS sheets were then used in the fabrication of mechanical resonators [123].

The main goal of this study was to investigate the possibility of elaborating a fiber-optic measurement head applying a ZnO coating and the nanocrystalline diamond sheet attached over it as a protection. The addition of the NDS provides a protective layer securing the film from the degrading influence of harsh environmental conditions while maintaining the sensing abilities. Further study on the application of NDS for securing fiber-optic measurement heads in chemically aggressive media is planned.

6. SUMMARY AND CONCLUSIONS

The research in the frame of this dissertation concerned 'Tuning of the finesse coefficient of optoelectronic devices'. The performed literature study presented the significance of optical devices using optical cavities and the constant need for their improvements as well as the research aim and theses of the study. It also covered the current state-of-the-art on tailoring the cavities of the optoelectronic device, with a focus on Fabry-Perot configuration. As the tuning is often achieved by applying new materials, the diamond in optoelectronics and current systems joining the optical and electrochemical methods were reviewed. The next step included a mathematical investigation of the cavities using diamond structures and their comparison with standard silver mirrors. The measurement system for the investigation of the Fabry-Perot cavities applying diamond structures was constructed. Interferometric measurements were performed and the comparison of modeled and measured data was presented. The study ends with a presentation of potential applications of the presented solution: fiber-optic sensors of distance and refractive index, optoelectrochemical system and nanocrystalline diamond sheet protective coating for securing measurement head elements. The full cycle of the research included:

- Design, construction and tuning of cavities using a nitrogen-doped diamond film, boron-doped diamond film, undoped nanocrystalline diamond sheet. Performing measurements with constructed devices to verify and validate their correct operation.
- Devising a method of a nanocrystalline diamond sheet transfer onto the fiber end-face and its successful application as a protective coating.
- Development of a hybrid optoelectrochemical system for optical monitoring of electrochemical reactions with the use of a boron-doped diamond as a linking element.

The dissertation is summed up with the list of all author's achievements reached within this study. The dissertation ends with a list of selected published articles thematically related to the presented research, further plans and bibliography. The full-text scientific papers along with co-authors' contribution statements are included.

The results obtained within the conducted research constitute proof for the following theses:

T1: Finesse coefficient of a Fabry-Perot cavity can be tailored by the use of diamond structures.

Diamond structures impact the finesse coefficient of the cavity, which was concluded in a theoretical and experimental way. To the best of the author's knowledge, such an approach was never described. As the parameters of the diamond materials can be changed during the deposition process, it is a neat solution for obtaining sensors dedicated to a given task. The first thesis was proven.

T2: Application of diamond structures enables construction of optoelectrochemical system for optical investigation of electrochemical processes.

A boron-doped diamond film can play a dual role of a working electrode and a reflective surface is a link between optical and electrochemical subsystems creating a hybrid measurement system for optical monitoring of electrochemical processes. The second thesis was proven.

The prime novelty of the research lies in the application of diamond structures to obtain finesse coefficient-tunable cavities, which also opened new application perspectives. To the best of the author's knowledge, a nanocrystalline diamond sheet was applied for the first time as a securing layer for the exposed single-mode fiber end-face while tailoring the finesse coefficient. The NDS transfer onto the fiber causes signal reduction of around 30% with the introduction of no additional signal modulation. Since the visibility values remain high and the information about the measurand is encoded in the frequency components of the signal, the loss of the intensity is acceptable to gain the protection of the measurement head. Comparable approach, where the NDS was placed on the multi-mode fiber end-face to test the transfer technique resulted in around 40% signal intensity reduction while changing the base signal through introducing additional modulation [123]. Application of boron-doped diamond in the cavity leads to finesse-tailoring to the desired need but also allows robust coupling of the interferometer and electrochemical cell. It is possible due to the properties of the selected material, fulfilling optical and electrochemical requirements for a dual-role operation, and assuring advantages of the optical fiber design. Using telecommunication fibers, immunity to electromagnetic interferences as well as small weight and dimensions of the optical part are achieved, leading to the effective coupling of the sub-systems. The resultant optoelectrochemical system is characterized by a fast response allowing real-time



monitoring and cost-saving configuration with the potential for further miniaturization to develop a lab-on-chip device.

6.1 Author's scientific achievements

The results of this study were published in numerous peer-reviewed renowned journals of international scope. They were also presented during international scientific conferences. Within the PhD studies, the author reached the following scientific achievements:

- 6-months foreign internship at Bar-Ilan University, Faculty of Engineering, and Institute of Nanotechnology and Advanced Materials BINA, Israel, in the frame of InterPhD2 program,
- 6-months foreign internship at Toronto University, Department of Medical Biophysics, and Princess Margaret Cancer Center, Canada, in the frame of Iwanowska Programme awarded by the National Agency for Academic Exchange – NAWA,
- publication of 14 papers, of which 12 were in JCR journals (in 5 as the first author). 5 publications were devoted to proving the theses and their full texts are included in the dissertation (Chapter 8).
- co-submission of 1 patent application,
- co-authoring of 1 granted national patent,
- receiving and working as a principal investigator in 2 research grants: 'Development of a setup for optical and electrochemical measurements' funded by Gdańsk University of Technology and 'Diamond films in optical sensors for monitoring electrochemical reactions' funded by National Agency for Academic Exchange (NAWA) as well as participating as a contractor in 2 research grants 'Low-coherence sensors with active nanodiamond layers' financed by National Science Center and 'Fiber-optic biosensors with metal-oxide ALD coatings' granted by NAWA,
- presentation of the research results during international scientific conferences (2 oral presentations, 7 poster presentations),

- member of the Optical Society of America OSA and the International Society for Optics and Photonics SPIE.

The author's achievements gained within work on this dissertation satisfy the goals set in the introduction:

- Conducting a mathematical investigation of diamond structures' impact on the cavity finesse. Devising a method of a nanocrystalline diamond sheet transfer onto the fiber end-face and its successful application as a protective coating.
- Conceiving, designing and fabricating the fiber-optic Fabry-Perot cavities with diamond structures to tune the finesse coefficient. Measurements for assessing the impact of diamond structures on the cavity properties were performed.
- Development of a diamond protection securing the measurement head end-face of the fiber-optic interferometric sensor.
- Development of a hybrid optoelectrochemical setup for monitoring of electrochemical reactions.

6.2 Planned further research

Further research on extending the study can be directed onto the investigation of wear-resistance improvements of the sensors and their novel applications. Future works can address the following subjects:

- Application of the nanocrystalline diamond sheet on the fiber-optic probe during electrochemical investigations.

As proved within the dissertation, a nanocrystalline diamond sheet can be transferred onto a fiber end-face to assure its protection or secure the layer underneath. Such sensor measuring abilities are maintained while having benefits of the diamond material. This approach can protect a measurement head covered with an additional layer from damaging or clogging by chemicals during electrochemical reactions.



- Investigation of dedicated algorithms and machine learning for data analysis.

The dedicated software for the investigation of the interferometric spectra could increase the amount of information obtained from the measurement data. The approach on machine learning application for predictions based on the interferometric data can further increase the capabilities and usability of the setup. Machine learning allows the development of models able to predict new values based on training datasets (which can be used for increasing the resolution) or to classify the data. This can be a powerful tool added to the biomedical interferometric sensors for preliminary tissue state assessment. A dedicated algorithm would enrich the data and label them as sick or healthy.



7. LIST OF PUBLISHED PAPERS

This chapter includes the list of all papers devoted to proving the formulated theses, and as such, relate the most to the presented research from all author's publications. Each article was shortly described in this section; the full texts are included at the end of the dissertation.

[MK1] Kosowska, M.; Pawłowska, S.; Sankaran, K.J.; Majchrowicz, D.; Haenen, K.; Dholakia, K.; Szczerska, M. Incorporation of Nitrogen in Diamond Films – a New Way of Tuning Parameters for Optical Passive Elements. *Diamond and Related Materials* 2021, 111, 108221, doi:10.1016/j.diamond.2020.108221.

The investigation of the impact of various nitrogen level incorporation in diamond films on an interferometric sensor of displacement is presented. Diamond films with various nitrogen levels (0%, 1%, 3%, 5%) were deposited on silicon substrates by microwave plasma-enhanced chemical vapor deposition. The nitrogen incorporated films were proved to be useful as mirrors as they achieve high visibility of the measurement signal.

[MK2] Kosowska, M.; Majchrowicz, D.; Sankaran, K.J.; Ficek, M.; Haenen, K.; Szczerska, M. Doped Nanocrystalline Diamond Films as Reflective Layers for Fiber-Optic Sensors of Refractive Index of Liquids. *Materials* 2019, 12, 2124, doi:10.3390/ma12132124.

The application of nitrogen-doped diamond film and boron-doped diamond film to tune cavities of interferometric sensors of the refractive index of liquids was presented. The measurements of refractive indices of liquids were carried out in the range of 1.3 to 1.6 for wavelengths 1310 and 1550 nm. A comparison of sensors parameters is provided.

[MK3] Kosowska, M.; Majchrowicz, D.; Ficek, M.; Wierzba, P.; Fleger, Y.; Fixler, D.; Szczerska, M. Nanocrystalline Diamond Sheets as Protective Coatings for Fiber-Optic Measurement Head. *Carbon* 2020, 156, 104–109, doi:10.1016/j.carbon.2019.09.042.

In this paper, the first use of a new nanocrystalline diamond structure in a fiber-optic measurement head as a protective coating of the fiber end-face is described. The sheet modifies cavity parameters while securing it from external damage. It was transferred from the deposition substrate onto the fiber tip. An interferometer for distance measurement comprising that fiber was built. The measurement results were compared with numerical modeling.

[MK4] Kosowska, M.; Jakóbczyk, P.; Rycewicz, M.; Vitkin, A.; Szczerska, M. Low-Coherence Photonic Method of Electrochemical Processes Monitoring. *Sci Rep* 2021, 11, 12600, doi:10.1038/s41598-021-91883-z.

An optoelectrochemical system for simultaneous optical and electrochemical measurements is presented. The combination of fiber-optic Fabry–Perot interferometer with a three-electrode electrochemical setup was possible due to the boron-doped diamond film application as a linking element. The film played the dual role of a mirror and a working electrode. Optical responses during the redox reactions of the electrochemical process are presented. This work proves that simultaneous optoelectrochemical measurements of liquids are possible.

[MK5] Kosowska, M.; Listewnik, P.; Majchrowicz, D.; Rycewicz, M.; Bechelany, M.; Fleger, Y.; Chen, M.; Fixler, D.; Dholakia, K.; Szczerska, M. Microscale Diamond Protection for a ZnO Coated Fiber Optic Sensor. *Sci Rep* 2020, 10, 19141, doi:10.1038/s41598-020-76253-5.

In this paper, the study on securing a sensor structure formed with a Zinc Oxide (ZnO) coating, deposited on the tip of a single-mode fiber, with a nanocrystalline diamond sheet is described. The deposition processes of the materials, the procedure of attaching NDS to the fiber end-face covered with ZnO, and the results of optical measurements are presented.

8. REFERENCES

1. Mikami, H.; Gao, L.; Goda, K. Ultrafast Optical Imaging Technology: Principles and Applications of Emerging Methods. *Nanophotonics* **2016**, *5*, 497–509, doi:10.1515/nanoph-2016-0026.
2. Larimer, C.; Brann, M.R.; Powell, J.D.; Marshall, M.J.; Suter, J.D.; Addleman, R.S. Rapid Nondestructive Measurement of Bacterial Cultures with 3D Interferometric Imaging. *Sci Rep* **2019**, *9*, 8055, doi:10.1038/s41598-019-43839-7.
3. Trivellin, N.; Buffolo, M.; De Santi, C.; Meneghini, M.; Forzan, M.; Dughiero, F.; Zaroni, E.; Meneghesso, G. Full Optical Contactless Thermometry Based on LED Photoluminescence. *IEEE Transactions on Instrumentation and Measurement* **2021**, *70*, 1–8, doi:10.1109/TIM.2020.3013873.
4. Eynaki, H.; Kiani, M.A.; Golmohammadi, H. Nanopaper-Based Screen-Printed Electrodes: A Hybrid Sensing Bioplatfrom for Dual Opto-Electrochemical Sensing Applications. *Nanoscale* **2020**, *12*, 18409–18417, doi:10.1039/D0NR03505J.
5. Alizadeh, N.; Ghoorchian, A. Hybrid Optoelectrochemical Sensor for Superselective Detection of 2,4,6-Trinitrotoluene Based on Electrochemical Reduced Meisenheimer Complex. *Anal. Chem.* **2018**, *90*, 10360–10368, doi:10.1021/acs.analchem.8b02183.
6. Bogdanowicz, R.; Sobaszek, M.; Ficek, M.; Gnyba, M.; Ryl, J.; Siuzdak, K.; Bock, W.J.; Śmietana, M. Opto-Electrochemical Sensing Device Based on Long-Period Grating Coated with Boron-Doped Diamond Thin Film. *Journal of the Optical Society of Korea* **2016**, *19*, 705–710, doi:10.3807/josk.2015.19.6.705.
7. Optical Resonance. In *Principles of Photonics*; Liu, J.-M., Ed.; Cambridge University Press: Cambridge, 2016; pp. 204–223 ISBN 978-1-107-16428-4.
8. Liu, S.; Fu, C.; Liao, C.; Wang, Y.; Wang, Y. High-Robustness Strain Sensor Based on in-Fiber Fabry-Perot Interferometer with an Elliptical Cavity. In Proceedings of the Asia Pacific Optical Sensors Conference (2016), paper W4A.38; Optical Society of America, October 11 2016; p. W4A.38.
9. Palma, P.D.; Natale, D.; Campopiano, S.; Iadicco, A. A Simple Fabry-Perot Pressure Sensor Fabricated on Fiber Optic Tip. In Proceedings of the Sixth European Workshop on Optical Fibre Sensors; SPIE, May 30 2016; Vol. 9916, pp. 138–141.
10. Shiokawa, K.; Otsuka, Y.; Oyama, S.; Nozawa, S.; Satoh, M.; Katoh, Y.; Hamaguchi, Y.; Yamamoto, Y.; Meriwether, J. Development of Low-Cost Sky-Scanning Fabry-Perot Interferometers for Airglow and Auroral Studies. *Earth Planet Sp* **2012**, *64*, 1033–1046, doi:10.5047/eps.2012.05.004.
11. Ben-Ami, S.; López-Morales, M.; Garcia-Mejia, J.; Abad, G.G.; Szentgyorgyi, A. High-Resolution Spectroscopy Using Fabry-Perot Interferometer Arrays: An Application to Searches for O₂ in Exoplanetary Atmospheres. *ApJ* **2018**, *861*, 79, doi:10.3847/1538-4357/aac835.
12. Wang, F.; Liu, Y.; Lu, Y.; Zhang, L.; Ma, J.; Wang, L.; Sun, W. High-Sensitivity Fabry-Perot Interferometer Temperature Sensor Probe Based on Liquid Crystal and the Vernier Effect. *Opt. Lett., OL* **2018**, *43*, 5355–5358, doi:10.1364/OL.43.005355.
13. Bitarafan, M.H.; DeCorby, R.G. On-Chip High-Finesse Fabry-Perot Microcavities for Optical Sensing and Quantum Information. *Sensors* **2017**, *17*, 1748, doi:10.3390/s17081748.
14. Zhu, M.; Wei, H.; Wu, X.; Li, Y. Fabry-Perot Interferometer with Picometer Resolution Referenced to an Optical Frequency Comb. *Optics and Lasers in Engineering* **2015**, *67*, 128–134, doi:10.1016/j.optlaseng.2014.11.010.



15. Ebermann, M.; Neumann, N.; Hiller, K.; Seifert, M.; Meinig, M.; Kurth, S. Tunable MEMS Fabry-Pérot Filters for Infrared Microspectrometers: A Review. In Proceedings of the MOEMS and Miniaturized Systems XV; International Society for Optics and Photonics, March 15 2016; Vol. 9760, p. 97600H.
16. Wang, P.; Chen, W.; Wan, F.; Wang, J.; Hu, J. A Review of Cavity-Enhanced Raman Spectroscopy as a Gas Sensing Method. *Applied Spectroscopy Reviews* **2020**, *55*, 393–417, doi:10.1080/05704928.2019.1661850.
17. Wuttke, C.; Becker, M.; Brückner, S.; Rothhardt, M.; Rauschenbeutel, A. Nanofiber Fabry-Perot Microresonator for Nonlinear Optics and Cavity Quantum Electrodynamics. *Opt. Lett., OL* **2012**, *37*, 1949–1951, doi:10.1364/OL.37.001949.
18. Lather, J.; Bhatt, P.; Thomas, A.; Ebbesen, T.W.; George, J. Cavity Catalysis by Cooperative Vibrational Strong Coupling of Reactant and Solvent Molecules. *Angewandte Chemie International Edition* **2019**, *58*, 10635–10638, doi:10.1002/anie.201905407.
19. Estudillo-Ayala, J.M.; Jauregui-Vazquez, D.; Haus, J.W.; Perez-Maciel, M.; Sierra-Hernandez, J.M.; Avila-Garcia, M.S.; Rojas-Laguna, R.; Lopez-Dieguez, Y.; Hernandez-Garcia, J.C. Multi-Wavelength Fiber Laser Based on a Fiber Fabry-Perot Interferometer. *Appl. Phys. B* **2015**, *121*, 407–412, doi:10.1007/s00340-015-6265-z.
20. Koerner, R.; Oehme, M.; Gollhofer, M.; Schmid, M.; KostECKI, K.; Bechler, S.; Widmann, D.; Kasper, E.; Schulze, J. Electrically Pumped Lasing from Ge Fabry-Perot Resonators on Si. *Opt. Express, OE* **2015**, *23*, 14815–14822, doi:10.1364/OE.23.014815.
21. Zhu, W.; Xu, T.; Wang, H.; Zhang, C.; Deotare, P.B.; Agrawal, A.; Lezec, H.J. Surface Plasmon Polariton Laser Based on a Metallic Trench Fabry-Perot Resonator. *Science Advances* **2017**, *3*, e1700909, doi:10.1126/sciadv.1700909.
22. Kuznetsov, M.; Atia, W.; Johnson, B.; Flanders, D. Compact Ultrafast Reflective Fabry-Perot Tunable Lasers for OCT Imaging Applications. In Proceedings of the Optical Coherence Tomography and Coherence Domain Optical Methods in Biomedicine XIV; International Society for Optics and Photonics, February 22 2010; Vol. 7554, p. 75541F.
23. Masson, J.; St-Gelais, R.; Poulin, A.; Peter, Y.-A. Tunable Fiber Laser Using a MEMS-Based in Plane Fabry-Pérot Filter. *IEEE Journal of Quantum Electronics* **2010**, *46*, 1313–1319, doi:10.1109/JQE.2010.2050299.
24. Jeong, Y.D.; Won, Y.H.; Choi, S.O.; Yoon, J.H. Tunable Single-Mode Fabry-Perot Laser Diode Using a Built-in External Cavity and Its Modulation Characteristics. *Opt. Lett., OL* **2006**, *31*, 2586–2588, doi:10.1364/OL.31.002586.
25. Xu, Z.; Wen, Y.J.; Zhong, W.-D.; Chae, C.-J.; Cheng, X.-F.; Wang, Y.; Lu, C.; Shankar, J. High-Speed WDM-PON Using CW Injection-Locked Fabry-Pérot Laser Diodes. *Opt. Express, OE* **2007**, *15*, 2953–2962, doi:10.1364/OE.15.002953.
26. Lin, Z.; Long, Y.; Zhu, X.; Dai, P.; Liu, F.; Zheng, M.; Zhou, Y.; Duan, H. Extending the Color of Ultra-Thin Gold Films to Blue Region via Fabry-Pérot-Cavity-Resonance-Enhanced Reflection. *Optik* **2019**, *178*, 992–998, doi:10.1016/j.ijleo.2018.09.184.
27. Kim, S.-J.; Choi, H.-K.; Lee, H.; Hong, S.-H. Solution-Processable Nanocrystal-Based Broadband Fabry-Perot Absorber for Reflective Vivid Color Generation. *ACS Appl. Mater. Interfaces* **2019**, *11*, 7280–7287, doi:10.1021/acsami.8b19157.
28. Chen, Y.-H.; Wang, C.-T.; Yu, C.-P.; Lin, T.-H. Polarization Independent Fabry-Pérot Filter Based on Polymer-Stabilized Blue Phase Liquid Crystals with Fast Response Time. *Opt. Express, OE* **2011**, *19*, 25441–25446, doi:10.1364/OE.19.025441.
29. Zhang, W.; Ehteshami, N.; Liu, W.; Yao, J. Silicon-Based on-Chip Electrically Tunable Sidewall Bragg Grating Fabry-Perot Filter. *Opt. Lett., OL* **2015**, *40*, 3153–3156, doi:10.1364/OL.40.003153.

30. Kilgus, J.; Duswald, K.; Langer, G.; Brandstetter, M. Mid-Infrared Standoff Spectroscopy Using a Supercontinuum Laser with Compact Fabry–Pérot Filter Spectrometers. *Appl Spectrosc* **2018**, *72*, 634–642, doi:10.1177/0003702817746696.
31. Lyubopytov, V.S.; Porfirev, A.P.; Gurbatov, S.O.; Paul, S.; Schumann, M.F.; Cesar, J.; Malekizandi, M.; Haidar, M.T.; Wegener, M.; Chipouline, A.; et al. Simultaneous Wavelength and Orbital Angular Momentum Demultiplexing Using Tunable MEMS-Based Fabry-Perot Filter. *Opt Express* **2017**, *25*, 9634–9646, doi:10.1364/OE.25.009634.
32. Egan, P.F.; Stone, J.A.; Hendricks, J.H.; Ricker, J.E.; Scace, G.E.; Strouse, G.F. Performance of a Dual Fabry–Perot Cavity Refractometer. *Opt. Lett., OL* **2015**, *40*, 3945–3948, doi:10.1364/OL.40.003945.
33. Wang, X.; Chen, C.; Pan, L.; Wang, J. A Graphene-Based Fabry–Pérot Spectrometer in Mid-Infrared Region. *Sci Rep* **2016**, *6*, 32616, doi:10.1038/srep32616.
34. Qin, F.; Gao, S.; Wei, G.; Luo, Q.; Mao, C.; Gu, C.; Xu, J.; Li, J. Wideband Circularly Polarized Fabry-Perot Antenna [Antenna Applications Corner]. *IEEE Antennas and Propagation Magazine* **2015**, *57*, 127–135, doi:10.1109/MAP.2015.2470678.
35. Attia, H.; Abdelghani, M.L.; Denidni, T.A. Wideband and High-Gain Millimeter-Wave Antenna Based on FSS Fabry–Perot Cavity. *IEEE Transactions on Antennas and Propagation* **2017**, *65*, 5589–5594, doi:10.1109/TAP.2017.2742550.
36. Çelik, M.; Şahin, E.; Yandayan, T.; Hamid, R.; Akgöz, A.; Özgür, B.; Çetintaş, M.; Demir, A. Application of the Differential Fabry–Perot Interferometer in Angle Metrology. *Meas. Sci. Technol.* **2016**, *27*, 035201, doi:10.1088/0957-0233/27/3/035201.
37. Durand, M.; Lawall, J.; Wang, Y. High-Accuracy Fabry–Perot Displacement Interferometry Using Fiber Lasers. *Meas. Sci. Technol.* **2011**, *22*, 094025, doi:10.1088/0957-0233/22/9/094025.
38. Zhu, M.; Wei, H.; Wu, X.; Li, Y. Fabry–Perot Interferometer with Picometer Resolution Referenced to an Optical Frequency Comb. *Optics and Lasers in Engineering* **2015**, *67*, 128–134, doi:10.1016/j.optlaseng.2014.11.010.
39. Vollmer, F.; Arnold, S. Whispering-Gallery-Mode Biosensing: Label-Free Detection down to Single Molecules. *Nat Methods* **2008**, *5*, 591–596, doi:10.1038/nmeth.1221.
40. Bergstein, D.A.; Ozkumur, E.; Wu, A.C.; Yalçın, A.; Colson, J.R.; Needham, J.W.; Irani, R.J.; Gershoni, J.M.; Goldberg, B.B.; Delisi, C.; et al. Resonant Cavity Imaging: A Means Toward High-Throughput Label-Free Protein Detection. *IEEE J Sel Top Quantum Electron* **2008**, *14*, 131–139, doi:10.1109/JSTQE.2007.913397.
41. Armani, A.M.; Kulkarni, R.P.; Fraser, S.E.; Flagan, R.C.; Vahala, K.J. Label-Free, Single-Molecule Detection with Optical Microcavities. *Science* **2007**, *317*, 783–787, doi:10.1126/science.1145002.
42. Curwen, C.A.; Reno, J.L.; Williams, B.S. Broadband Continuous Single-Mode Tuning of a Short-Cavity Quantum-Cascade VECSEL. *Nat. Photonics* **2019**, *13*, 855–859, doi:10.1038/s41566-019-0518-z.
43. Chen, Y.; Li, C.; Chen, J.-H.; Zheng, Z.; Sun, T.; Grattan, K.T.V.; Xu, F. Demonstration of a Microelectromechanical Tunable Fabry–Pérot Cavity Based on Graphene-Bonded Fiber Devices. *Opt Lett* **2019**, *44*, 1876–1879, doi:10.1364/OL.44.001876.
44. Sikdar, D.; Kornyshev, A.A. An Electro-Tunable Fabry–Perot Interferometer Based on Dual Mirror-on-Mirror Nanoplasmonic Metamaterials. *Nanophotonics* **2019**, *8*, 2279–2290, doi:10.1515/nanoph-2019-0317.
45. Fuscaldo, W.; Tofani, S.; Zografopoulos, D.C.; Baccarelli, P.; Burghignoli, P.; Beccherelli, R.; Galli, A. Tunable Fabry–Perot Cavity THz Antenna Based on Leaky-Wave Propagation in

- Nematic Liquid Crystals. *IEEE Antennas and Wireless Propagation Letters* **2017**, *16*, 2046–2049, doi:10.1109/LAWP.2017.2695324.
46. Ding, T. Controllable Tuning of Fabry–Perot Cavities via Laser Printing. *Journal of Materials Chemistry C* **2020**, *8*, 10825–10830, doi:10.1039/D0TC01662D.
 47. Braakman, R.; Blake, G.A. Principles and Promise of Fabry–Perot Resonators at Terahertz Frequencies. *Journal of Applied Physics* **2011**, *109*, 063102, doi:10.1063/1.3560771.
 48. Alligood DePrince, B.; Rocher, B.E.; Carroll, A.M.; Widicus Weaver, S.L. Extending High-Finesse Cavity Techniques to the Far-Infrared. *Review of Scientific Instruments* **2013**, *84*, 075107, doi:10.1063/1.4813274.
 49. Mitra, A.; Harutyunyan, H.; Palomba, S.; Novotny, L. Tuning the Cavity Modes of a Fabry–Perot Resonator Using Gold Nanoparticles. *Opt. Lett., OL* **2010**, *35*, 953–955, doi:10.1364/OL.35.000953.
 50. Hirsch, M.; Wierzba, P.; Jędrzejewska-Szczerska, M. Tuning Transfer Function of Fiber-Optic Fabry–Pérot Interferometer via Introduction of Birefringence in the Cavity. *Optica Applicata* **2019**, Vol. 49, doi:10.5277/oa190205.
 51. Isaacs, S.; Placido, F.; Abdulhalim, I. Investigation of Liquid Crystal Fabry–Perot Tunable Filters: Design, Fabrication, and Polarization Independence. *Appl. Opt., AO* **2014**, *53*, H91–H101, doi:10.1364/AO.53.000H91.
 52. Williams, R.J.; Kitzler, O.; Bai, Z.; Sarang, S.; Jasbeer, H.; McKay, A.; Antipov, S.; Sabella, A.; Lux, O.; Spence, D.J.; et al. High Power Diamond Raman Lasers. *IEEE Journal of Selected Topics in Quantum Electronics* **2018**, *24*, 1–14, doi:10.1109/JSTQE.2018.2827658.
 53. Rodionov, N.B.; Pal', A.F.; Bol'shakov, A.P.; Ral'chenko, V.G.; Khmel'nitskiy, R.A.; Dravin, V.A.; Malykhin, S.A.; Altukhov, I.V.; Kagan, M.S.; Paprotskiy, S.K. Diamond Diode Structures Based on Homoepitaxial Films. *J. Commun. Technol. Electron.* **2018**, *63*, 828–834, doi:10.1134/S1064226918070148.
 54. Angelone, M.; Aielli, G.; Almaviva, S.; Cardarelli, R.; Lattanzi, D.; Marinelli, M.; Milani, E.; Prestopino, G.; Pillon, M.; Santonico, R.; et al. Neutron Detectors Based Upon Artificial Single Crystal Diamond. *IEEE Transactions on Nuclear Science* **2009**, *56*, 2275–2279, doi:10.1109/TNS.2009.2025177.
 55. Kleimeier, N.F.; Haarlammert, T.; Witte, H.; Schühle, U.; Hochedez, J.-F.; BenMoussa, A.; Zacharias, H. Autocorrelation and Phase Retrieval in the UV Using Two-Photon Absorption in Diamond Pin Photodiodes. *Opt. Express, OE* **2010**, *18*, 6945–6956, doi:10.1364/OE.18.006945.
 56. Bae, H.; Giri, A.; Kolawole, O.; Azimi, A.; Jackson, A.; Harris, G. Miniature Diamond-Based Fiber Optic Pressure Sensor with Dual Polymer–Ceramic Adhesives. *Sensors (Basel)* **2019**, *19*, doi:10.3390/s19092202.
 57. Dang, C.; Chou, J.-P.; Dai, B.; Chou, C.-T.; Yang, Y.; Fan, R.; Lin, W.; Meng, F.; Hu, A.; Zhu, J.; et al. Achieving Large Uniform Tensile Elasticity in Microfabricated Diamond. *Science* **2021**, *371*, 76–78, doi:10.1126/science.abc4174.
 58. Nazempour, R.; Zhang, Q.; Fu, R.; Sheng, X. Biocompatible and Implantable Optical Fibers and Waveguides for Biomedicine. *Materials (Basel)* **2018**, *11*, 1283, doi:10.3390/ma11081283.
 59. Henderson, P.J. Advanced Materials and Techniques for Fibre-Optic Sensing. *IOP Conf. Ser.: Mater. Sci. Eng.* **2014**, *60*, 012072, doi:10.1088/1757-899X/60/1/012072.
 60. Jędrzejewska-Szczerska, M.; Majchrowicz, D.; Hirsch, M.; Struk, P.; Bogdanowicz, R.; Bechelany, M.; Tuchin, V.V. Chapter 14 - Nanolayers in Fiber-Optic Biosensing. In *Nanotechnology and Biosensors*; Nikolelis, D.P., Nikoleli, G.-P., Eds.; Advanced Nanomaterials; Elsevier, 2018; pp. 395–426 ISBN 978-0-12-813855-7.



61. Bogdanowicz, R. Characterization of Optical and Electrical Properties of Transparent Conductive Boron-Doped Diamond thin Films Grown on Fused Silica. *Metrology and Measurement Systems* **2014**, *21*, 685–698, doi:10.2478/mms-2014-0059.
62. Cheng, H.-Y.; Yang, C.-Y.; Yang, L.-C.; Peng, K.-C.; Chia, C.-T.; Liu, S.-J.; Lin, I.-N.; Lin, K.-H. Effective Thermal and Mechanical Properties of Polycrystalline Diamond Films. *Journal of Applied Physics* **2018**, *123*, 165105, doi:10.1063/1.5016919.
63. Gracio, J.J.; Fan, Q.H.; Madaleno, J.C. Diamond Growth by Chemical Vapour Deposition. *J. Phys. D: Appl. Phys.* **2010**, *43*, 374017, doi:10.1088/0022-3727/43/37/374017.
64. Giustino, F.; Louie, S.G.; Cohen, M.L. Electron-Phonon Renormalization of the Direct Band Gap of Diamond. *Phys. Rev. Lett.* **2010**, *105*, 265501, doi:10.1103/PhysRevLett.105.265501.
65. Tang, H.; Wang, M.; He, D.; Zou, Q.; Ke, Y.; Zhao, Y. Synthesis of Nano-Polycrystalline Diamond in Proximity to Industrial Conditions. *Carbon* **2016**, *108*, 1–6, doi:10.1016/j.carbon.2016.07.004.
66. Hébert, C.; Scorsone, E.; Mermoux, M.; Bergonzo, P. Porous Diamond with High Electrochemical Performance. *Carbon* **2015**, *90*, 102–109, doi:10.1016/j.carbon.2015.04.016.
67. Bogdanowicz, R.; Ficek, M.; Malinowska, N.; Gupta, S.; Meek, R.; Niedziałkowski, P.; Ryciewicz, M.; Sawczak, M.; Ryl, J.; Ossowski, T. Electrochemical Performance of Thin Free-Standing Boron-Doped Diamond Nanosheet Electrodes. *Journal of Electroanalytical Chemistry* **2020**, *862*, 114016, doi:10.1016/j.jelechem.2020.114016.
68. Jacobson, P.; Stoupin, S. Thermal Expansion Coefficient of Diamond in a Wide Temperature Range. *Diamond and Related Materials* **2019**, *97*, 107469, doi:10.1016/j.diamond.2019.107469.
69. Zkria, A.; Abdel-Wahab, F.; Katamune, Y.; Yoshitake, T. Optical and Structural Characterization of Ultrananocrystalline Diamond/Hydrogenated Amorphous Carbon Composite Films Deposited via Coaxial Arc Plasma. *Current Applied Physics* **2019**, *19*, 143–148, doi:10.1016/j.cap.2018.11.012.
70. Yang, K.-H.; Narayan, R.J. Biocompatibility and Functionalization of Diamond for Neural Applications. *Current Opinion in Biomedical Engineering* **2019**, *10*, 60–68, doi:10.1016/j.cobme.2019.03.002.
71. Zhang, Q.; Liu, Y.; Chen, S.; Quan, X.; Yu, H. Nitrogen-Doped Diamond Electrode Shows High Performance for Electrochemical Reduction of Nitrobenzene. *Journal of Hazardous Materials* **2014**, *265*, 185–190, doi:10.1016/j.jhazmat.2013.11.065.
72. Deshmukh, S.; Sankaran, K.J.; Korneychuk, S.; Verbeeck, J.; Mclaughlin, J.; Haenen, K.; Roy, S.S. Nanostructured Nitrogen Doped Diamond for the Detection of Toxic Metal Ions. *Electrochimica Acta* **2018**, *283*, 1871–1878, doi:10.1016/j.electacta.2018.07.067.
73. Raina, S.; Kang, W.P.; Davidson, J.L. Nitrogen Incorporated Nanodiamond Film with ‘Ridge’ Surface Morphology for Detection of Bio-Analyte. *Diamond and Related Materials* **2009**, *18*, 574–577, doi:10.1016/j.diamond.2008.11.016.
74. Raina, S.; Kang, W.P.; Davidson, J.L. Optimizing Nitrogen Incorporation in Nanodiamond Film for Bio-Analyte Sensing. *Diamond and Related Materials* **2009**, *18*, 718–721, doi:10.1016/j.diamond.2009.02.030.
75. Raina, S.; Kang, W.P.; Davidson, J.L. Fabrication of Nitrogen-Incorporated Nanodiamond Ultra-Microelectrode Array for Dopamine Detection. *Diamond and Related Materials* **2010**, *19*, 256–259, doi:10.1016/j.diamond.2009.10.013.
76. Shalini, J.; Sankaran, K.J.; Dong, C.-L.; Lee, C.-Y.; Tai, N.-H.; Lin, I.-N. In Situ Detection of Dopamine Using Nitrogen Incorporated Diamond Nanowire Electrode. *Nanoscale* **2013**, *5*, 1159–1167, doi:10.1039/c2nr32939e.



77. Zhou, Y.; Zhi, J. The Application of Boron-Doped Diamond Electrodes in Amperometric Biosensors. *Talanta* **2009**, *79*, 1189–1196, doi:10.1016/j.talanta.2009.05.026.
78. Niedziałkowski, P.; Bogdanowicz, R.; Zięba, P.; Wysocka, J.; Ryl, J.; Sobaszek, M.; Ossowski, T. Melamine-Modified Boron-Doped Diamond towards Enhanced Detection of Adenine, Guanine and Caffeine. *Electroanalysis* **2016**, *28*, 211–221, doi:https://doi.org/10.1002/elan.201500528.
79. Feier, B.; Gui, A.; Cristea, C.; Săndulescu, R. Electrochemical Determination of Cephalosporins Using a Bare Boron-Doped Diamond Electrode. *Anal Chim Acta* **2017**, *976*, 25–34, doi:10.1016/j.aca.2017.04.050.
80. Suzuki, A.; Ivandini, T.A.; Yoshimi, K.; Fujishima, A.; Oyama, G.; Nakazato, T.; Hattori, N.; Kitazawa, S.; Einaga, Y. Fabrication, Characterization, and Application of Boron-Doped Diamond Microelectrodes for in Vivo Dopamine Detection. *Anal. Chem.* **2007**, *79*, 8608–8615, doi:10.1021/ac071519h.
81. Zhao, W.; Xu, J.-J.; Qiu, Q.-Q.; Chen, H.-Y. Nanocrystalline Diamond Modified Gold Electrode for Glucose Biosensing. *Biosensors and Bioelectronics* **2006**, *22*, 649–655, doi:10.1016/j.bios.2006.01.026.
82. Panizza, M.; Cerisola, G. Application of Diamond Electrodes to Electrochemical Processes. *Electrochimica Acta* **2005**, *51*, 191–199, doi:10.1016/j.electacta.2005.04.023.
83. Bai, H.; He, P.; Pan, J.; Chen, J.; Chen, Y.; Dong, F.; Li, H. Boron-Doped Diamond Electrode: Preparation, Characterization and Application for Electrocatalytic Degradation of m-Dinitrobenzene. *Journal of Colloid and Interface Science* **2017**, *497*, 422–428, doi:10.1016/j.jcis.2017.03.017.
84. Montanaro, D.; Lavecchia, R.; Petrucci, E.; Zuorro, A. UV-Assisted Electrochemical Degradation of Coumarin on Boron-Doped Diamond Electrodes. *Chemical Engineering Journal* **2017**, *323*, 512–519, doi:10.1016/j.cej.2017.04.129.
85. Švorc, L.; Rievaj, M.; Bustin, D. Green Electrochemical Sensor for Environmental Monitoring of Pesticides: Determination of Atrazine in River Waters Using a Boron-Doped Diamond Electrode. *Sensors and Actuators B: Chemical* **2013**, *181*, 294–300, doi:10.1016/j.snb.2013.02.036.
86. Lamberti, F.; Brigo, L.; Favaro, M.; Luni, C.; Zoso, A.; Cattelan, M.; Agnoli, S.; Brusatin, G.; Granozzi, G.; Giomo, M.; et al. Optoelectrochemical Biorecognition by Optically Transparent Highly Conductive Graphene-Modified Fluorine-Doped Tin Oxide Substrates. *ACS Appl. Mater. Interfaces* **2014**, *6*, 22769–22777, doi:10.1021/am506941u.
87. Narakathu, B.B.; Reddy, A.S.G.; Eshkeiti, A.; Bazuin, B.J.; Atashbar, M.Z. Opto-Electrochemical Based Dual Detection of Heavy Metal Compounds Using a Novel Flow Cell. In Proceedings of the 2013 IEEE SENSORS; IEEE: Baltimore, MD, USA, November 2013; pp. 1–4.
88. Liu, W.; Li, M.; Luo, Z.; Jin, G. Using Electrochemistry - Total Internal Reflection Ellipsometry Technique to Observe the Dissolved Oxygen Reduction on Clark Electrode. *Electrochimica Acta* **2014**, *142*, 371–377, doi:10.1016/j.electacta.2014.07.114.
89. Cobet, C.; Oppelt, K.; Hingerl, K.; Neugebauer, H.; Knör, G.; Sariciftci, N.S.; Gasiorowski, J. Ellipsometric Spectroelectrochemistry: An in Situ Insight in the Doping of Conjugated Polymers. *J. Phys. Chem. C* **2018**, *122*, 24309–24320, doi:10.1021/acs.jpcc.8b08602.
90. Sobaszek, M.; Strąkowski, M.; Skowroński, Ł.; Siuzdak, K.; Sawczak, M.; Własny, I.; Wyszomółek, A.; Wieloszyńska, A.; Pluciński, J.; Bogdanowicz, R. In-Situ Monitoring of Electropolymerization Processes at Boron-Doped Diamond Electrodes by Mach-Zehnder Interferometer. *Sensors and Actuators B: Chemical* **2020**, *304*, 127315, doi:10.1016/j.snb.2019.127315.

91. Janczuk-Richter, M.; Piestrzyńska, M.; Burnat, D.; Sezemský, P.; Stranak, V.; Bock, W.; Bogdanowicz, R.; Niedziółka-Jönsson, J.; Smietana, M. Optical Investigations of Electrochemical Processes Using a Long-Period Fiber Grating Functionalized by Indium Tin Oxide. *Sensors and Actuators B Chemical* **2018**, *279*, 223–229, doi:10.1016/j.snb.2018.10.001.
92. Janczuk-Richter, M.; Piestrzyńska, M.; Burnat, D.; Szot-Karpińska, K.; Sezemsky, P.; Stranak, V.; Bock, W.J.; Bogdanowicz, R.; Niedziółka-Jönsson, J.; Śmietana, M. Optical Monitoring of Electrochemical Processes with ITO-Coated Long-Period Fiber Grating. In Proceedings of the 26th International Conference on Optical Fiber Sensors; OSA: Lausanne, 2018; p. ThE54.
93. Dolan, P.R.; Hughes, G.M.; Grazioso, F.; Patton, B.R.; Smith, J.M. Femtoliter Tunable Optical Cavity Arrays. *Opt Lett* **2010**, *35*, 3556–3558, doi:10.1364/OL.35.003556.
94. Hunger, D.; Steinmetz, T.; Colombe, Y.; Deutsch, C.; Hänsch, T.W.; Reichel, J. A Fiber Fabry–Perot Cavity with High Finesse. *New J. Phys.* **2010**, *12*, 065038, doi:10.1088/1367-2630/12/6/065038.
95. Muller, A.; Flagg, E.B.; Lawall, J.R.; Solomon, G.S. Ultrahigh-Finesse, Low-Mode-Volume Fabry-Perot Microcavity. *Opt Lett* **2010**, *35*, 2293–2295, doi:10.1364/OL.35.002293.
96. Flores, R.; Janeiro, R.; Viegas, J. Optical Fibre Fabry-Pérot Interferometer Based on Inline Microcavities for Salinity and Temperature Sensing. *Sci Rep* **2019**, *9*, 9556, doi:10.1038/s41598-019-45909-2.
97. Born, M. *Principles of Optics: Electromagnetic Theory of Propagation, Interference and Diffraction of Light*; 7th edition.; Cambridge University Press: Cambridge ; New York, 1999; ISBN 978-0-521-64222-4.
98. Pedrotti, F.L. *Introduction to Optics*; 3rd edition.; Cambridge University Press: Cambridge, 2017; ISBN 978-1-108-42826-2.
99. Santos, J.L.; Leite, A.P.; Jackson, D.A. Optical Fiber Sensing with a Low-Finesse Fabry–Perot Cavity. *Appl. Opt., AO* **1992**, *31*, 7361–7366, doi:10.1364/AO.31.007361.
100. Lodes, M.A.; Kachold, F.S.; Rosiwal, S.M. Mechanical Properties of Micro- and Nanocrystalline Diamond Foils. *Philosophical Transactions of the Royal Society A: Mathematical, Physical and Engineering Sciences* **2015**, *373*, 20140136, doi:10.1098/rsta.2014.0136.
101. Engenhorst, M.; Fecher, J.; Notthoff, C.; Schierning, G.; Schmechel, R.; Rosiwal, S.M. Thermoelectric Transport Properties of Boron-Doped Nanocrystalline Diamond Foils. *Carbon* **2015**, *81*, 650–662, doi:10.1016/j.carbon.2014.10.002.
102. Kato, H.; Nagatomo, H.; Nakai, M.; Sakaiya, T.; Terasaki, H.; Kondo, T.; Hironaka, Y.; Shimizu, K.; Shigemori, K. Surface Structure on Diamond Foils Generated by Spatially Nonuniform Laser Irradiation. *Sci Rep* **2020**, *10*, 9017, doi:10.1038/s41598-020-66036-3.
103. Kamińska, A.M.; Ficek, M.; Bogdanowicz, R.; Pluciński, J. Studies of Free-Standing Boron-Doped Diamond Sheets Using Optical Coherence Tomography. In Proceedings of the Biophotonics Congress: Biomedical Optics 2020 (Translational, Microscopy, OCT, OTS, BRAIN) (2020), paper JTU3A.22; Optical Society of America, April 20 2020; p. JTU3A.22.
104. Kostovski, G.; Stoddart, P.R.; Mitchell, A. The Optical Fiber Tip: An Inherently Light-Coupled Microscopic Platform for Micro- and Nanotechnologies. *Adv Mater* **2014**, *26*, 3798–3820, doi:10.1002/adma.201304605.
105. Ran, Z.; He, X.; Rao, Y.; Sun, D.; Qin, X.; Zeng, D.; Chu, W.; Li, X.; Wei, Y. Fiber-Optic Microstructure Sensors: A Review. *Photonic Sens* **2021**, *11*, 227–261, doi:10.1007/s13320-021-0632-7.

106. Zhang, L.; Tang, Y.; Tong, L. Micro-/Nanofiber Optics: Merging Photonics and Material Science on Nanoscale for Advanced Sensing Technology. *iScience* **2020**, *23*, 100810, doi:10.1016/j.isci.2019.100810.
107. Urrutia, A.; Goicoechea, J.; Arregui, F.J. Optical Fiber Sensors Based on Nanoparticle-Embedded Coatings. *Journal of Sensors* **2015**, *2015*, e805053, doi:10.1155/2015/805053.
108. Luo, J.; Yao, J.; Lu, Y.; Ma, W.; Zhuang, X. A Silver Nanoparticle-Modified Evanescent Field Optical Fiber Sensor for Methylene Blue Detection. *Sensors* **2013**, *13*, 3986–3997, doi:10.3390/s130303986.
109. Rithesh Raj, D.; Prasanth, S.; Vineeshkumar, T.V.; Sudarsanakumar, C. Surface Plasmon Resonance Based Fiber Optic Sensor for Mercury Detection Using Gold Nanoparticles PVA Hybrid. *Optics Communications* **2016**, *367*, 102–107, doi:10.1016/j.optcom.2016.01.027.
110. Yang, M.; Peng, J.; Wang, G.; Dai, J. Fiber Optic Sensors Based on Nano-Films. In *Fiber Optic Sensors: Current Status and Future Possibilities*; Matias, I.R., Ikezawa, S., Corres, J., Eds.; Smart Sensors, Measurement and Instrumentation; Springer International Publishing: Cham, 2017; pp. 1–30 ISBN 978-3-319-42625-9.
111. Wang, Q.; Zhao, W.-M. A Comprehensive Review of Lossy Mode Resonance-Based Fiber Optic Sensors. *Optics and Lasers in Engineering* **2018**, *100*, 47–60, doi:10.1016/j.optlaseng.2017.07.009.
112. Azad, S.; Sadeghi, E.; Parvizi, R.; Mazaheri, A. Fast Response Relative Humidity Clad-Modified Multimode Optical Fiber Sensor with Hydrothermally Dimension Controlled ZnO Nanorods. *Materials Science in Semiconductor Processing* **2017**, *66*, 200–206, doi:10.1016/j.mssp.2017.04.024.
113. Coelho, L.; Viegas, D.; Santos, J.L.; de Almeida, J.M.M.M. Characterization of Zinc Oxide Coated Optical Fiber Long Period Gratings with Improved Refractive Index Sensing Properties. *Sensors and Actuators B: Chemical* **2016**, *223*, 45–51, doi:10.1016/j.snb.2015.09.061.
114. Tynell, T.; Karppinen, M. Atomic Layer Deposition of ZnO: A Review. *Semicond. Sci. Technol.* **2014**, *29*, 043001, doi:10.1088/0268-1242/29/4/043001.
115. Chen, Z.; Shum, K.; Salagaj, T.; Zhang, W.; Strobl, K. ZnO Thin Films Synthesized by Chemical Vapor Deposition. In Proceedings of the 2010 IEEE Long Island Systems, Applications and Technology Conference; May 2010; pp. 1–6.
116. Znaidi, L. Sol–Gel-Deposited ZnO Thin Films: A Review. *Materials Science and Engineering: B* **2010**, *174*, 18–30, doi:10.1016/j.mseb.2010.07.001.
117. Zhang, Z.; Bao, C.; Yao, W.; Ma, S.; Zhang, L.; Hou, S. Influence of Deposition Temperature on the Crystallinity of Al-Doped ZnO Thin Films at Glass Substrates Prepared by RF Magnetron Sputtering Method. *Superlattices and Microstructures* **2011**, *49*, 644–653, doi:10.1016/j.spmi.2011.04.002.
118. Postica, V.; Lupan, O.; Gapeeva, A.; Hansen, L.; Khaledialidusti, R.; Mishra, A.K.; Drewes, J.; Kersten, H.; Faupel, F.; Adelung, R.; et al. Improved Long-Term Stability and Reduced Humidity Effect in Gas Sensing: SiO₂ Ultra-Thin Layered ZnO Columnar Films. *Advanced Materials Technologies* **2021**, *6*, 2001137, doi:10.1002/admt.202001137.
119. Behroudj, A.; Strehle, S. Transfer of Nanocrystalline Diamond Films Grown by Chemical Vapor Deposition for Sensors and Other Applications. In Proceedings of the Micro-Nano-Integration; 6. GMM-Workshop; October 2016; pp. 1–4.
120. Lodes, M.A.; Kachold, F.S.; Rosiwal, S.M. Mechanical Properties of Micro- and Nanocrystalline Diamond Foils. *Philosophical Transactions of the Royal Society A: Mathematical, Physical and Engineering Sciences* **2015**, *373*, 20140136, doi:10.1098/rsta.2014.0136.

121. Engenhorst, M.; Fecher, J.; Notthoff, C.; Schierning, G.; Schmechel, R.; Rosiwal, S.M. Thermoelectric Transport Properties of Boron-Doped Nanocrystalline Diamond Foils. *Carbon* **2015**, *81*, 650–662, doi:10.1016/j.carbon.2014.10.002.
122. Bogdanowicz, R.; Ficek, M.; Sobaszek, M.; Nosek, A.; Gołuński, Ł.; Karczewski, J.; Jaramillo-Botero, A.; Goddard, W.A.; Bockrath, M.; Ossowski, T. Growth and Isolation of Large Area Boron-Doped Nanocrystalline Diamond Sheets: A Route toward Diamond-on-Graphene Heterojunction. *Advanced Functional Materials* **2019**, *29*, 1805242, doi:10.1002/adfm.201805242.
123. Seshan, V.; Island, J.O.; Leeuwen, R. van; Venstra, W.J.; Schneider, B.H.; Janssens, S.D.; Haenen, K.; Sudhölter, E.J.R.; Smet, L.C.P.M. de; Zant, H.S.J. van der; et al. Pick-up and Drop Transfer of Diamond Nanosheets. *Nanotechnology* **2015**, *26*, 125706, doi:10.1088/0957-4484/26/12/125706.



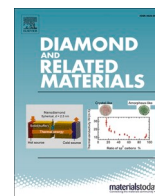
[MK1] Incorporation of Nitrogen in Diamond Films – a New Way of Tuning Parameters for Optical Passive Elements.

Kosowska, M.; Pawłowska, S.; Sankaran, K.J.; Majchrowicz, D.; Haenen, K.; Dholakia, K.;
Szczerska, M.

Diamond and Related Materials 2021, 111, 108221, doi:10.1016/j.diamond.2020.108221.

The author's contributions were:

conceptualization, methodology, analysis of optical data and writing selected parts of an original manuscript.



Incorporation of nitrogen in diamond films – A new way of tuning parameters for optical passive elements

Monika Kosowska^{a,*}, Sandra Pawłowska^a, Kamatchi J. Sankaran^b, Daria Majchrowicz^{a,c,*}, Ken Haenen^{d,e}, Kishan Dholakia^c, Małgorzata Szczerska^{a,**}

^a Department of Metrology and Optoelectronics, Faculty of Electronics, Telecommunications and Informatics, Gdańsk University of Technology, 11/12 Narutowicza Street, 80-233 Gdańsk, Poland

^b CSIR-Institute of Minerals and Materials Technology, Bhubaneswar 751013, India

^c SUPA, School of Physics and Astronomy, University of St Andrews, North Haugh, St Andrews KY16 9SS, United Kingdom

^d Institute for Materials Research (IMO), Hasselt University, B-3590 Diepenbeek, Belgium

^e IOMEC, IMEC vzw, B-3590 Diepenbeek, Belgium

ARTICLE INFO

Keywords:

Nitrogen incorporated diamond
Nitrogen doping
Diamond film
Diamond passive optical element
Optoelectronics
Fiber-optic

ABSTRACT

This paper investigates the impact of nitrogen incorporation in diamond films for the construction of an interferometric sensor to measure displacement. Diamond films with different nitrogen levels (0–5%) were deposited on silicon substrates by microwave plasma enhanced chemical vapor deposition. The structural characteristics of these samples are characterized using scanning electron microscopy (SEM), atomic force microscopy (AFM), confocal micro-Raman spectroscopy, and electron energy loss spectroscopy (EELS). The homogeneous and continuous surface morphology of the films is observed through SEM. In the micro-Raman and electron energy loss spectroscopy studies, it is evident that there is a formation of sp^2 -bonded carbon phases due to the increase in the concentration of nitrogen. This investigation gives a strong basis for utilizing these diamond films as reflective layers in fiber-optic devices. The interferometric measurement setup is constructed as a Fabry-Pérot interferometer. The nitrogen incorporated films are proved to be useful as mirrors as they achieve a measurement signal with high contrast. The achieved visibility values for the investigated samples are higher than 94% in the range of 40–100 μm .

1. Introduction

Fiber-optic sensors belong to the most popular technologies we have today. They can be found in many industries such as the automotive, aviation and maritime, and energy industries [1,2] and may be used for medical purposes. They have many advantages, that include: high measurement sensitivity [3]; they are easy to install in hard-to-reach places [4] and have low weight and size [5]. Fiber-optic sensors enable measurements of physical and chemical values, such as temperature [6], refractive index [7], pressure [8] and displacement [9]. Research on the prospects of using optical fibers is still ongoing and the use of new materials in the construction of such sensors may lead to further advantages.

The development of nanotechnology and deposition techniques (e.g.

chemical vapor deposition, atomic layer deposition) has opened up new possibilities in the use of thin films to build unique optoelectronic and electronic components with parameters that are virtually impossible to obtain as a result of using other materials. One such material is a diamond film. Parameters of the resulting film can be tailored during the deposition process to match the requirements of the planned application [10,11].

Nanocrystalline diamond has found a number of key applications. This is due to its optical [12], mechanical and thermal [13], and chemical [14] properties. It is particularly valued as an abrasive layer [15], is chemically inert, and has a high refractive index for optical dielectric material [16]. Nanocrystalline diamond structures are used in electronics and optoelectronics for the construction of high-frequency electronic components [17] as well as building membranes [18]. The

* Corresponding authors.

** Correspondence to: M. Szczerska, Department of Metrology and Optoelectronics, Faculty of Electronics, Telecommunications and Informatics, Gdańsk University of Technology, 11/12 Narutowicza Street, 80-233 Gdańsk, Poland.

E-mail addresses: monkosow@student.pg.edu.pl (M. Kosowska), darmajch@pg.edu.pl (D. Majchrowicz), malszcze@pg.edu.pl (M. Szczerska).

<https://doi.org/10.1016/j.diamond.2020.108221>

Received 4 August 2020; Received in revised form 3 December 2020; Accepted 3 December 2020

Available online 11 December 2020

0925-9635/© 2020 Elsevier B.V. All rights reserved.

high-quality synthetic diamond crystals are used for laser manufacturing [19].

Their use in the field of interferometry has opened up many developments for new fiber-optic sensor designs, namely fiber-optic Bragg sensors [20] and fiber-optic interferometric sensors, where diamond plays the role of protective [21] or reflective layers [22,23]. As diamond films have satisfying optical properties, they are also chemically stable and resistant to mechanical damage making them superior to standard silver mirrors. Moreover, diamond films enable the measurements of biological materials because of their well-known biocompatibility. There is no risk of poisoning the test organism, and the biological samples do not damage the diamond structure. Undoped diamond is transparent in the broad range of wavelengths, but proper doping transforms the structure into a reflective layer. Our previous research on diamond films doped with boron proved that doping changes the behavior of the diamond in terms of transparency [7,24].

On the other hand, nitrogen is known to be a good source for doping in diamond films. Nitrogen incorporated diamond films have found interest in the field of optical applications including photovoltaic solar cells [24] or biosensors [25]. A number of experimental studies have been carried out to accomplish effective changes in the properties of diamond films by adding nitrogen in the plasma during film deposition. In the work on nitrogen dopant in nanocrystalline diamond (NCD) films, it is discovered that the addition of an appropriate amount of nitrogen can increase the sp^2 bonding structure in NCD films, avert clustering on the diamond surface, endorse the smoothness of diamond surface, and efficiently raise the conductivity, thus making the films possessing n-type conducting property [26]. The resistivity decreased significantly via the deposition of NCD films in $CH_4/H_2/N_2$ plasma [27]. Based on the analysis of vibrational and optical properties of ultrananocrystalline diamond (UNCD) films grown in an argon-rich $Ar/CH_4/H_2$ microwave plasma with nitrogen gas added in amounts of 0%–20% proves that nitrogen stimulates the transition from amorphous carbon into an ordered graphite-like structure with a narrowed optical bandgap, which is supposed to be responsible for the high electrical conductivity of the N-doped UNCD [28]. Teng et al. synthesized nitrogen incorporated UNCD films in $CH_4/Ar/N_2$ plasma and found an increase of amorphous sp^2 -bonded carbons in the grain boundaries and decrease in the size of diamond grains to nanosize that are well correlated to the reported enhancement of conductivity and structural changes of UNCD films [29]. Ficek et al., reported relatively high refractive index (2.6 ± 0.25 at 550 nm) and extinction coefficient (0.05 ± 0.02 at 550 nm) with a transmittance of 60% for the nitrogen doped diamond films grown using $CH_4/H_2/N_2$ (1%–8%) plasma [30]. Cuenca et al. [31] developed a microwave cavity perturbation system to measure non-contact and non-destructive electrical conductivity measurements of nitrogen doped nanocrystalline diamond (NCD) films grown using $CH_4/H_2/N_2$ plasma by varying the CH_4 concentration. Also, 0 to 10% nitrogen was incorporated in $CH_4/H_2/N_2$ plasma to synthesis UNCD films, and the obtained highly concentrated nitrogen content UNCD films exhibit good electrically conducting behavior with enhanced field electron emission and cyclic voltammetry characteristics [32]. Ralchenko et al. synthesized UNCD films using $CH_4/H_2/Ar$ plasma with 25% of nitrogen addition and the obtained films possess a very smooth surface, low thermal conductivity, and high optical absorption [33].

This gives us a strong basis to extend the research for the construction of an interferometric sensor using the nitrogen incorporated NCD films. An added advantage of NCD films is that their properties and therefore the applications can be tailored during the deposition process to fit the specific requirements of fiber-optic sensors.

In this work, we show the use of diamond films with different nitrogen incorporation levels in the construction of a fiber-optic measurement head. The diamond samples were deposited with the use of a microwave plasma enhanced chemical vapor deposition system. During the deposition process, we can control e.g. temperature, pressure, deposition time, microwave power, and doping level [34]. In the

presented investigation, all the above-mentioned parameters are kept the same among all samples, apart from the nitrogen doping level. Consequently, for representative nitrogen incorporation levels, the diamond films have been transformed from the transparent material into reflective layers, which can be used as mirrors. Therefore, we study the possibility of using nitrogen incorporated diamond films as mirrors in the construction of the sensor. A fiber-optic interferometer in the Fabry-Pérot configuration with a low reflection coefficient ($r \approx 0.26$) has been constructed. This low reflection coefficient is critical to obtain two-beam Fabry-Pérot, which transfer function is the same as two-beam interferometers.

It enables the implementation of almost point measurements and avoiding electromagnetic interference in the examined area, as the measurement head does not use electricity. Moreover, such a sensor is insensitive to changes in the intensity of the optical signal, as information about the value of the measured value is contained in the spectrum of the measurement signal.

2. Materials and methods

2.1. Growth of nitrogen incorporated diamond films

N-type mirror-polished (100)-oriented silicon (Si) substrates (10–20 $k\Omega\cdot cm$) were used to grow nitrogen incorporated diamond (NiD) films. First, the Si substrates were exposed to an O_2 plasma for 1 min at 200 W and 50 sccm total flux in order to prepare the surface for diamond seeding. Oxygen plasma was used to clean the surface of organic contamination as well as to improve the hydrophilicity of the surface. Then the Si substrates were seeded by drop casting with water based colloidal suspension of ultra-dispersed detonation nanodiamond of size 6–7 nm (NanoCarbon Institute Co., Ltd.) and subsequent spin-drying. The diamond film growth was carried out in a Seki ASTeX 6500 (Tokyo, Japan) microwave plasma enhanced chemical vapor deposition (MWPECVD) reactor. A mixture of CH_4 , H_2 , and N_2 gases was used with a total flow rate of 300 sccm. While the concentration of CH_4 was kept constant as 3% (9 standard cubic centimeter (sccm)), the concentration of N_2 was varied as 0% (0 sccm), 1% (3 sccm), 3% (9 sccm) and 5% (15 sccm) and complemented by H_2 to maintain the total flow rate. The grown samples were labeled as NiD-0, NiD-1, NiD-3, and NiD-5 films for 0%, 1%, 3%, and 5% nitrogen concentrations, respectively. The working pressure and microwave power were set at 30 Torr and 3000 W, respectively. All the samples were grown for a thickness of ~ 500 nm. The substrates were heated due to the bombardment of the plasma species and the growth temperature was measured by a single color optical pyrometer with the emissivity set to 0.3. The growth temperatures were estimated to be around 675 °C, 700 °C, 720 °C, and 750 °C for NiD-0, NiD-1, NiD-3, and NiD-5 films, respectively. Table 1 summarizes the growth conditions used for each sample.

2.2. Material characterization

The surface morphology and the thicknesses of the NiD films were characterized using a FEI R1.2 Quanta 200 FEG scanning electron microscope (SEM) operated at 15 kV. The surface roughness of the NiD films was estimated from an atomic force microscope (AFM) (NX-10, Park Systems) in a tapping mode. The crystalline quality of the films was examined using a Horiba Jobin Yvon T64000 microRaman spectrometer (equipped with a BXM Olympus 9/128 microscope, a Horiba JY Symphoony CCD detector with a 488 nm Lexell SHG laser). The bonding structure of the films was investigated by core-loss electron energy loss spectroscopy (EELS, Gatan Enfina) in transmission electron microscopy, respectively.

2.3. Interferometric measurement setup

The measurement setup was designed and constructed as a Fabry-

Table 1Growth conditions of nitrogen incorporated diamond films grown using CH₄, H₂, and N₂ plasma.

Sample	CH ₄ concentration	H ₂ concentration	N ₂ concentration	Pressure (Torr)	Microwave power (W)	Temperature (°C)	Thickness (nm)
NiD-0	3%	97%	0%	30	3000	675	500
NiD-1	3%	96%	1%	30	3000	700	500
NiD-3	3%	94%	3%	30	3000	720	500
NiD-5	3%	92%	5%	30	3000	750	500

Pérot interferometer operating in the reflective mode. The interferometer was composed of standard single-mode telecommunication fibers with a fiber-optic coupler (Lightel, WA, USA) with 1 × 2 power split (50/50 symmetrical system). The coupler was connected to a broadband light source operating at a central wavelength of $\lambda = 1550$ nm (SLD-1550-13, FiberLabs Inc., Japan) and to an optical spectrum analyzer (Ando AQ 6319, Yokogawa, Japan). The third arm of the coupler played the role of a measurement head. It was placed in the mechanical setup with a micrometer screw and positioned over the reflective layer, parallel to its surface. The scheme of the prepared setup and the normalized source characteristics can be seen in Fig. 1.

During measurements, the micrometer screw increased the distance between the fiber head and the reflecting layer, the increment was set to 10 μm in the range of 0–100 μm . Each measurement series was repeated for both silver (which acted as a reference) and for NiD films, each with different nitrogen content. Following the measurement procedure described above, we registered sets of optical spectra for the cavity lengths from 0 μm to 100 μm , using all prepared diamond samples in succession as mirrors. As a reference, the measurements on a standard silver mirror were performed with the same settings as for the diamond samples.

3. Results and discussion

3.1. Surface characteristics

Fig. 2 shows the SEM images of the NiD films.

At 0% N₂, the NiD-0 films show rough, faceted and randomly oriented micron-sized diamond grains. A dramatic change in the morphology of the NiD films was observed when nitrogen was added to the plasma. The micron-sized diamond grains disappeared and instead, “cauliflower-like” morphological nano-sized diamond grains of size ~20 nm appeared for NiD-1, NiD-3 and NiD-5 films, respectively.

The AFM images shown in Fig. 3 reveal that the NiD-0 films display high surface RMS roughness of 71.4 nm because of the presence of micron-sized diamond grains as shown in Fig. 2a.

Increasing the concentration of nitrogen decreases the roughness of the films due to the decrease in the grain size of the diamond films. The RMS roughness values of 30.1 nm, 29.7 nm, and 28.5 nm for NiD-1, NiD-3 and NiD-5 films, respectively.

The bonding structure of the NiD films was characterized using confocal micro-Raman spectroscopy operating at 488 nm with an acquisition time of 60 s. Fig. 4 shows the micro-Raman spectra of I. NiD-0, II. NiD-1, III. NiD-3 and IV. NiD-5, respectively.

The NiD-0 films show a characteristic peak at 1332 cm^{-1} (spectrum I of Fig. 4) that indicates the presence of sp^3 -bonded carbon. As the nitrogen concentration increases, the intensity of the diamond peak starts to diminish, which indicates the presence of smaller diamond grains and the formation of sp^2 -phases in the grain boundaries of the NiD-1, NiD-3 and NiD-5 films, respectively. There are peaks at around 1140 cm^{-1} and 1520 cm^{-1} , which are ascribed to the ν_1 and ν_3 modes of a *trans*-polyacetylene (*t*-PA) phase existing in the grain boundaries [35]. The broadened peaks at around 1352 cm^{-1} (D-band) and 1560 cm^{-1} (G-band) correspond to disordered carbon and graphitic phases, respectively [36]. The Raman spectra show I_D/I_G values (ratio of intensities of D-peak to G-peak) of 0.74, 0.83, and 1.05 for NiD-1, NiD-3 and NiD-5 films, respectively. The increase of the I_D/I_G value from 0.74 to 1.05 implies the formation of nanographite and decrease in sp^3 content according to a three stage model of increasing disorder in carbon materials [36,37], i.e., there is a conversion of sp^3 to sp^2 content due to the incorporation of nitrogen in the growth plasma. The absence of ν_1 and ν_3 bands in the NiD-5 sample also indicates the conversion of *t*-PA to nanographitic phases in the grain boundaries of NiD-5 films. It is to be noted that the scattering cross-section for sp^2 -bonded carbon to incident laser in micro-Raman is markedly larger than that for sp^3 -bonded carbon that induced larger background noise in Raman spectra of these materials [37]. The carbon edge core-loss EELS spectra corresponding to the NiD films are presented in Fig. 5.

Obtained spectra indicate that, for all of the NiD films, there is present an abrupt rise near 289.5 eV (σ^* -band) and a large dip in the vicinity of 302 eV, entailing the diamond nature of these materials [38,39]. Moreover, there is a π^* -band at 285.0 eV in core-loss EELS

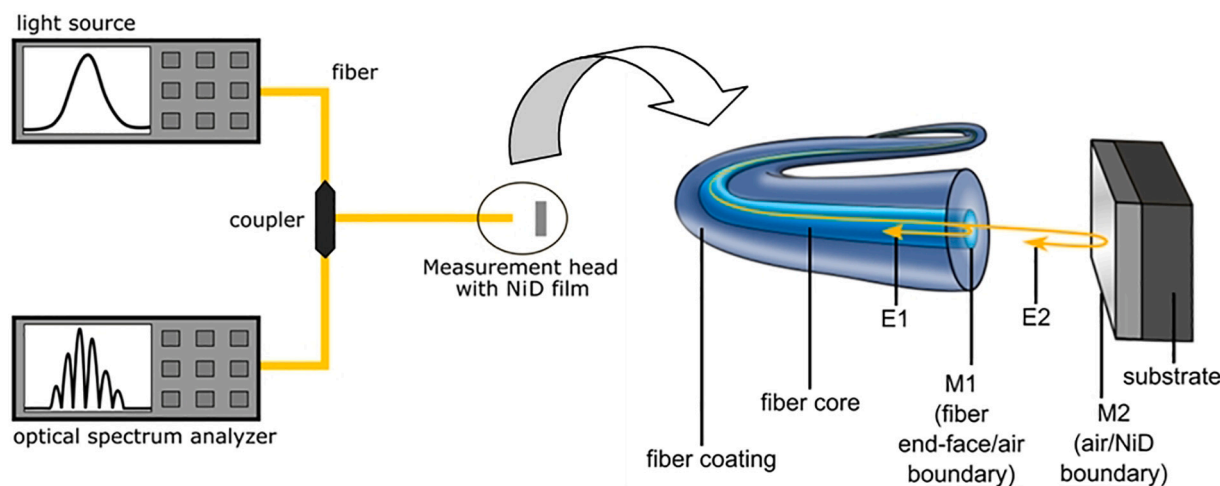


Fig. 1. Measurement setup of the prepared laboratory model of the sensor applying nitrogen incorporated diamond (NiD) film: M1, M2 – mirrors, E1, E2 – electric vectors of the wave reflected on the first and second mirror, respectively.

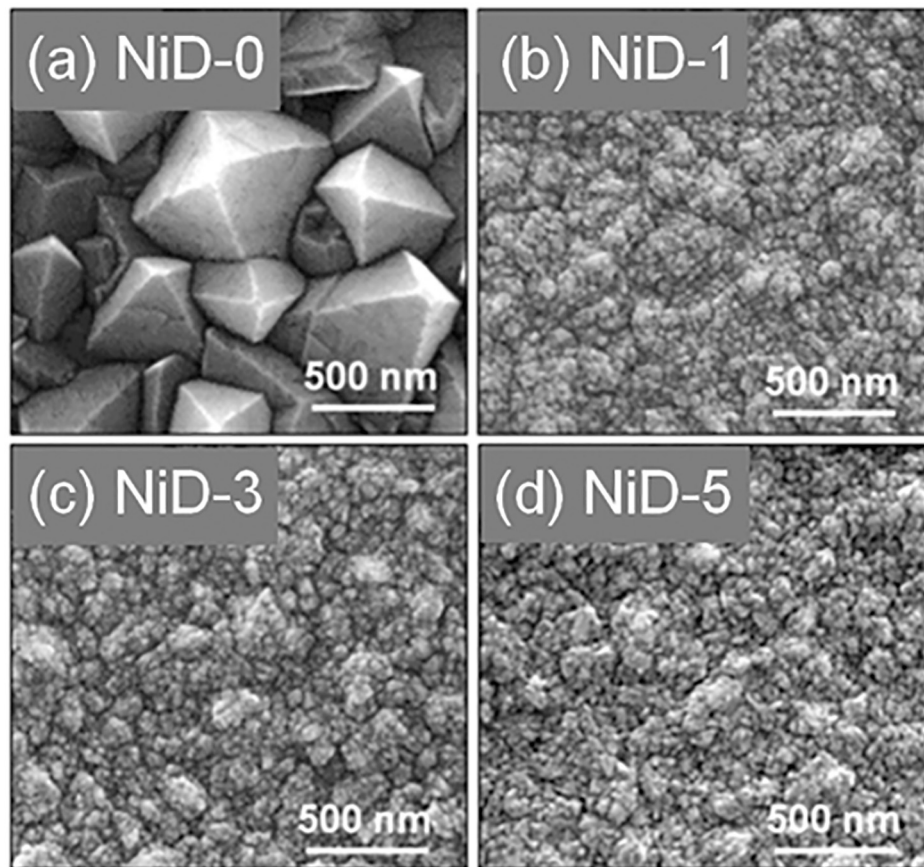


Fig. 2. SEM micrographs of NiD films deposited on silicon substrates at various concentrations of nitrogen in $\text{CH}_4/\text{H}_2/\text{N}_2$ plasma, (a) NiD-0 (0% N_2), (b) NiD-1 (1% N_2), (c) NiD-3 (3% N_2) and (d) NiD-5 (5% N_2).

spectra, especially for NiD-3 (spectrum III) and NiD-5 films (spectrum IV), indicating the formation of sp^2 -bonded carbon due to the increase of nitrogen concentration in the gas mixtures. The EELS investigations are in accord with the Raman analysis (cf. Fig. 4).

In line with the report of Birrell et al. even after the incorporation of nitrogen to the film the diamond grains stay pure diamond [40]. So the increase of sp^2 -bonded carbon is major happened at the grain boundaries. The nitrogen incorporation significantly affects the chemical bonds of the deposited films, which induces the formation of sp^2 -bonded carbon at the grain boundaries of the NiD films [41,42]. So it is confirmed that when the diamond grain size decreases, the amount of sp^2 -bonded carbon increases, as observed in Raman and EELS analyses.

3.2. Interferometric fiber-optic sensor

NiD films were then applied as passive elements in an interferometric fiber-optic sensor. In this set-up, we recorded a series of optical spectra and analyzed the modulation of the measured signals. The representative spectrum obtained for a standard silver mirror is shown in Fig. 6a, and spectra of measurement signals obtained with an interferometric setup with the NiD samples are shown in Fig. 6b–d. The cavity length was equal to 90 μm and the light source operating on a central wavelength of 1550 nm was used. The optical path of the interferometer changes during measurements, hence the optical signal obtained from the light source is modulated.

Changes in the optical properties of investigated samples are caused by different refractive indices due to various nitrogen levels. Ficek et al. described an ellipsometric investigation of diamond samples with nitrogen, showing that the increase in nitrogen content results in the decrease in refractive index [31]. As we have shown in Raman

spectroscopy investigation (Fig. 4), ratio values of D-peak to G-peak (noted as I_D/I_G) increase with the nitrogen content increase. This indicates the decrease in sp^3 content due to the conversion of sp^3 to sp^2 content, as a result of the incorporation of nitrogen in the films [38,39]. Different refractive indices of samples lead to various values of their reflectivity. The lowest I_D/I_G was obtained for NiD-1, hence its highest refractive index among the samples.

In the constructed sensors, the refractive index inside the cavity formed by the fiber end-face and an external mirror is constant ($n = 1$ for air) and therefore, changes occur due to the variation of the geometrical path of the Fabry-Pérot cavity. From the measured spectra we can also acquire information about maximum and minimum signal intensity. Those values have direct impact on the visibility value, describing the contrast. This can be expressed by the following formula [43]:

$$V = \frac{I_{\max} - I_{\min}}{I_{\max} + I_{\min}} \quad (1)$$

where I_{\max} is the maximum intensity of the measured signal, and I_{\min} is the minimum intensity of the measured signal. Calculations were performed for the diamond samples and presented as percentages in Table 2.

The value of visibility of measured spectra is dependent fundamentally upon the intensity of the signal reflected by the mirror. Therefore, the reflection coefficient of the mirror which depends on the material of the mirror has the biggest impact on visibility.

Different refractive indices of samples lead to various values of reflectivity R , which can be calculated using Fresnel formula [44]:

$$R = \left(\frac{n_2 - n_1}{n_1 + n_2} \right)^2,$$

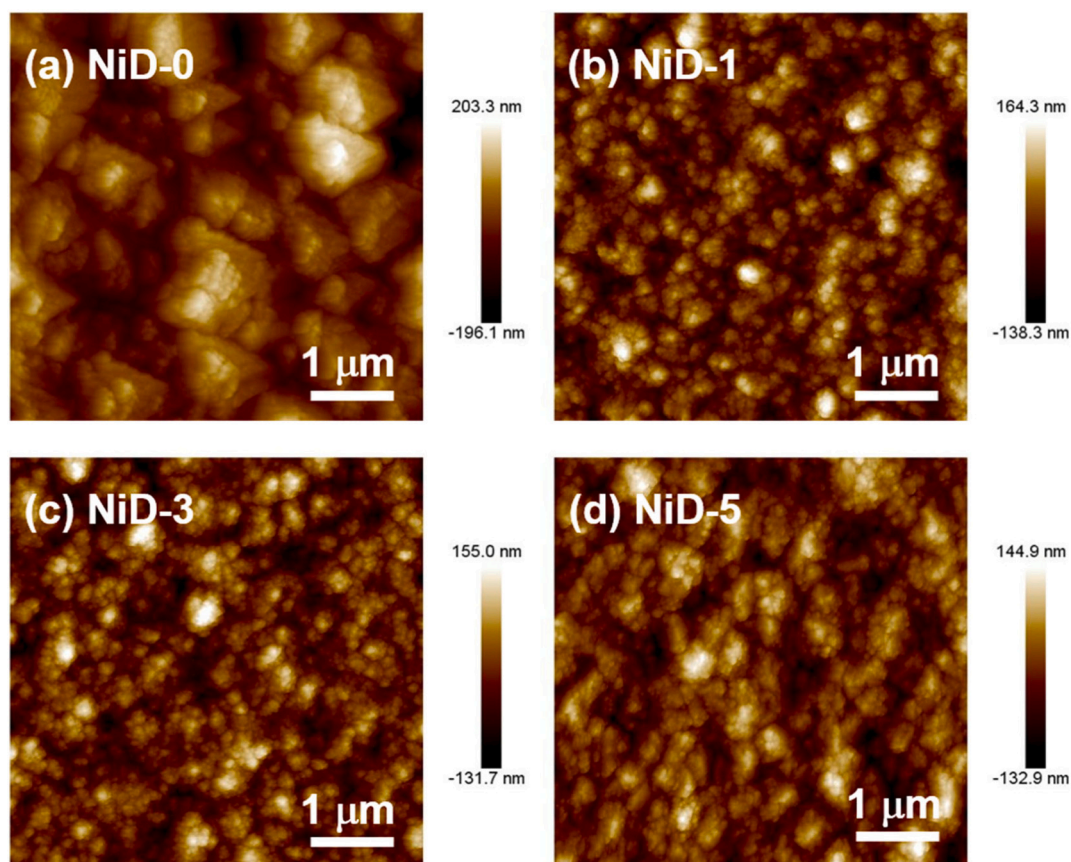


Fig. 3. AFM micrographs of NiD films deposited on silicon substrates at various concentrations of nitrogen in $\text{CH}_4/\text{H}_2/\text{N}_2$ plasma, (a) NiD-0 (0% N_2), (b) NiD-1 (1% N_2), (c) NiD-3 (3% N_2) and (d) NiD-5 (5% N_2).

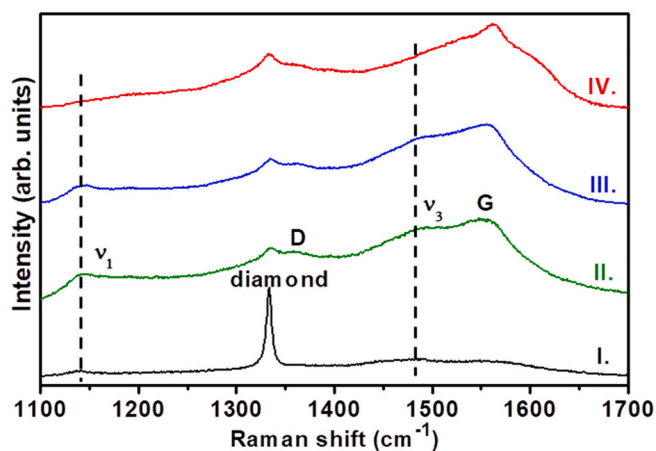


Fig. 4. Micro-Raman spectra of I. NiD-0, II. NiD-1, III. NiD-3 and IV. NiD-5 films.

where n_1 - refractive index of the optical fiber, n_2 - refractive index of the NiD film.

The differences in refractive indices of samples due to different nitrogen content influence the measured signal, as refractive index directly impacts the reflectivity of the mirror. According to Raman studies, NiD-1 has the highest refractive index due to the lowest I_D/I_G ratio.

It can be noted that for NiDs the highest contrast is achieved for very short cavity lengths. NiD-1 and NiD-3 provide the greatest values of visibility for 40–60 μm , while NiD-5 for 80–100 μm . In this range, silver

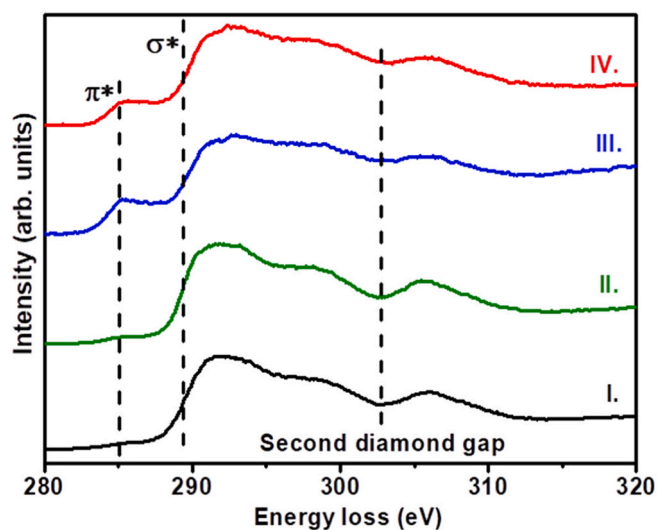


Fig. 5. Carbon edge core-loss EELS spectra of I. NiD-0, II. NiD-1, III. NiD-3 and IV. NiD-5 films.

assures much lower visibility which shows that diamond films can serve as mirrors with better signal visibility for smaller cavity lengths. The obtained visibility values assure a good contrast quality of interferometric signal meaning nitrogen incorporated diamond films work properly as reflective surfaces.



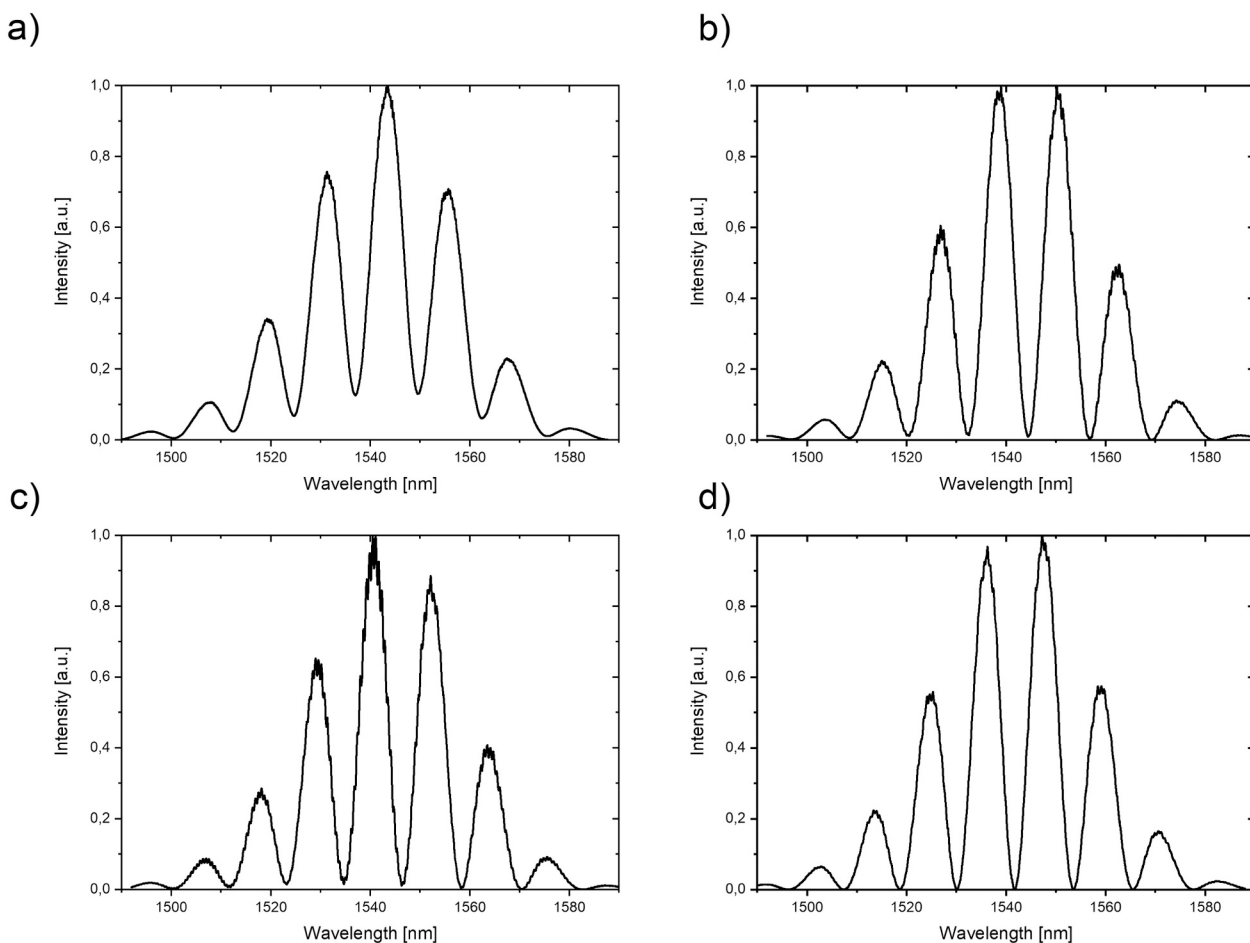


Fig. 6. Representative spectra recorded for investigated diamond mirrors and silver with the cavity lengths set to 90 μm and the light source with a central wavelength of 1550 nm: a) silver, b) NiD-1, c) NiD-3, d) NiD-5.

Table 2

Comparison of visibility values for representative cavity lengths on nitrogen incorporated diamond films and silver.

Cavity length [μm]	Ag	NiD-1	NiD-3	NiD-5
40	75.1%	99.9%	99.8%	94.0%
60	76.0%	99.9%	99.9%	97.3%
80	77.0%	99.5%	98.6%	99.2%
100	81.1%	97.6%	97.0%	99.9%

4. Conclusions

This study has shown results on the application of nitrogen incorporated diamond films in fiber-optic sensors, taking into account the level of nitrogen-doping in the resulting films. Our research showed that the best visibility is achieved for a nitrogen doping level of 1%. We compared the obtained visibility values for representative cavity lengths with those achieved for a conventional mirror – silver.

It can be noted that the utilization of nitrogen incorporated diamond as a mirror results in obtaining visibility values greater than 90% For the cavity length of e.g. 80 μm , the standard silver mirror assures the visibility equal to 77%, while diamond films provide this value to be greater than 98%. We presented that different values of nitrogen in the working gas mixture composition impact properties of resulting nanocrystalline diamond films which translate directly into their reflective properties. With different nitrogen content, the bonding and surface characteristics change, resulting in a decrease of the grain size and the increase of the boundary phases. We presented that the smallest nitrogen doping – 1% –

provides the best material for the mirror, as the NiD-1 sample gives the highest contrast (>0.99%). Other diamond samples also provide good results in comparison to silver, however, a higher degree of nitrogen doping slowly reduces the contrast in the range of the interest. This clearly shows that the silver provides good signal visibility, but diamond mirrors are a better choice. The use of nanocrystalline diamond films in optical fiber sensors reduces the required sample volume due to high visibility for shorter cavities. Numerous benefits of diamond material application are introduced along with better signal contrast. Those are mechanical and chemical resistance, and biocompatibility, which could open new applications of fiber-optic sensors. Further investigations on the use of NiD films can lead to the development of chemical sensors and biosensors [45,46]. Their metrological parameters could be tailored by e.g. proper doping of the diamond film.

CRediT authorship contribution statement

Monika Kosowska: Conceptualization, Methodology, Investigation, Formal analysis, Visualization, Funding acquisition, Writing – original draft. **Sandra Pawłowska:** Validation, Investigation, Data Curation, Formal analysis, Writing – original draft. **Kamatchi J. Sankaran:** Conceptualization, Methodology, Validation, Investigation, Data curation, Formal Analysis, Visualization, Writing – original draft. **Daria Majchrowicz:** Conceptualization, Methodology, Funding acquisition, Writing – original draft. **Ken Haenen:** Writing – review & editing, Funding acquisition. **Kishan Dholakia:** Writing – review & editing, Funding acquisition. **Małgorzata Szczerska:** Conceptualization, Methodology, Formal analysis, Supervision, Funding acquisition, Writing –

review & editing.

Declaration of competing interest

The authors declare that they have no known competing financial interests or personal relationships that could have appeared to influence the work reported in this paper.

Acknowledgements

This research was funded by Polish National Science Centre (NCN) grant number 2017/25/N/ST7/01610, Polish National Agency for Academic Exchange under Iwanowska Programme PPN/IWA/2018/00026/U/00001 and Iwanowska Programme PPN/IWA/2018/1/00058/U/0001, and the DS funds of the Faculty of Electronics, Telecommunications, and Informatics of the Gdańsk University of Technology. Financial support of these studies from Gdańsk University of Technology by the 11/2020/IDUB/I.3/CC grant under the COMBATING CORONAVIRUS - EIRU program is gratefully acknowledged. KH acknowledges the Research Foundation Flanders (FWO) via Research Project GOD4920N. KD thanks the UK Engineering and Physical Sciences Research Council through grant EP/P030017/1.

References

- [1] A. Davanlou, Integration of fiber-optic sensors in measuring machines, *Measurement*. 57 (2014) 25–32, <https://doi.org/10.1016/j.measurement.2014.07.004>.
- [2] K. Bohnert, P. Gabus, J. Kostovic, H. Brändle, Optical fiber sensors for the electric power industry, *Opt. Lasers Eng.* 43 (2005) 511–526, <https://doi.org/10.1016/j.optlaseng.2004.02.008>.
- [3] D. Tosi, S. Poeggel, G. Leen, E. Lewis, Adaptive filter-based interrogation of high-sensitivity fiber optic Fabry-Perot interferometry sensors, *Sensors Actuators A Phys.* 206 (2014) 144–150, <https://doi.org/10.1016/j.sna.2013.12.010>.
- [4] J. Weng, Z. Zhang, L. Sun, J.A. Wang, High sensitive detection of cancer cell with a folic acid-based boron-doped diamond electrode using an AC impedimetric approach, *Biosens. Bioelectron.* 26 (2011) 1847–1852, <https://doi.org/10.1016/j.bios.2010.01.027>.
- [5] Y.-J. Rao, Recent progress in fiber-optic extrinsic Fabry-Perot interferometric sensors, *Opt. Fiber Technol.* 12 (2006) 227–237, <https://doi.org/10.1016/j.yofte.2006.03.004>.
- [6] A. Leal-Junior, A. Frizzera-Netoc, C. Marques, M.J. Pontes, A polymer optical fiber temperature sensor based on material features, *Sensors (Basel)*. 18 (2018). doi:<https://doi.org/10.3390/s18010301>.
- [7] M. Kosowska, D. Majchrowicz, K.J. Sankaran, M. Ficek, K. Haenen, M. Szczerska, Doped nanocrystalline diamond films as reflective layers for fiber-optic sensors of refractive index of liquids, *Materials (Basel)*. 12 (2019). doi:<https://doi.org/10.3390/ma12132124>.
- [8] Q. Zhao, H. Zheng, R. Lv, Y. Gu, Y. Zhao, Y. Yang, Novel integrated optical fiber sensor for temperature, pressure and flow measurement, *Sensors Actuators A Phys.* 280 (2018) 68–75, <https://doi.org/10.1016/j.sna.2018.07.034>.
- [9] D. Milewska, K. Karpienko, M. Jędrzejewska-Szczerska, Application of thin diamond films in low-coherence fiber-optic Fabry Perot displacement sensor, *Diam. Relat. Mater.* 64 (2016) 169–176, <https://doi.org/10.1016/j.diamond.2016.02.015>.
- [10] V. Baranauskas, B.B. Li, A. Peterlevitz, M.C. Tosin, S.F. Durrant, Nitrogen-doped diamond films, *J. Appl. Phys.* 85 (1999) 7455–7458, <https://doi.org/10.1063/1.369378>.
- [11] S. Jin, T.D. Moustakas, Effect of nitrogen on the growth of diamond films, *Appl. Phys. Lett.* 65 (1994) 403–405, <https://doi.org/10.1063/1.12315>.
- [12] R. Bogdanowicz, M. Śmietana, M. Gnyba, Ł. Gołuski, J. Ryl, M. Gardas, Optical and structural properties of polycrystalline CVD diamond films grown on fused silica optical fibres pre-treated by high-power sonication seeding, *Appl. Phys. A Mater. Sci. Process.* 116 (2014) 1927–1937, <https://doi.org/10.1007/s00339-014-8355-x>.
- [13] H.-Y. Cheng, C.-Y. Yang, L.-C. Yang, K.-C. Peng, C.-T. Chia, S.-J. Liu, I.-N. Lin, K.-H. Lin, Effective thermal and mechanical properties of polycrystalline diamond films, *J. Appl. Phys.* 123 (2018) 165105, <https://doi.org/10.1063/1.5016919>.
- [14] R.S. Balmer, J.R. Brandon, S.L. Clewes, H.K. Dhillon, J.M. Dodson, I. Friel, P.N. Inglis, T.D. Madgwick, M.L. Markham, T.P. Mollart, N. Perkins, G.A. Scarsbrook, D. J. Twitchen, A.J. Whitehead, J.J. Wilman, S.M. Woollard, Chemical vapour deposition synthetic diamond: materials, technology and applications, *J. Phys.: Condens. Matter*. 21 (2009) 364221. doi:<https://doi.org/10.1088/0953-8984/21/36/364221>.
- [15] M.A. Hayat, Y. Zhang, Care and use of diamond knives, *Micron*. 29 (1998) 411–414, [https://doi.org/10.1016/S0968-4328\(98\)00016-X](https://doi.org/10.1016/S0968-4328(98)00016-X).
- [16] M. Sobaszek, Ł. Skowronski, R. Bogdanowicz, K. Siuzdak, A. Cirocka, P. Zięba, M. Gnyba, M. Naparty, Ł. Gołuski, P. Płotka, Optical and electrical properties of ultrathin transparent nanocrystalline boron-doped diamond electrodes, *Opt. Mater.* 42 (2015) 24–34, <https://doi.org/10.1016/j.optmat.2014.12.014>.
- [17] B. Bayram, Diamond-based capacitive micromachined ultrasonic transducers, *Diam. Relat. Mater.* 22 (2012) 6–11, <https://doi.org/10.1016/j.diamond.2011.11.006>.
- [18] K. Xiao, P. Giusto, L. Wen, L. Jiang, M. Antonietti, Nanofluidic ion transport and energy conversion through ultrathin free-standing polymeric carbon nitride membranes, *Angew. Chem. Int. Ed.* 57 (2018) 10123–10126, <https://doi.org/10.1002/anie.201804299>.
- [19] R.J. Williams, O. Kitzler, Z. Bai, S. Sarang, H. Jasbeer, A. McKay, S. Antipov, A. Sabella, O. Lux, D.J. Spence, R.P. Mildren, High power diamond Raman lasers, *IEEE J. Sel. Top. Quantum Electron.* 24 (2018) 1–14, <https://doi.org/10.1109/JSTQE.2018.2827658>.
- [20] R. Bogdanowicz, M. Sobaszek, M. Ficek, M. Gnyba, J. Ryl, K. Siuzdak, W.J. Bock, M. Śmietana, Opto-electrochemical sensing device based on long-period grating coated with boron-doped diamond thin film, *J. Opt. Soc. Korea*. 19 (2015) 705–710.
- [21] M. Kosowska, D. Majchrowicz, M. Ficek, P. Wierzbna, Y. Flegler, D. Fixler, M. Szczerska, Nanocrystalline diamond sheets as protective coatings for fiber-optic measurement head, *Carbon*. 156 (2020) 104–109, <https://doi.org/10.1016/j.carbon.2019.09.042>.
- [22] D. Majchrowicz, M. Kosowska, K.J. Sankaran, P. Struk, M. Wałowicz, M. Sobaszek, K. Haenen, M. Jędrzejewska-Szczerska, Nitrogen-doped diamond film for optical investigation of hemoglobin concentration, *Materials*. 11 (2018) 109, <https://doi.org/10.3390/ma11010109>.
- [23] D. Majchrowicz, M. Kosowska, P. Struk, M. Jędrzejewska-Szczerska, Tailoring the optical parameters of optical fiber interferometer with dedicated boron-doped nanocrystalline diamond thin film (*Phys. Status Solidi A* 11/2017), *Physica Status Solidi (A)*. 214 (2017) 1770164. doi:<https://doi.org/10.1002/pssa.201770164>.
- [24] Y. Tanaka, M. Furuta, K. Kuriyama, R. Kuwabara, Y. Katsuki, T. Kondo, A. Fujishima, K. Honda, Electrochemical properties of N-doped hydrogenated amorphous carbon films fabricated by plasma-enhanced chemical vapor deposition methods, *Electrochim. Acta* 56 (2011) 1172–1181, <https://doi.org/10.1016/j.electacta.2010.11.006>.
- [25] A. Härtl, E. Schmich, J.A. Garrido, J. Hernando, S.C.R. Catharino, S. Walter, P. Feulner, A. Kromka, D. Steinmüller, M. Stutzmann, Protein-modified nanocrystalline diamond thin films for biosensor applications, *Nat. Mater.* 3 (2004) 736–742, <https://doi.org/10.1038/nmat1204>.
- [26] J. Birrell, J.A. Carlisle, O. Auciello, D.M. Gruen, J.M. Gibson, Morphology and electronic structure in nitrogen-doped ultrananocrystalline diamond, *Appl. Phys. Lett.* 81 (2002) 2235–2237, <https://doi.org/10.1063/1.1503153>.
- [27] K.L. Ma, W.J. Zhang, Y.S. Zou, Y.M. Chong, K.M. Leung, I. Bello, S.T. Lee, Electrical properties of nitrogen incorporated nanocrystalline diamond films, *Diam. Relat. Mater.* 15 (2006) 626–630, <https://doi.org/10.1016/j.diamond.2005.11.017>.
- [28] I.I. Vlasov, E. Goovaerts, V.G. Ralchenko, V.I. Konov, A.V. Khomich, M. V. Kanzyuba, Vibrational properties of nitrogen-doped ultrananocrystalline diamond films grown by microwave plasma CVD, *Diam. Relat. Mater.* 16 (2007) 2074–2077, <https://doi.org/10.1016/j.diamond.2007.07.007>.
- [29] C.-C. Teng, S.-M. Song, C.-M. Sung, C.-T. Lin, Structural transformation upon nitrogen doping of ultrananocrystalline diamond films by microwave plasma CVD, *J. Nanomater.* 621208 (2009), <https://doi.org/10.1155/2009/621208>.
- [30] M. Ficek, K.J. Sankaran, J. Ryl, R. Bogdanowicz, I.-N. Lin, K. Haenen, K. Darowicki, Ellipsometric investigation of nitrogen doped diamond thin films grown in microwave CH₄/H₂/N₂ plasma enhanced chemical vapor deposition, *Appl. Phys. Lett.* 108 (2016) 241906, <https://doi.org/10.1063/1.4953779>.
- [31] J.A. Cuenca, K.J. Sankaran, P. Pobedinskas, K. Panda, I.-N. Lin, A. Porch, K. Haenen, O.A. Williams, Microwave cavity perturbation of nitrogen doped nanocrystalline diamond films, *Carbon*. 145 (2019) 740–750, <https://doi.org/10.1016/j.carbon.2018.12.025>.
- [32] Y.C. Lin, K.J. Sankaran, Y.C. Chen, C.Y. Lee, H.C. Chen, I.N. Lin, N.H. Tai, Enhancing electron field emission properties of UNCD films through nitrogen incorporation at high substrate temperature, *Diam. Relat. Mater.* 20 (2011) 191–195, <https://doi.org/10.1016/j.diamond.2010.11.026>.
- [33] V. Ralchenko, S. Pimenov, V. Konov, A. Khomich, A. Saveliev, A. Popovich, I. Vlasov, E. Zavedeev, A. Bozhko, E. Loubnin, R. Khmel'nitskii, Nitrogenated nanocrystalline diamond films: thermal and optical properties, *Diam. Relat. Mater.* 16 (2007) 2067–2073, <https://doi.org/10.1016/j.diamond.2007.05.005>.
- [34] M. Ficek, M. Sobaszek, M. Gnyba, J. Ryl, Ł. Gołuski, M. Śmietana, J. Jasiński, P. Caban, R. Bogdanowicz, Optical and electrical properties of boron doped diamond thin conductive films deposited on fused silica glass substrates, *Appl. Surf. Sci.* 387 (2016) 846–856, <https://doi.org/10.1016/j.apsusc.2016.06.165>.
- [35] Z. Sun, J.R. Shi, B.K. Tay, S.P. Lau, UV Raman characteristics of nanocrystalline diamond films with different grain size, *Diam. Relat. Mater.* 9 (2000) 1979–1983, [https://doi.org/10.1016/S0925-9635\(00\)00349-6](https://doi.org/10.1016/S0925-9635(00)00349-6).
- [36] A.C. Ferrari, J. Robertson, Origin of the 1150-cm⁻¹ Raman mode in nanocrystalline diamond, *Phys. Rev. B* 63 (2001) 121405, <https://doi.org/10.1103/PhysRevB.63.121405>.
- [37] A.C. Ferrari, J. Robertson, Interpretation of Raman spectra of disordered and amorphous carbon, *Phys. Rev. B* 61 (2000) 14095–14107, <https://doi.org/10.1103/PhysRevB.61.14095>.
- [38] S. Praver, J.L. Peng, J.O. Orwa, J.C. McCallum, D.N. Jamieson, L.A. Bursill, Size dependence of structural stability in nanocrystalline diamond, *Phys. Rev. B* 62 (2000) R16360–R16363, <https://doi.org/10.1103/PhysRevB.62.R16360>.
- [39] R. Arenal, P. Bruno, D.J. Miller, M. Bleuel, J. Lal, D.M. Gruen, Diamond nanowires and the insulator-metal transition in ultrananocrystalline diamond films, *Phys. Rev. B* 75 (2007) 195431, <https://doi.org/10.1103/PhysRevB.75.195431>.

- [40] J. Birrell, J.E. Gerbi, O. Auciello, J.M. Gibson, D.M. Gruen, J.A. Carlisle, Bonding structure in nitrogen doped ultrananocrystalline diamond, *J. Appl. Phys.* 93 (2003) 5606–5612, <https://doi.org/10.1063/1.1564880>.
- [41] Y.L. Li, J.J. Li, X.X. Xia, C. Lu, H. Jin, C.Z. Gu, Effect of grain boundary on local surface conductivity of diamond film, *J. Appl. Phys.* 105 (2009), 013706, <https://doi.org/10.1063/1.3056381>.
- [42] F. Lloret, K.J. Sankaran, J. Millan-Barba, D. Desta, R. Rouzbahani, P. Pobedinskas, M. Gutierrez, H.-G. Boyen, K. Haenen, Improved field electron emission properties of phosphorus and nitrogen Co-doped nanocrystalline diamond films, *Nanomaterials (Basel)*. 10 (2020). doi:<https://doi.org/10.3390/nano10061024>.
- [43] P. Hariharan, P. (School of P.H. Australia) University of Sydney Sydney, *Optical Interferometry*, 2e, Academic Press, 2003.
- [44] L.S. Grattan, B.T. Meggitt (Eds.), *Optical Fiber Sensor Technology: Fundamentals*, Springer US, 2000. <https://www.springer.com/la/book/9780792378525>. (Accessed 23 June 2019).
- [45] A. Tereshchenko, G.R. Yazdi, I. Konup, V. Smyntyna, V. Khranovskyy, R. Yakimova, A. Ramanavicius, Application of ZnO nanorods based whispering gallery mode resonator in optical immunosensors, *Colloids Surf. B: Biointerfaces* 191 (2020) 110999, <https://doi.org/10.1016/j.colsurfb.2020.110999>.
- [46] I. Brice, K. Grundsteins, A. Atvars, J. Alnis, R. Viter, A. Ramanavicius, Whispering gallery mode resonator and glucose oxidase based glucose biosensor, *Sensors Actuators B Chem.* 318 (2020) 128004, <https://doi.org/10.1016/j.snb.2020.128004>.

**[MK2] Doped Nanocrystalline Diamond Films as Reflective Layers for Fiber-Optic Sensors
of Refractive Index of Liquids.**

Kosowska, M.; Majchrowicz, D.; Sankaran, K.J.; Ficek, M.; Haenen, K.; Szczerska, M.






Materials 2019, 12, 2124, doi:10.3390/ma12132124.

The author's contributions were:

conceptualization, performing measurements, data analysis and writing selected parts of the manuscript.

Article

Doped Nanocrystalline Diamond Films as Reflective Layers for Fiber-Optic Sensors of Refractive Index of Liquids

Monika Kosowska ¹, Daria Majchrowicz ¹, Kamatchi J. Sankaran ^{2,3}, Mateusz Ficek ¹, Ken Haenen ^{2,3} and Małgorzata Szczerska ^{1,*}

¹ Department of Metrology and Optoelectronics, Faculty of Electronics, Telecommunications and Informatics, Gdansk University of Technology, 11/12 Narutowicza Street, 80-233 Gdansk, Poland

² Institute for Materials Research (IMO), Hasselt University, Wetenschapspark 1, B-3590 Diepenbeek, Belgium

³ IMOMEC, IMEC vzw, Wetenschapspark 1, B-3590 Diepenbeek, Belgium

* Correspondence: mjedrzej@eti.pg.edu.pl; Tel.: +48-583-471-361

Received: 28 May 2019; Accepted: 29 June 2019; Published: 2 July 2019



Abstract: This paper reports the application of doped nanocrystalline diamond (NCD) films—nitrogen-doped NCD and boron-doped NCD—as reflective surfaces in an interferometric sensor of refractive index dedicated to the measurements of liquids. The sensor is constructed as a Fabry–Pérot interferometer, working in the reflective mode. The diamond films were deposited on silicon substrates by a microwave plasma enhanced chemical vapor deposition system. The measurements of refractive indices of liquids were carried out in the range of 1.3 to 1.6. The results of initial investigations show that doped NCD films can be successfully used in fiber-optic sensors of refractive index providing linear work characteristics. Their application can prolong the lifespan of the measurement head and open the way to measure biomedical samples and aggressive chemicals.

Keywords: doped nanocrystalline diamond films; refractive index sensor; fiber-optic; nitrogen-doping; boron-doping; optical fiber sensor

1. Introduction

The field of biomedical measurements is rapidly growing, and optical sensors play a significant role in its development. The use of optical fibers in the construction of sensors provides many advantages [1]. Such sensors require only a small amount of sample, give a rapid response, measurements are non-invasive and chemical pretreatment is not needed [2]. Moreover, they assure no risk of electrical sparks and immunity to ionizing radiation [3]. This group of sensors is widely used for the determination of refractive index, one of the most important optical properties describing materials. The precise determination of its value allows for the identification of the investigated substance and its concentration [4,5]. Therefore, fiber-optic measurements of refractive index attracted considerable attention in finding applications in many fields including biomedicine, chemistry, environmental analysis and the food industry [6–10].

However, measurements of biological samples, hazardous and chemically aggressive substances are still a challenge. Investigation of such materials carries a high risk of damaging the elements of the measurement heads. In conventional Fabry–Pérot interferometers, the most exposed part is a mirror that has direct contact with the sample. In standard solutions it is made of metallic layers such as silver or aluminum. Even though they have satisfactory optical parameters, they are susceptible to mechanical damage and have limited chemical resistance. Aluminum can cause poisoning of the investigated tissues. This results in permanent damaging of the measurement head and the necessity

of replacing the damaged part, which is inconvenient and causes additional costs. In performing measurements of biomedical substances, apart from the risk of damaging the sensor, there is a high chance of polluting the investigated sample, which can affect the results giving a false response. Thus, there is a need for new materials which can be used in the production of reflective surfaces that provide good optical parameters, as well as great resistance to chemicals. These features can be found in diamond materials.

Diamond films deposited in chemical vapor deposition (CVD) process are very hard, chemically inert and stable materials, which are transparent in a broad wavelength range [11–13]. The properties of diamond film structures produced in a CVD system can be tailored by changing the deposition process parameters. The use of dopants in the working gas mixture has an impact on the resulting film, including the optical properties. Hence it is possible to tune the process to achieve a suitable structure for the reflective layer in the interferometer [14–16].

In this work we present the application of diamond films doped with boron and nitrogen. The diamond films were deposited on silicon substrates and utilized as mirrors in fiber-optic sensors dedicated to measuring refractive indices of liquids. This solution combines the advantages of the fiber-optic Fabry–Pérot interferometer with benefits introduced by the extraordinary parameters of the diamond films, solving the problem of standard mirrors being susceptible to chemical damage.

This study is a continuation of our investigation regarding the use of diamond films in fiber-optic sensors. Previously, we proved that doped diamond films can be successfully applied in distance sensors and that they assure the biocompatibility [17,18]. This paper reports refractive index sensors utilizing two kinds of doped diamond films.

2. Materials and Methods

2.1. Nanocrystalline Diamond Films

Boron-doped nanocrystalline diamond (BD-NCD) films were synthesized in a microwave plasma enhanced CVD (MW PE CVD) system (SEKI Technotron AX5400S, Tokyo, Japan) on p-type Si (100) substrates. In our experiments, dedicated NCD suspensions were used to seed the substrates [19,20]. The pressure before growth in the vacuum chamber was kept at 10^{-4} Torr. A special truncated cone-shaped shim and 500 °C was used during the growth of BD-NCD films. The plasma microwave power, optimized for diamond synthesis, was kept at 1300 W [21]. In this study, the molar ratio of the $\text{CH}_4:\text{H}_2$ mixture was kept at 1% of gas volume at 300 sccm of the total flow rate. The boron level, expressed as the (B)/(C) ratio, in the gas phase was 10,000 ppm. The growth time was 3 h. After the growth process, the substrate temperature was slowly reduced ($5\text{ °C}\cdot\text{min}^{-1}$) down to room temperature.

Nitrogen-doped NCD (ND-NCD) film was grown on silicon substrate in a MW PE CVD system (SEKI ASTeX 6500, Tokyo, Japan). Prior to the diamond film growth, the silicon substrate was seeded with a colloidal suspension containing 5 nm detonation nanodiamonds and distilled water using a spin-coating technique. The ND-NCD film was grown on a silicon substrate in a $\text{CH}_4(9)/\text{H}_2(282)/\text{N}_2(3)$ sccm plasma excited by 3000 W microwave power with 65 Torr pressure for 180 min. The substrate temperature was about 650 °C, which was measured using a single-color optical pyrometer.

The samples were made in two different universities. Two different pressures result from differences in the standard growth procedures developed in each scientific team. For convenient referencing to each sample, we adopted the following abbreviations: BD-NCD-Si—boron-doped nanocrystalline diamond deposited on a silicon substrate, and ND-NCD-Si—nitrogen-doped nanocrystalline diamond deposited on a silicon substrate.

Diamond Film Characterization

In order to be able to use a diamond film as a mirror, it has to fulfill specific requirements considering its surface. The film has to be homogenous, continuously covering the substrate. No cracks should be detected to provide reliable resistance to chemicals.

The diamond films used in this experiment were previously applied in fiber-optic sensors for determining their potential in measurements of biological samples and for distance measurements [14,22], hence, their detailed characterizations can be found there. The investigation has shown that the thickness of the doped NCD films is around 300 nm, and the root mean square roughness is equal to 22 nm and 49 nm for BD-NCD-Si and ND-NCD-Si, respectively [22]. The aforementioned examinations proved that the deposited diamond films can work as reflective surfaces.

2.2. Measurement Setup

The fiber-optic setup for measuring the refractive index of liquid samples based on a Fabry–Pérot interferometer was constructed. The experiment was carried out with two superluminescent diodes working at the central wavelength of 1290 nm and 1560 nm, respectively. The system was built with a light source (S-1290-G-I-20, and S1560-G-I-10, Superlum, Ireland), an optical spectrum analyzer (ANDO AQ6319, Yokogawa, Japan), single-mode telecommunication optical fibers (SMF-28, Thorlabs, Newton, NJ, USA), and a 2×1 50:50 coupler. The tip of the fiber and the doped NCD films were used as a measurement head. The principle of the operation of this setup was described elsewhere [22]. Figure 1 shows the schema of the measurement setup with a close-up of the measurement head.

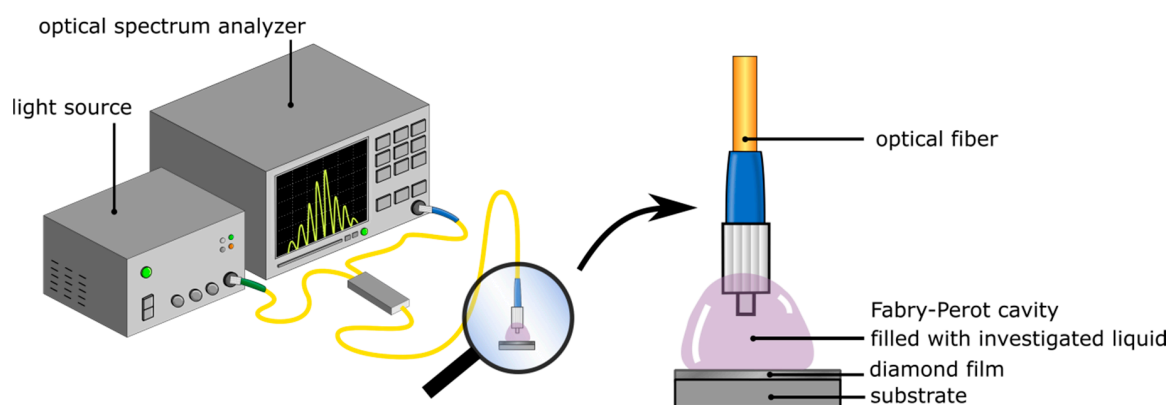


Figure 1. Measurement setup with a close-up of the measurement head.

The measurement field, called a Fabry–Pérot cavity, is formed between the face of a fiber and the nanocrystalline diamond film deposited on silicon substrate. Measurements of refractive indices in the range of 1.3–1.6 were performed with the use of refractive index liquids provided by Cargille®. In the experiment and data analysis we considered the refractive indices of liquids at 1290 nm and 1560 nm according to the datasheets. However, in the text, we refer to each solution by a rounded value of its refractive index to provide greater clarity. Before placing the sample, the cavity was cleaned with isopropyl alcohol. The block diagram of the experiment is shown in Figure 2.

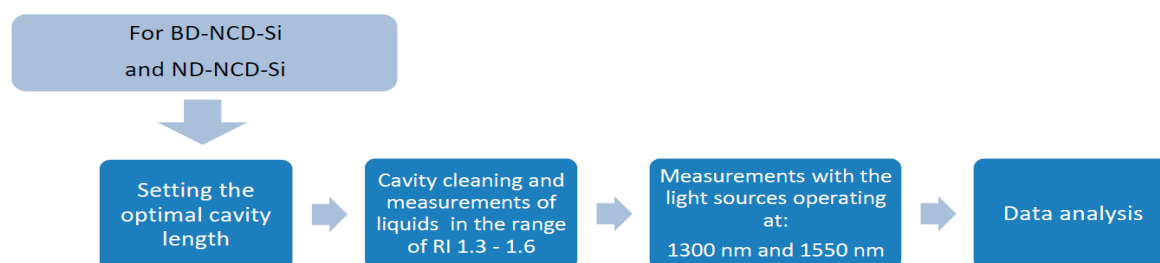


Figure 2. The block diagram of the experiment.

The distance between the fiber and the reflective surface in the device influences the visibility of the interferometric fringes, as the light beam diverges and is coupled back into the fiber with differing efficiency. Therefore, before carrying out refractive index measurements, the cavity length of the

interferometer was set to achieve the highest visibility value of the measured signal. To calculate the visibility V , the following formula was used:

$$V = \frac{I_{\max} - I_{\min}}{I_{\max} + I_{\min}} \quad (1)$$

where I_{\max} is the maximum intensity of the measured signal and I_{\min} is the minimum intensity of the measured signal. Table 1 shows values of visibility for the investigated films calculated for representative cavity lengths for given working wavelengths.

Table 1. Visibility values calculated for representative cavity lengths filled with air measured on BD-NCD-Si and ND-NCD-Si for central wavelength of 1290 nm and 1560 nm.

BD-NCD-Si			
Wavelength—1290 nm		Wavelength—1560 nm	
Cavity Length	Visibility	Cavity Length	Visibility
80 μm	0.9915	110 μm	0.9950
160 μm	0.8239	200 μm	0.8727
ND-NCD-Si			
Wavelength—1290 nm		Wavelength—1560 nm	
Cavity Length	Visibility	Cavity Length	Visibility
60 μm	0.9917	90 μm	0.9939
120 μm	0.8394	190 μm	0.7905

BD-NCD-Si: boron-doped nanocrystalline diamond deposited on a silicon substrate; ND-NCD-Si: nitrogen-doped nanocrystalline diamond deposited on a silicon substrate.

The above calculations of visibility were based on spectra presented in Figures 3 and 4.

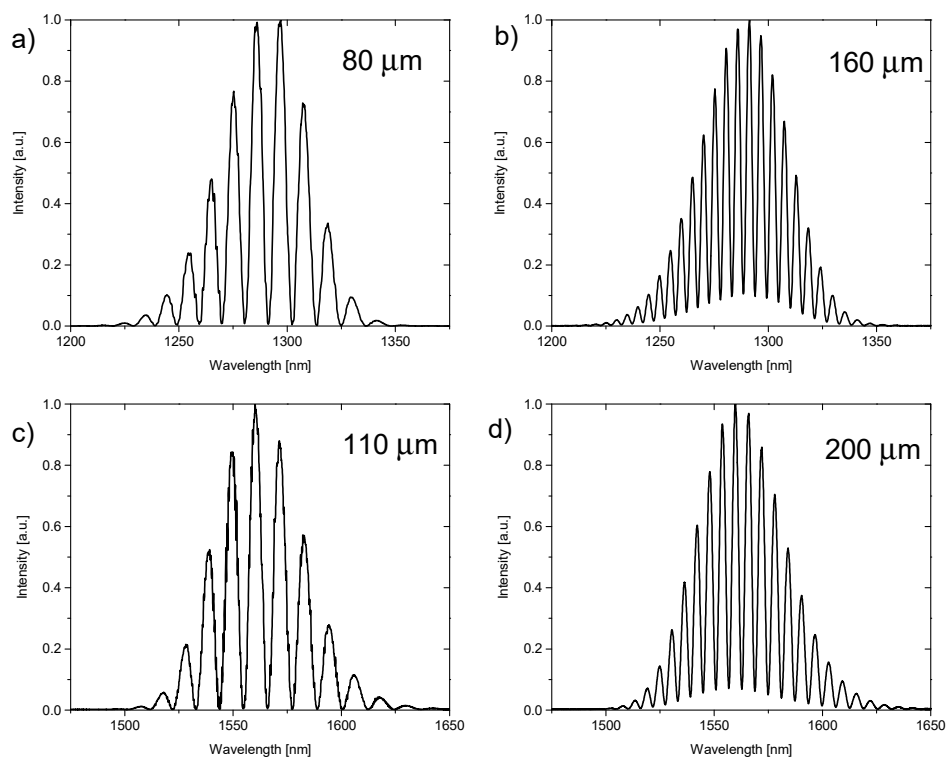


Figure 3. Spectra measured on BD-NCD-Si while the cavity was filled with air. Spectra obtained for 1290 nm and cavity lengths (a) 80 μm and (b) 160 μm . Spectra obtained for 1560 nm and cavity lengths (c) 110 μm and (d) 200 μm .

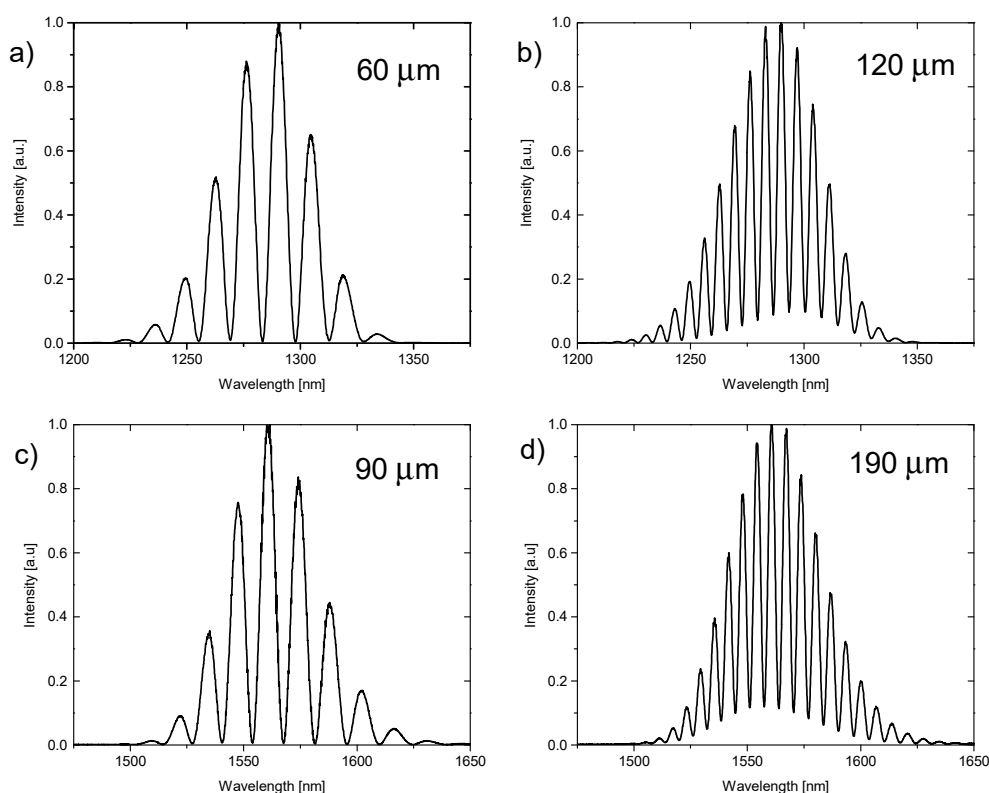


Figure 4. Spectra measured on ND-NCD-Si while the cavity was filled with air. Spectra obtained for 1290 nm and cavity lengths (a) 60 μm and (b) 120 μm . Spectra obtained for 1560 nm and cavity lengths (c) 90 μm and (d) 190 μm .

3. Results

The measurement signals were recorded with the use of an optical spectrum analyzer. The representative spectra are shown in Figure 5.

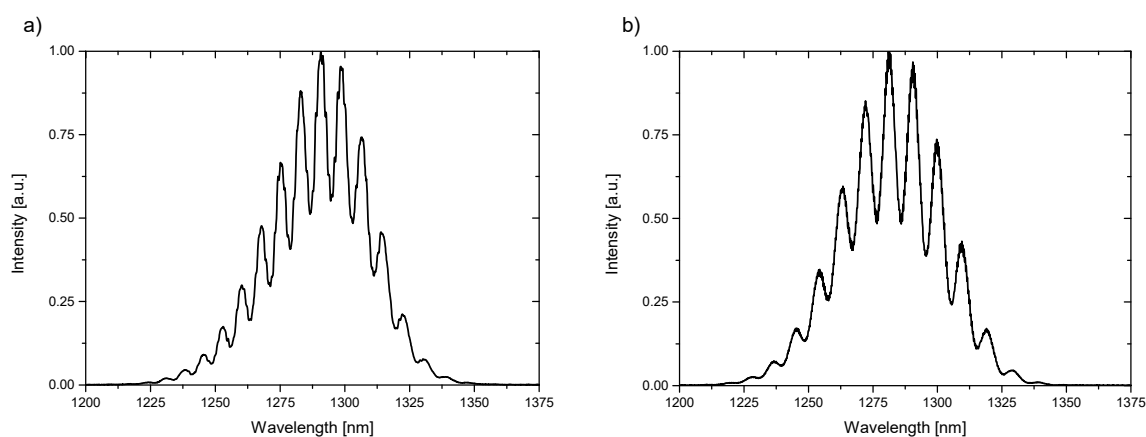


Figure 5. Spectra of liquid with refractive index $n = 1.4$ measured with a wavelength of 1290 nm (a) BD-NCD-Si, (b) ND-NCD-Si.

The obtained spectra were analyzed regarding the spectral separation between the maxima in the spectra for measured refractive indices of liquids. The results of these investigations for the light sources with a central wavelength equal to 1290 nm are presented in Figure 6.

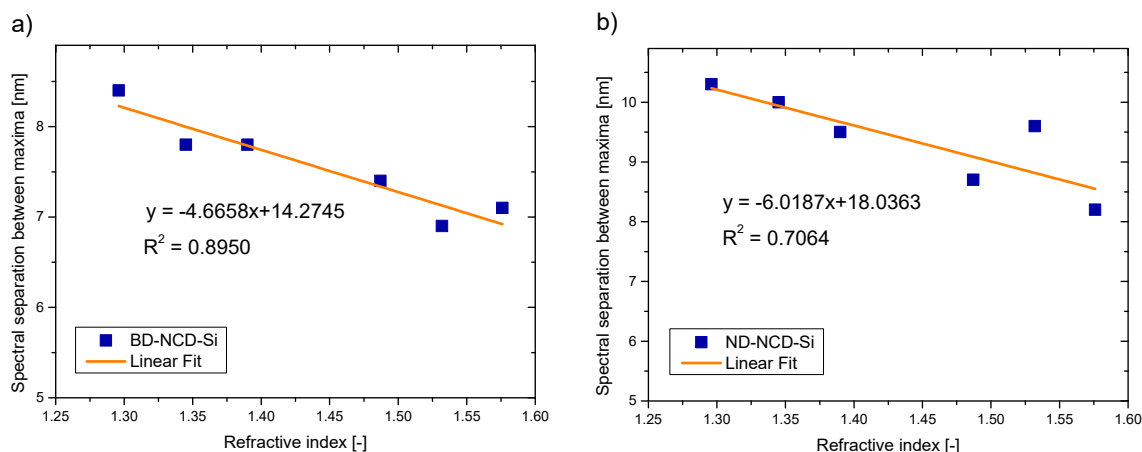


Figure 6. Measurement results: spectral separation between maxima as a function of refractive index for wavelength equal to 1290 nm (a) BD-NCD-Si, (b) ND-NCD-Si.

The values of correlation coefficient R^2 and sensitivity S for each sensor working at central wavelength of 1290 nm are presented in Table 2. The sensitivity can be directly found from the slope of the linear fit [9]. The values of R^2 parameter in the range of 0.7–0.9 indicate high positive/negative correlation, while values higher than 0.9 mean very high positive/negative correlation [23].

Table 2. Correlation coefficient (R^2) and sensitivity (S) values for sensors working at 1290 nm.

Parameters	BD-NCD-Si	ND-NCD-Si
R^2	0.8950	0.7064
S (nm/a.u.)	−4.6658	−6.0187

Similarly, the same procedure of data analysis was applied to the measurement data collected with the use of a source working at central wavelength of 1560 nm. The representative measurement spectra are shown in Figure 7.

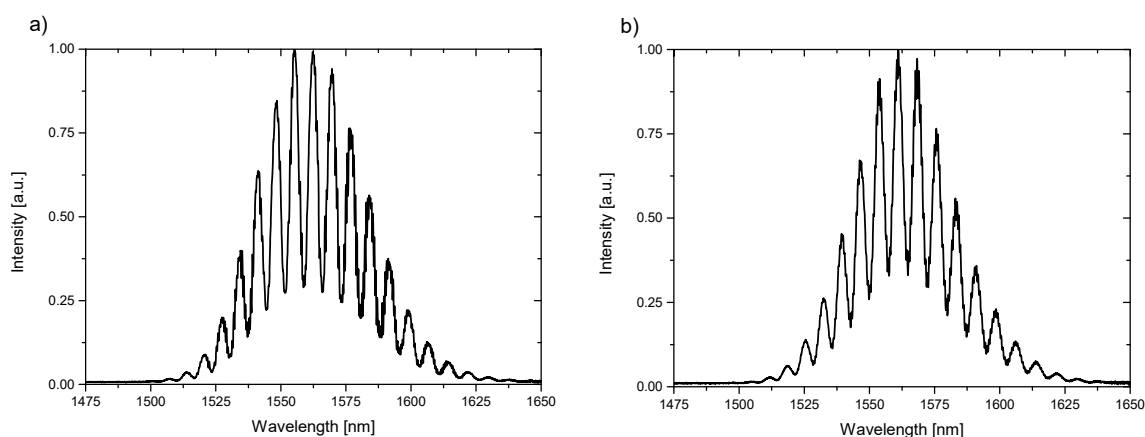


Figure 7. Spectra of liquid with refractive index $n = 1.6$ measured with a wavelength of 1560 nm (a) BD-NCD-Si, (b) ND-NCD-Si.

Figure 8 presents the relationship between the spectral separation of the interferometric fringes and the refractive index.

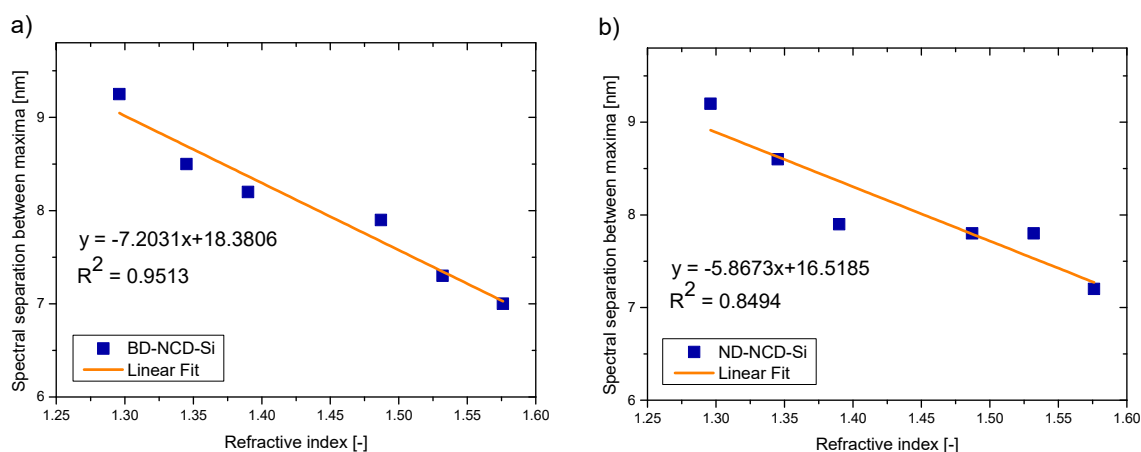


Figure 8. Measurement results: spectral separation between maxima as a function of refractive index for wavelength equal to 1560 nm (a) BD-NCD-Si, (b) ND-NCD-Si.

The values of correlation coefficient R^2 and sensitivity S for each sensor working at central wavelength of 1560 nm are calculated and presented in Table 3.

Table 3. Correlation coefficient (R^2) and sensitivity (S) values for sensors working at 1560 nm.

Parameters	BD-NCD-Si	ND-NCD-Si
R^2	0.9513	0.8494
S (nm/a.u.)	-7.2031	-5.8673

It can be noted that all investigated samples can be applied as reflective surfaces in fiber-optic sensors of refractive index. The dependence between the spectral separation and refractive index is linear in each case, with a high or very high value of correlation coefficient R^2 .

The small reduction in sensitivity for the nitrogen-doped NCD can result from the lower value of reflectivity assured by this film in comparison with the boron-doped NCD film. The sensitivity is directly related to the reflection assured by the reflective film implemented in the sensor. The reflectivity of the surface is dependent on its refractive index. Reflectivity R at the boundary between the diamond film and the medium can be calculated by use of the Fresnel equation [24]:

$$R = \left(\frac{n_2 - n_1}{n_1 + n_2} \right)^2 \quad (2)$$

where: n_1, n_2 are the refractive indices of the medium and NCD diamond film, respectively.

For the BD-NCD-Si sample, the value of the refractive index increases with the increase of wavelength, which results in a higher value of reflectivity. For the ND-NCD-Si sample, the value of the refractive index decreases with the increase of wavelength, which results in a lower value of reflectivity. The reflectivity for the BD-NCD-Si sample increased by 3.6% with the wavelength, while the reflectivity of the ND-NCD-Si sample decreased by 0.79%.

4. Conclusions

In this paper we reported the application of doped NCD films to fiber-optic interferometric sensors. The sensors are dedicated to the measurement of the refractive index of liquids. The experiments included NCD films doped with nitrogen and boron. The diamond films were produced using a microwave plasma enhanced chemical vapor deposition system. The investigation was performed in the refractive index range between 1.3–1.6. The linear mathematical models were adopted to the measurement data, allowing for determination of correlation coefficients R^2 and sensitivity values for

each sensor. The achieved values of R^2 in the range of 0.7–0.9 and higher than 0.9 show high and very high negative correlation between the spectral separation of the fringes in the spectrum and the value of the refractive index. The initial study showed that the use of doped diamond films as reflective surfaces in sensors of refractive index is possible. This approach assures better resistance to chemical and mechanical damage prolonging the lifespan of sensors and allowing measurements of aggressive chemicals and biological samples.

Author Contributions: Conceptualization M.K., D.M. and M.S.; methodology D.M. and M.S.; validation M.K.; data analysis M.K. and D.M.; investigation M.K.; samples preparation K.J.S., M.F. and K.H.; data curation M.K.; writing—original draft preparation M.K., K.J.S., D.M., M.F., K.H. and M.S.; writing—review and editing K.H. and M.S.; visualization M.K.; supervision, K.H. and M.S.; project administration M.S. and D.M.; funding acquisition M.K., D.M. and M.S.

Funding: The authors want to acknowledge the financial support of the Polish National Science Centre under Grant No. 2017/25/N/ST7/01610, the Polish National Centre for Research and Development under the project Techmatstrateg Diamsec 347324, DS Programs of Faculty of Electronics, Telecommunications and Informatics of Gdańsk University of Technology and the project no MNiD/2018/2019/4. M.S. acknowledges the scholarship from the Bekker Programme PPN/BEK/2018/1/00185 funded by the Polish National Agency for Academic Exchange. K.J.S. and K.H. want to acknowledge the financial support from the Methusalem “NANO” network.

Conflicts of Interest: The authors declare no conflict of interest.

References

- Chiavaioli, F.; Baldini, F.; Tombelli, S.; Trono, C.; Giannetti, A. Biosensing with optical fiber gratings. *Nanophotonics* **2017**, *6*, 663–679. [[CrossRef](#)]
- Chaudhari, A.L.; Shaligram, A.D. Fiber optic sensor for the measurement of concentration and refractive index of liquids based on intensity modulation. *Int. J. Mod. Phys. Conf. Ser.* **2012**, *6*, 589–593. [[CrossRef](#)]
- Ahsani, V.; Ahmed, F.; Jun, M.B.G.; Bradley, C. Tapered Fiber-Optic Mach-Zehnder Interferometer for Ultra-High Sensitivity Measurement of Refractive Index. *Sensors* **2019**, *19*, 1652. [[CrossRef](#)] [[PubMed](#)]
- Zhang, T.; Feng, G.; Song, Z.; Zhou, S. A single-element interferometer for measuring refractive index of transparent liquids. *Opt. Commun.* **2014**, *332*, 14–17. [[CrossRef](#)]
- Kaneko, K.; Yoshimura, Y.; Shimizu, A. Water concentration dependence of the refractive index of various ionic liquid-water mixtures. *J. Mol. Liquids* **2018**, *250*, 283–286. [[CrossRef](#)]
- Rodionov, S.A.; Remnev, M.A.; Klimov, V.V. Refractive index sensor based on all-dielectric gradient metasurface. *Sens. Bio-Sens. Res.* **2019**, *22*, 100263. [[CrossRef](#)]
- Nath, P.; Singh, H.K.; Datta, P.; Sarma, K.C. All-fiber optic sensor for measurement of liquid refractive index. *Sens. Actuators A Phys.* **2008**, *148*, 16–18. [[CrossRef](#)]
- Yüksel, K. Optical fiber sensor system for remote and multi-point refractive index measurement. *Sens. Actuators A Phys.* **2016**, *250*, 29–34. [[CrossRef](#)]
- Chiavaioli, F.; Gouveia, C.A.J.; Jorge, P.A.S.; Baldini, F. Towards a Uniform Metrological Assessment of Grating-Based Optical Fiber Sensors: From Refractometers to Biosensors. *Biosensors* **2017**, *7*, 23. [[CrossRef](#)]
- Chiavaioli, F.; Zubiarte, P.; Del Villar, I.; Zamarreño, C.R.; Giannetti, A.; Tombelli, S.; Trono, C.; Arregui, F.J.; Matias, I.R.; Baldini, F. Femtomolar Detection by Nanocoated Fiber Label-Free Biosensors. *ACS Sens.* **2018**, *3*, 936–943. [[CrossRef](#)]
- Sobaszek, M.; Skowroński, Ł.; Bogdanowicz, R.; Siuzdak, K.; Cirocka, A.; Zięba, P.; Gnyba, M.; Naparty, M.; Gołński, Ł.; Płotka, P. Optical and electrical properties of ultrathin transparent nanocrystalline boron-doped diamond electrodes. *Opt. Mater.* **2015**, *42*, 24–34. [[CrossRef](#)]
- Ficek, M.; Sobaszek, M.; Gnyba, M.; Ryl, J.; Gołński, Ł.; Smietana, M.; Jasiński, J.; Caban, P.; Bogdanowicz, R. Optical and electrical properties of boron doped diamond thin conductive films deposited on fused silica glass substrates. *Appl. Surf. Sci.* **2016**, *387*, 846–856. [[CrossRef](#)]
- Ficek, M.; Sankaran, K.J.; Ryl, J.; Bogdanowicz, R.; Lin, I.-N.; Haenen, K.; Darowicki, K. Ellipsometric investigation of nitrogen doped diamond thin films grown in microwave CH₄/H₂/N₂ plasma enhanced chemical vapor deposition. *Appl. Phys. Lett.* **2016**, *108*, 241906. [[CrossRef](#)]
- Majchrowicz, D.; Kosowska, M.; Struk, P.; Jędrzejewska-Szczerska, M. Tailoring the Optical Parameters of Optical Fiber Interferometer with Dedicated Boron-Doped Nanocrystalline Diamond Thin Film. *Phys. Status Solidi A* **2017**, *214*, 1700222. [[CrossRef](#)]

15. Milewska, D.; Karpienko, K.; Jędrzejewska-Szczerska, M. Application of thin diamond films in low-coherence fiber-optic Fabry Pérot displacement sensor. *Diam. Mater.* **2016**, *64*, 169–176. [[CrossRef](#)]
16. Kosowska, M.; Majchrowicz, D.; Sankaran, K.J.; Ficek, M.; Jędrzejewska-Szczerska, M.; Haenen, M.K. Nitrogen-doped diamond thin films: Potential application in Fabry-Pérot interferometer. *Proc. SPIE* **2017**, *10716*, 1071614.
17. Majchrowicz, D.; Kosowska, M.; Sankaran, K.J.; Struk, P.; Wąsowicz, M.; Sobaszek, M.; Haenen, K.; Jędrzejewska-Szczerska, M. Nitrogen-Doped Diamond Film for Optical Investigation of Hemoglobin Concentration. *Materials* **2018**, *11*, 109. [[CrossRef](#)]
18. Jędrzejewska-Szczerska, M.; Majchrowicz, D.; Hirsch, M.; Struk, P.; Bogdanowicz, R.; Bechelany, M.; Tuchin, V.V. *Nanotechnology and Biosensors: Nanolayers in Fiber-Optic Biosensing*; Elsevier: Amsterdam, The Netherlands, 2018.
19. Ficek, M.; Bogdanowicz, R.; Ryl, J. Nanocrystalline CVD Diamond Coatings on Fused Silica Optical Fibers: Optical Properties Study. *Acta Phys. Polonica A* **2015**, *127*, 868–873. [[CrossRef](#)]
20. Bogdanowicz, R.; Śmietana, M.; Gnyba, M.; Ficek, M.; Straňák, V.; Goluński, Ł.; Sobaszek, M.; Ryl, J. Nucleation and growth of CVD diamond on fused silica optical fibres with titanium dioxide interlayer. *Phys. Status Solidi A* **2013**, *210*, 1991–1997. [[CrossRef](#)]
21. Dec, B.; Ficek, M.; Ryciewicz, M.; Macewicz, Ł.; Gnyba, M.; Sawczak, M.; Sobaszek, M.; Bogdanowicz, R. Gas Composition Influence on the Properties of Boron-Doped Diamond Films Deposited on the Fused Silica. *Mater. Sci.-Poland* **2018**, *36*, 288–296. [[CrossRef](#)]
22. Hirsch, M.; Majchrowicz, D.; Wierzba, P.; Weber, M.; Bechelany, M.; Jędrzejewska-Szczerska, M. Low-Coherence Interferometric Fiber-Optic Sensors with Potential Applications as Biosensors. *Sensors* **2017**, *17*, 261. [[CrossRef](#)] [[PubMed](#)]
23. Mukaka, M. A guide to appropriate use of Correlation coefficient in medical research. *Malawi Med J.* **2012**, *24*, 69–71. [[PubMed](#)]
24. Grattan, L.S.; Meggitt, B.T. *Optical Fiber Sensor Technology*; Springer: Boston, MA, USA, 2000.



© 2019 by the authors. Licensee MDPI, Basel, Switzerland. This article is an open access article distributed under the terms and conditions of the Creative Commons Attribution (CC BY) license (<http://creativecommons.org/licenses/by/4.0/>).

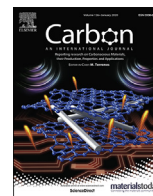
**[MK3] Nanocrystalline Diamond Sheets as Protective Coatings for Fiber-Optic
Measurement Head.**

Kosowska, M.; Majchrowicz, D.; Ficek, M.; Wierzba, P.; Fleger, Y.; Fixler, D.; Szczerska, M.

Carbon 2020, 156, 104–109, doi:10.1016/j.carbon.2019.09.042.

The author's contributions were:

conceiving and designing the experiments, developing a procedure of NDS transfer, performing measurements, data analysis and writing selected parts of the original manuscript.



Nanocrystalline diamond sheets as protective coatings for fiber-optic measurement head

Monika Kosowska^a, Daria Majchrowicz^{a,*}, Mateusz Ficek^a, Paweł Wierzba^a,
Yafit Fleger^b, Dror Fixler^{b,c}, Małgorzata Szczerska^{a,**}

^a Department of Metrology and Optoelectronics, Faculty of Electronics, Telecommunications and Informatics, Gdańsk University of Technology, 11/12 Narutowicza Street, 80-233, Gdańsk, Poland

^b Institute for Nanotechnology and Advanced Materials, Bar-Ilan University, Ramat-Gan, 52900, Israel

^c Faculty of Engineering, Institute of Nanotechnology and Advanced Materials, Bar-Ilan University, Ramat-Gan, 52900, Israel

ARTICLE INFO

Article history:

Received 8 July 2019

Received in revised form

12 September 2019

Accepted 14 September 2019

Available online 17 September 2019

ABSTRACT

Fiber-optic sensors find numerous applications in science and industry, but their full potential is limited because of the risk of damaging the measurement head, in particular, due to the vulnerability of unprotected tips of the fiber to mechanical damage and aggressive chemical agents. In this paper, we report the first use of a new nanocrystalline diamond structure in a fiber-optic measurement head as a protective coating of the fiber tip. The nanocrystalline sheet structures, produced with the use of Microwave Plasma Assisted Chemical Vapor Deposition System (MW PA CVD), were characterized by Scanning Electron Microscopy (SEM) and successfully transferred from the deposition substrate onto the surface of the tip of a single-mode fiber sensor head. A Fabry-Perot sensing interferometer for distance measurement comprising that fiber was built. The measurement results were compared with numerical modeling. High values of achieved correlation coefficients ($R^2 > 0.99$) between a linear model and distance measurements data indicate that the diamond sheet does not affect the correct operation of the sensor while extending its potential scope of applications.

© 2019 Elsevier Ltd. All rights reserved.

1. Introduction

Fiber-optic sensors are used in many fields of science and technology [1]. They have become an alternative to conventional measurement methods due to their excellent properties, such as high sensitivity and wide dynamic range of measurements or resistance to ionizing radiation. They are used in the automotive industry [2], aviation and marine [3], power engineering [4], chemistry [5] and medicine [6]. They are used to measure values of physical and chemical quantities, such as: temperature [7,8], refractive index [9–11], pH [12,13], pressure [14,15], displacement [16,17], stress [18,19] and others [20–25]. They enable measurements in places hard to reach and in difficult working conditions, in particular, in the presence of strong electromagnetic fields or radiation. A wide range of potential applications of fiber-optic sensors

makes it necessary to search for new materials whose optical properties would enable their use in the sensor structure [26].

One of the biggest scientific interest of many group is the use of new materials in fiber-optic sensors to enhance their metrological parameters and extend possibilities of their use thanks to e.g. higher mechanical resistance of their components. The development of nanotechnology and thin film deposition techniques (e.g. CVD, ALD) has opened up new possibilities in the construction of fiber optic sensors. This allowed the use of thin (tens of nanometers) dielectric layers (e.g. ZnO, TiO₂) as well as thin, translucent metal layers made of silver, aluminum or gold [27–29]. The use of different materials for the optical fiber sensors achieves new constructions of measurement heads with tailored properties for desired use. The metrological parameters of fiber-optic sensors are strongly determined by the optical parameters of the materials used for their construction. Thin metallic layers, e.g. ZnO, show greater sensitivity to various physical factors, such as temperature or humidity, which as result increase the sensitivity of an interferometric sensor applying them. Those materials do not show high chemical and mechanical resistance to damage.

* Corresponding author.

** Corresponding author.

E-mail addresses: darmajch@pg.edu.pl (D. Majchrowicz), mjdrzej@eti.pg.edu.pl (M. Szczerska).

The metrological parameters of fiber-optic sensors are strongly determined by the optical parameters of the materials used for their construction. Hence, it is necessary to protect the elements of the measuring head (fiber tip, mirrors). Materials protecting the elements of the sensor structure have to be characterized by high chemical stability, resistance to mechanical damage and biocompatibility in case of biomedical measurements. In the case of chemically aggressive substances measurements, failure to protect the tip of the optical fiber can result in permanent damage to the optical fiber [30,31]. The lack of protection for photonic devices, may cause poisoning of the tested biological samples or damaging them by degraded elements of measurement heads. Therefore, there is a need for elaborating new materials for protection of photonic devices.

The use of diamond structures extends the possibilities of using fiber-optic sensors dedicated for studying biological or chemically aggressive materials. Diamond structures are characterized by very high hardness (about 10,000 on the Vickers scale) [32], chemical stability, biocompatibility [33] and transparency in a wide range of optical radiation - from ultraviolet to far infrared [34]. They are particularly appreciated as hardening, abrasive [35] films, as well as being chemically inert and having a high, for dielectric material, refractive index ($n = 2.419$) [36]. Due to biocompatibility [37], chemical resistance [38] and very good mechanical properties [32] the use of diamond structures carries great potential. According to the authors' knowledge, so far, the only diamond structures used in the fiber-optic sensors have been diamond films. They were used as protection of the reflective surface or reflective surfaces themselves in the Fabry-Perot interferometer.

In this article, we report for the first time the application of nanocrystalline diamond sheet (NDS) produced in the process of Microwave Plasma Assisted Chemical Vapor Deposition (MW PA CVD) [39] as a protection of the optical fiber sensor head. The NDS was attached to the face of the fiber increasing its resistance to damage. The proper selection of the parameters for the deposition process of diamond structures allowed their use as protecting surfaces of the optical fiber heads. The use of diamond sheets in fiber-optic sensors will allow the measurements of biological materials that have been very difficult to date and in some cases impossible to perform, as well as enable the examination of chemically aggressive substances that damage the fiber-optic sensor measuring heads.

2. Numerical modeling

The sensing interferometer considered in this study is a Fabry-Perot interferometer operating in the reflective mode, connected to the measurement system by a standard single-mode fiber SMF-28 [40]. The cavity of this interferometers is planar, formed by a plane mirror and the end-face of the fiber. A diamond sheet on the fiber end-face modifies reflective properties of the fiber and protects it against mechanical damage and chemical aggression, as shown in Fig. 1.

The propagation of optical radiation in such interferometers can be described using the Gaussian beam formalism [41–44]. Since the thickness of the nanocrystalline diamond sheet compared to the length of the cavity is small, it is assumed that the Gaussian beam does not expand appreciably when traversing this film. Therefore, in further analysis, the diamond film is to be replaced by a planar reflective surface, whose reflection and transmission coefficients are calculated using the plane wave approach [43]. This results in a tractable single-cavity model of the sensing interferometer.

First, the reflectance of the nanocrystalline diamond sheet deposited on the fiber was calculated, assuming that the fiber and the nanocrystalline diamond sheet are placed in the air ($n = 1.00$).

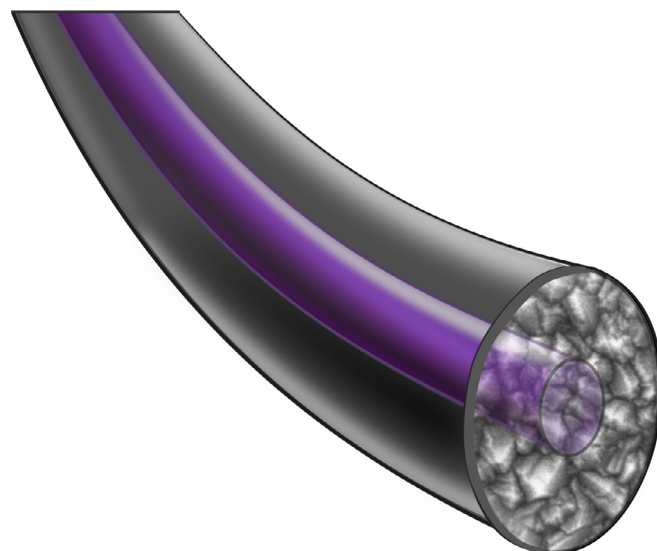


Fig. 1. Sensing head with a nanocrystalline diamond sheet (NDS).

Refractive indices for the fiber and diamond obtained from Refs. [45,46] respectively, were used in the modeling. The thickness of the NDS was assumed to be in the range from 100 nm to 1100 nm, depending on the time of growth. The calculations were conducted for the wavelength equal to 1560 nm, which is the central wavelength of the superluminescent source used in the experimental part of this study. Reflectance as a function of the thickness of the NDS is presented in Fig. 2.

As expected, the reflectance varies periodically with the thickness of the nanocrystalline diamond sheet from 0.033 to 0.265. By selecting the proper thickness of the sheet, it is possible to obtain either reflectance close to that of a bare fiber tip, or much higher.

3. Materials

3.1. Nanocrystalline diamond sheet fabrication

The NDS were synthesized in an MW PA CVD system (SEKI

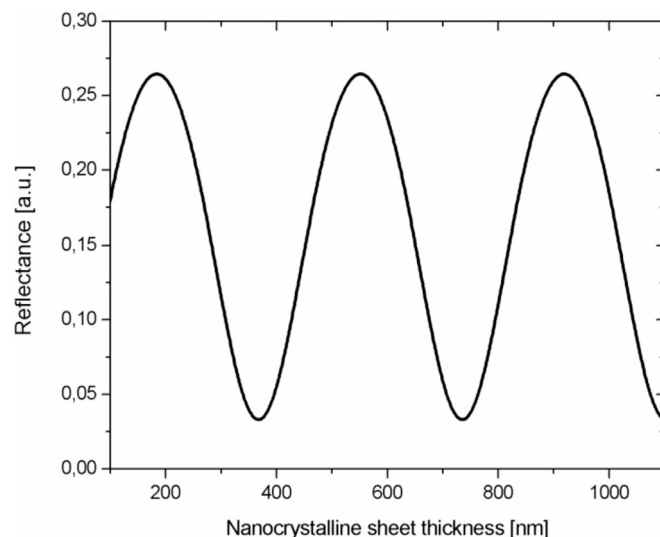


Fig. 2. Numerical modeling of the reflectance as a function of nanocrystalline diamond sheet thickness.

Technotron Ax5400S) on mirror-polished tantalum sheets (Sigma-Aldrich Chemie, 0.025 mm thick, 99.9+% metal basis). Substrates were seeded in an ultrasonic bath [46]. During the growth process, the graphite stage was heated to 500 °C and controlled by the thermocouple. The purities of the gases H₂ and CH₄ were 6.0 N and 5.5 N respectively. The CH₄:H₂ molar ratio of the mixture was set at 1% of gas volume at 300 sccm total flow rate. The optimized plasma microwave power of 1100 W was applied during the synthesis of diamond sheets. The growth time was 120 min. NDS are showing low adhesion to the tantalum substrate. Mechanical delamination of a diamond foil with internal strain and stress allows to form free-standing sheets, which can be easily transferred to the optical fiber head. The main difficulty in NDS fabrication in comparison to well-known fabrication process of nanocrystalline diamond films [33,43] is that we must obtain samples with very low adhesion to the substrate which allows us to extract sheets and apply them to the fiber head, whereas nanocrystalline diamond film fabrication process have been always optimized to obtain as good adhesion to the substrates as possible.

3.2. Nanocrystalline diamond sheet characterization

Characterization of the investigated NDS sample was performed to determine surface properties and to assess the possibility of using it as a protective film. In order to detect the morphology as well as the thickness of the NDS, the measurements were performed using Dual-beam system Helios 600 (FEI, Hillsboro, Oregon, USA) with SEM voltage-current of 2 kV and 0.17 nA. Cross-section cuts were done using Ga FIB with voltage-current of 30 kV and 0.28 nA. The results are presented in Fig. 3.

As can be noticed from Fig. 3a, the film consists of nanocrystallites. The NDS sheet is continuous and the crystallites are equally distributed. The surface is homogenous and continuous without any cracks. The image captured with 65 000x magnification shows that the size of the crystallites is smaller than 1 μm. Fig. 3b presents the cross-section of the investigated sample that allowed us to determine its thickness - 807 nm.

3.3. Measurement setup

The measurements were performed with the use of a fiber-optic interferometer in a Fabry-Perot configuration shown in Fig. 4. The sensor was operating in reflective mode. The setup was constructed of a superluminescent diode (S1550-G-I-10, Superlum, Ireland) with central wavelength $\lambda = 1560$ nm and full width at half maximum $\lambda\text{FWHM} = 45$ nm, single-mode telecommunication

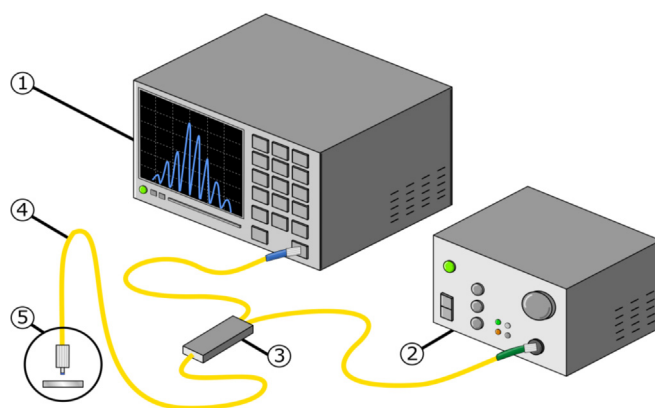


Fig. 4. Measurement setup: 1 – optical spectrum analyzer, 2 – superluminescent diode, 3 – fiber-optic 2x1 coupler, 4 – single-mode fiber-optic, 5 – measurement head with NDS and silver mirror.

optical fibers (SMF-28, Thorlabs, USA), 2x1 fiber-optic coupler and optical spectrum analyzer (AQ6319, Ando, Japan). The polished tip of the optical fiber was used as the measurement head, the principle of operation of this setup is described in detail by Majchrowicz et al. [47].

In the implemented setup the optical path difference (OPD) has an impact on a phase difference between interfering beams. The change of OPD can be caused by the change of the refractive index of the medium inside the cavity or by the change of a geometrical path length. In order to assess the influence of NDS on the operation of the sensor, we performed distance measurements. Firstly, the reference measurements were performed with the use of a silver mirror and fiber-optic measurement head without the NDS. Secondly, the NDS was transferred onto the fiber-optic measurement head. The free-standing NDS was attached to the fiber by touching it with the fiber head, resulting in joining them with the means of van der Waals forces. The distance was measured to 1000 μm, the increment up to 300 μm was equal to 20 μm, and in the range of 300–1000 μm the increment was 100 μm.

4. Results and discussion

The reflectance spectra calculations for the interferometer with a silver mirror and NDS illuminated by a superluminescent source whose central wavelength was 1560 nm and full width at half maximum of the spectrum was 45 nm were performed. The

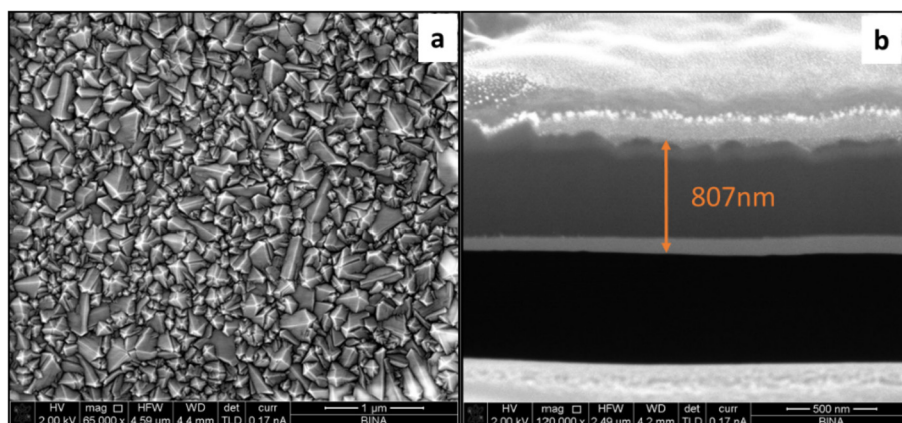


Fig. 3. SEM images of the nanocrystalline diamond sheet sample: a) morphology of the sheet, b) cross-section image in order to measure the thickness.

thickness of the NDS was set to 807 nm, as measured by Scanning Electron Microscope (c.f. subsection 3.2.). Calculations were performed for the cavity filled with air ($n = 1.00$) whose length was determined from experimental data.

The achieved measurement results were plotted in Fig. 5 for nominal values of cavity length of 100 μm , 160 μm , 500 μm , and 900 μm . The spectra obtained by the means of numerical modeling were superimposed on experimental data in Fig. 5. Experimental data corresponding to cavity length of 900 μm has a markedly smaller amplitude of the spectral fringes than that of the calculated spectrum. This phenomenon is most probably caused by the fact that the optical spectrum analyzer does not sample the spectrum in discrete wavelength points but records intensity in a sequence of wavelength intervals leading to some averaging in the recorded signal. Since for the 900 μm cavity the number of intervals per one fringe is the smallest, the averaging effect is most readily apparent.

The obtained measurement spectra were used to investigate the measurement characteristics of the sensing head, i.e. the relationship between the length of the cavity and the number of spectral fringes in the wavelength range of 1520–1620 nm. The experimental data showed a linear relationship between a number of maxima in the spectrum and a cavity length. Thus, the linear mathematical model was fitted to them, as shown in Fig. 6, along with the formula and value of correlation coefficient R^2 .

The very high value of the correlation coefficient R^2 (0.999)

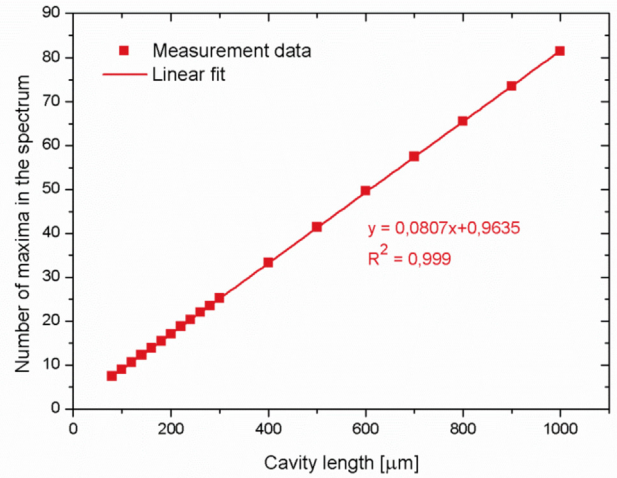


Fig. 6. Measurements results – number of maxima in the spectrum as a function of the cavity length.

indicates that the fitting quality of the mathematical model to the measurement data is excellent. The investigated sensing head can provide accurate measurement results without any detectable

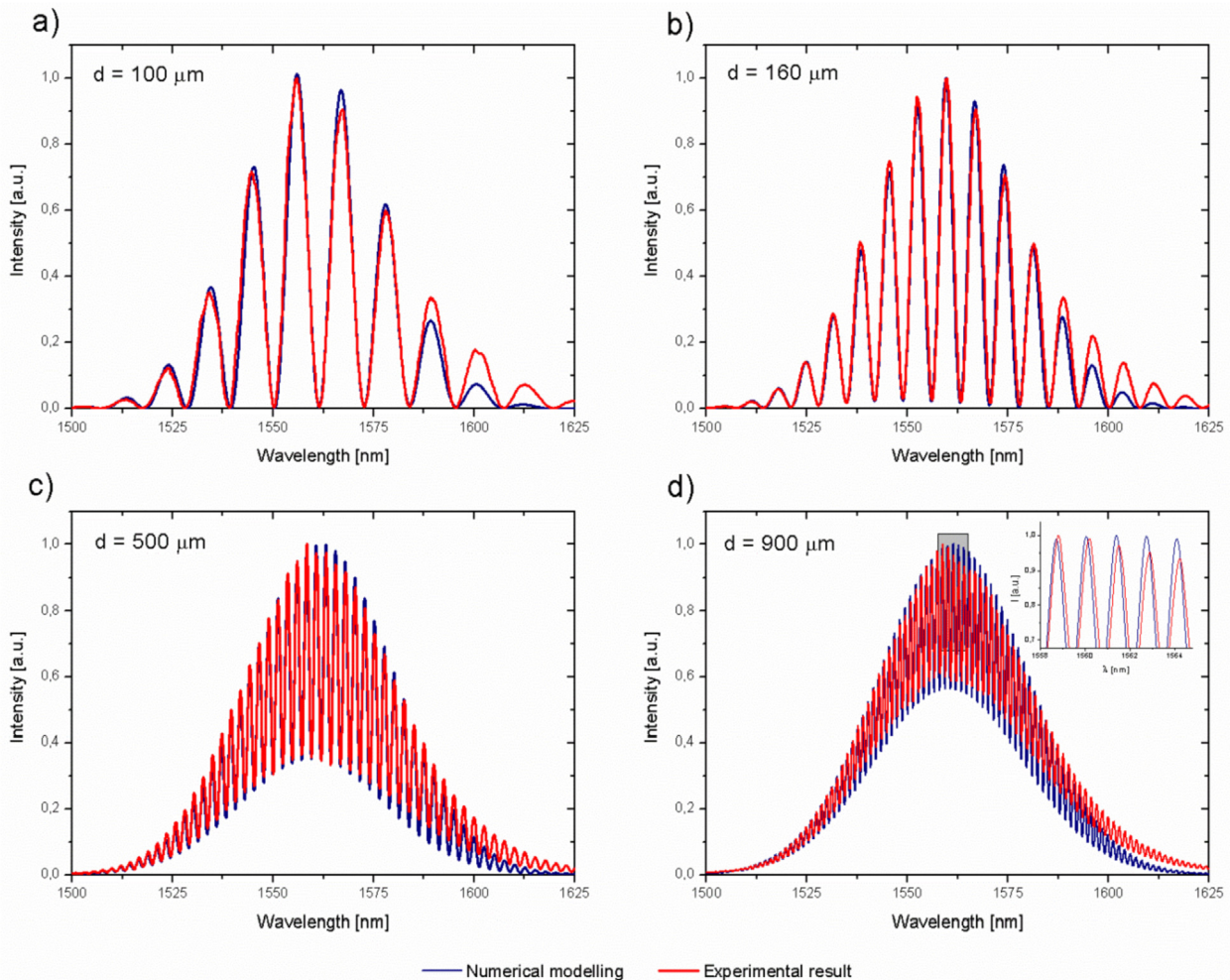


Fig. 5. Comparison of numerical modeling and measurement results. The cavity length was set to a) 100 μm b) 160 μm c) 500 μm d) 900 μm .

degradation introduced by the nanodiamond structure. Therefore, NDS can be successfully used as protective coatings for fiber-optic measurement heads.

5. Conclusion

In this paper, we reported for the first time the use of NDS in a fiber-optic measurement head. The NDS transferred onto the fiber head served as a protective coating. Numerical modeling and experiments were performed to assess the impact of the NDS on the performance of a Fabry–Perot interferometric sensing head. The results of experiments are consistent with those of numerical modeling confirming the successful implementation of the proposed solution. Data analysis of the distance measurements showed correlation coefficient $R^2 > 0.99$ indicating that the NDS does not affect the correct operation of the sensor. Moreover, its application can prolong the lifespan of the sensors and extend their scope of applications, especially in harsh environmental conditions. The promising results of the research constitute a strong basis for future research on the use of NDS in optical fiber sensors.

Acknowledgements

This work was supported by the Polish National Science Centre under Grant No. 2017/25/N/ST7/01610, the Polish National Center for Research and Development under the project Technatstrateg Diamsec 347324, DS Programs of Faculty of Electronics, Telecommunications and Informatics of Gdańsk University of Technology.

References

- [1] E. Udd, An overview of fiber-optic sensors, *Rev. Sci. Instrum.* 66 (1995) 4015–4030, <https://doi.org/10.1063/1.1145411>.
- [2] A. Davanlou, Integration of fiber-optic sensors in measuring machines, *Measurement* 57 (2014) 25–32, <https://doi.org/10.1016/j.measurement.2014.07.004>.
- [3] C. Baldwin, *Opto-Mechanical Fiber Optic Sensors*, Butterworth-Heinemann, 2018, <https://doi.org/10.1016/B978-0-12-803131-5.00008-8>.
- [4] K. Bohnert, P. Gabus, J. Kostovic, H. Brändle, Optical fiber sensors for the electric power industry, *Opt. Lasers Eng.* 43 (2005) 511–526, <https://doi.org/10.1016/j.optlaseng.2004.02.008>.
- [5] G. Liu, N. Hu, Z. Ma, R. Li, A portable analyzer based on a novel optical structure for urine dry-chemistry analysis, *J. Inst. Met.* 13 (2018) T07002, <https://doi.org/10.1088/1748-0221/13/07/T07002>.
- [6] K. Wysockiński, D. Budnicki, J. Fidelus, E. Szostkiewicz, Ł. Ostrowski, M. Murawski, M. Staniszewski, M. Staniszevska, M. Napierala, T. Nasitowski, Dual-core all-fiber integrated immunosensor for detection of protein antigens, *Biosens. Bioelectron.* 114 (2018) 22–29, <https://doi.org/10.1016/j.bios.2018.05.008>.
- [7] A. Leal-Junior, A. Frizzera-Neto, C. Marques, M.J. Pontes, A polymer optical fiber temperature sensor based on material features, *Sensors* 18 (2018) 301, <https://doi.org/10.3390/s18010301>.
- [8] S. Poeggel, D. Duraibabu, K. Kalli, G. Leen, G. Dooly, E. Lewis, J. Kelly, M. Munroe, Recent improvement of medical optical fibre pressure and temperature sensors, *Biosensors* 5 (2015) 432–449, <https://doi.org/10.3390/bios5030432>.
- [9] M. Jędrzejewska-Szczerska, Measurement of complex refractive index of human blood by low-coherence interferometry, *Eur. Phys. J. Spec. Top.* 222 (2013) 2367–2372, <https://doi.org/10.1140/epjst/e2013-02018-7>.
- [10] N. Uddin, Microfluidic enhanced fabry-perot etalon based optical biosensor for the detection of biological substances in liquid with refractive index measurement, electronic theses and dissertations. <https://openprairie.sdstate.edu/etd/1667>, 2017.
- [11] Z. Zhang, S. Li, Q. Liu, X. Feng, S. Zhang, Y. Wang, J. Wu, Groove micro-structure optical fiber refractive index sensor with nanoscale gold film based on surface plasmon resonance, *Opt. Fiber Technol.* 43 (2018) 45–48, <https://doi.org/10.1016/j.yofte.2018.04.009>.
- [12] S. Islam, H. Bakhtiar, S. Naseem, M.S.B. Abd Aziz, N. Bidin, S. Riaz, J. Ali, Surface functionality and optical properties impact of phenol red dye on mesoporous silica matrix for fiber optic pH sensing, *Sens. Actuators.A.Phys.* 276 (2018) 267–277, <https://doi.org/10.1016/j.sna.2018.04.027>.
- [13] A.K. Pathak, D.K. Chaudhary, V.K. Singh, Broad range and highly sensitive optical pH sensor based on Hierarchical ZnO microflowers over tapered silica fiber, *Sens. Actuators.A.Phys.* (2018), <https://doi.org/10.1016/j.sna.2018.08.013>.
- [14] J. Eom, C.-J. Park, B.H. Lee, J.-H. Lee, I.-B. Kwon, E. Chung, Fiber optic Fabry–Perot pressure sensor based on lensed fiber and polymeric diaphragm, *Sens. Actuators.A.Phys.* 225 (2015) 25–32, <https://doi.org/10.1016/j.sna.2015.01.023>.
- [15] K. Chen, Z. Gong, M. Guo, S. Yu, C. Qu, X. Zhou, Q. Yu, Fiber-optic Fabry–Perot interferometer based high sensitive cantilever microphone, *Sens. Actuators.A.Phys.* 279 (2018) 107–112, <https://doi.org/10.1016/j.sna.2018.06.010>.
- [16] Y. Huang, J. Tao, X. Huang, Y.W. Huang, J. Tao, X.G. Huang, Research progress on F-P interference—based fiber-optic sensors, *Sensors* 16 (2016) 1424, <https://doi.org/10.3390/s16091424>.
- [17] Y. Zheng, D. Huang, Z.-W. Zhu, Theoretical and experimental study on fiber-optic displacement sensor with bowknot bending modulation, *Opt. Fiber Technol.* 41 (2018) 12–20, <https://doi.org/10.1016/j.yofte.2017.12.008>.
- [18] P. Jia, G. Fang, Z. Li, H. Liang, Y. Hong, T. Liang, J. Xiong, “Bellows spring-shaped” ultrasensitive fiber-optic Fabry–Perot interferometric strain sensor, *Sens. Actuators.A.Phys.* 277 (2018) 85–91, <https://doi.org/10.1016/j.sna.2018.04.041>.
- [19] P. Li, Z. Zhang, J. Zhang, Simultaneously identifying displacement and strain flexibility using long-gauge fiber optic sensors, *Mech. Syst. Signal Process.* 114 (2019) 54–67, <https://doi.org/10.1016/j.ymssp.2018.05.005>.
- [20] D. Sun, Y. Ran, G. Wang, Label-free detection of cancer biomarkers using an in-line taper fiber-optic interferometer and a fiber bragg grating, *Sensors* 17 (2017) 2559, <https://doi.org/10.3390/s17112559>.
- [21] P.J. Rivero, J. Goicoechea, F.J. Arregui, Optical fiber sensors based on polymeric sensitive coatings, *Polymers* 10 (2018) 280, <https://doi.org/10.3390/polym10030280>.
- [22] L. Zhang, Y. Jiang, J. Jia, P. Wang, S. Wang, L. Jiang, Fiber-optic micro vibration sensors fabricated by a femtosecond laser, *Opt. Lasers Eng.* 110 (2018) 207–210, <https://doi.org/10.1016/j.optlaseng.2018.06.003>.
- [23] T. Liu, Y. Wei, G. Song, B. Hu, L. Li, G. Jin, J. Wang, Y. Li, C. Song, Z. Shi, L. Zhao, J. Hu, W. Zhao, M. Hou, R. Li, J. Wang, Fibre optic sensors for coal mine hazard detection, *Measurement* 124 (2018) 211–223, <https://doi.org/10.1016/j.measurement.2018.03.046>.
- [24] M. Li, T. Dubaniewicz, H. Dougherty, J. Addis, Evaluation of fiber optic methane sensor using a smoke chamber, *International Journal of Mining Science and Technology* (2018), <https://doi.org/10.1016/j.ijmst.2018.05.010>.
- [25] P.J. Thomas, J.O. Hellevang, A high response polyimide fiber optic sensor for distributed humidity measurements, *Sens. Actuators B Chem.* 270 (2018) 417–423, <https://doi.org/10.1016/j.snb.2018.05.011>.
- [26] M. Pisco, F. Galeotti, G. Quero, A. Iadicco, M. Giordano, A. Cusano, Miniaturized sensing probes based on metallic dielectric crystals self-assembled on optical fiber tips, *ACS Photonics* 1 (2014) 917–927, <https://doi.org/10.1021/ph500126v>.
- [27] M. Hirsch, D. Majchrowicz, P. Wierzbza, M. Weber, M. Bechelany, M. Jędrzejewska-Szczerska, Low-Coherence interferometric fiber-optic sensors with potential applications as biosensors, *Sensors (Basel)* 17 (2017), <https://doi.org/10.3390/s17020261>.
- [28] D. Majchrowicz, M. Hirsch, P. Wierzbza, M. Bechelany, R. Viter, M. Jędrzejewska-Szczerska, Application of thin ZnO ALD layers in fiber-optic fabry-perot sensing interferometers, *Sensors (Basel)* 16 (2016), <https://doi.org/10.3390/s16030416>.
- [29] M. Jędrzejewska-Szczerska, P. Wierzbza, A.A. Chaaya, M. Bechelany, P. Miele, R. Viter, A. Mazikowski, K. Karpienko, M. Wróbel, ALD thin ZnO layer as an active medium in a fiber-optic Fabry–Perot interferometer, *Sens. Actuators.A.Phys.* 221 (2015) 88–94, <https://doi.org/10.1016/j.sna.2014.11.001>.
- [30] H.E. Joe, H. Yun, S.H. Jo, M.B.G. Jun, B.-K. Min, A review on optical fiber sensors for environmental monitoring, *Int. J. Precis. Eng.Manuf.Green Technol.* 5 (2018) 173–191, <https://doi.org/10.1007/s40684-018-0017-6>.
- [31] D.D. Nolte, *Optical Interferometry for Biology and Medicine*, Springer-Verlag, New York, 2012. www.springer.com/ja/book/9781461408895. (Accessed 9 August 2018).
- [32] J. Philip, P. Hess, T. Feygelson, J.E. Butler, S. Chattopadhyay, K.H. Chen, L.C. Chen, Elastic, mechanical, and thermal properties of nanocrystalline diamond films, *J. Appl. Phys.* 93 (2003) 2164–2171, <https://doi.org/10.1063/1.1537465>.
- [33] L. Tang, C. Tsai, W.W. Gerberich, L. Kruckeberg, D.R. Kania, Biocompatibility of chemical-vapour-deposited diamond, *Biomaterials* 16 (1995) 483–488, [https://doi.org/10.1016/0142-9612\(95\)98822-V](https://doi.org/10.1016/0142-9612(95)98822-V).
- [34] X. Checoury, D. Néel, P. Boucaud, C. Gesset, H. Girard, S. Saada, P. Bergonzo, Nanocrystalline diamond photonics platform with high quality factor photonic crystal cavities, *Appl. Phys. Lett.* 101 (2012) 171115, <https://doi.org/10.1063/1.4764548>.
- [35] J. Konstanty, Chapter 8 - main application areas and operating guidelines for diamond-impregnated tools, in: *Powder Metallurgy Diamond Tools*, Elsevier Science, Amsterdam, 2005, pp. 129–147, <https://doi.org/10.1016/B978-185617440-4/50085-7>.
- [36] M. Sobaszek, Ł. Skowroński, R. Bogdanowicz, K. Siuzdak, A. Cirocka, P. Zięba, M. Gnyba, M. Naparty, Ł. Goliński, P. Piotka, Optical and electrical properties of ultrathin transparent nanocrystalline boron-doped diamond electrodes, *Opt. Mater.* 42 (2015) 24–34, <https://doi.org/10.1016/j.optmat.2014.12.014>.
- [37] M. Amaral, A.G. Dias, P.S. Gomes, M.A. Lopes, R.F. Silva, J.D. Santos, M.H. Fernandes, Nanocrystalline diamond: in vitro biocompatibility assessment by MG63 and human bone marrow cells cultures, *J. Biomed. Mater. Res.* A 87 (2008) 91–99, <https://doi.org/10.1002/jbm.a.31742>.
- [38] S.J. Bull, A. Matthews, Diamond for wear and corrosion applications, *Diam.*

- Relat. Mater. 1 (1992) 1049–1064, [https://doi.org/10.1016/0925-9635\(92\)90075-Y](https://doi.org/10.1016/0925-9635(92)90075-Y).
- [39] P. Wroczynski, R. Bogdanowicz, M. Gnyba, Optoelectronic system for investigation of CVD diamond/DLC layers growth, *Adv. Mater. Sci.* 9 (2009) 47–53, <https://doi.org/10.2478/v10077-009-0015-z>.
- [40] Corning SMF-28e Optical Fiber, (n.d.) 4.
- [41] D. Marcuse, Loss analysis of single-mode fiber splices, *The Bell System Technical Journal* 56 (1977) 703–718.
- [42] D. Marcuse, Theory of Dielectric Optical Waveguides, Elsevier, 1991, <https://doi.org/10.1016/B978-0-12-470951-5.X5001-X>.
- [43] M. Born, E. Wolf, Principles of Optics, Elsevier, 1980. <https://www.sciencedirect.com/science/book/9780080264820>. (Accessed 25 July 2018).
- [44] B.E.A. Saleh, Fundamentals of Photonics, second ed., John Wiley & Sons, Ltd, Canada, 1991. <https://www.wiley.com/en-us/Fundamentals+of+Photonics%2C+2nd+Edition-p-9780471358329>. (Accessed 25 July 2018).
- [45] Refractive index of SiO₂ (silicon dioxide, silica, quartz) - malitson (n.d.), <https://refractiveindex.info/?shelf=main&book=SiO2&page=Malitson>. (Accessed 8 April 2019).
- [46] M. Ficek, M. Sobaszek, M. Gnyba, J. Ryl, Ł. Gołuński, M. Smietana, J. Jasiński, P. Caban, R. Bogdanowicz, Optical and electrical properties of boron doped diamond thin conductive films deposited on fused silica glass substrates, *Appl. Surf. Sci.* 387 (2016) 846–856, <https://doi.org/10.1016/j.apsusc.2016.06.165>.
- [47] D. Milewska, K. Karpienko, M. Jędrzejewska-Szczerska, Application of thin diamond films in low-coherence fiber-optic Fabry Pérot displacement sensor, *Diam. Relat. Mater.* 64 (2016) 169–176, <https://doi.org/10.1016/j.diamond.2016.02.015>.

[MK4] Low-Coherence Photonic Method of Electrochemical Processes Monitoring.

Kosowska, M.; Jakóbczyk, P.; Rycewicz, M.; Vitkin, A.; Szczerska, M.

Scientific Reports 2021, 11, 12600, doi:10.1038/s41598-021-91883-z.

The author's contributions were:

conceiving, designing and performing the experiments, data analysis, graphical visualization and writing the original manuscript draft.



OPEN

Low-coherence photonic method of electrochemical processes monitoring

Monika Kosowska¹✉, Paweł Jakóbczyk¹, Michał Rycewicz¹, Alex Vitkin^{2,3,4} & Małgorzata Szczerska¹✉

We present an advanced multimodality characterization platform for simultaneous optical and electrochemical measurements of ferrocyanides. Specifically, we combined a fiber-optic Fabry–Perot interferometer with a three-electrode electrochemical setup to demonstrate a proof-of-principle of this hybrid characterization approach, and obtained feasibility data in its monitoring of electrochemical reactions in a boron-doped diamond film deposited on a silica substrate. The film plays the dual role of being the working electrode in the electrochemical reaction, as well as affording the reflectivity to enable the optical interferometry measurements. Optical responses during the redox reactions of the electrochemical process are presented. This work proves that simultaneous opto-electrochemical measurements of liquids are possible.

Global research trends are aimed at combining multiple measurement techniques using different modalities. This increases the attractive possibility of obtaining more information because of the synergy between different methods. More and complementary data can be correlated to yield new insights into the investigated samples or processes^{1,2}. For example, the combination of electrochemical and optical methods appears very promising, as these are characterized by high sensitivity and accuracy as well as the possibility of miniaturization and automation.

Different approaches to combining these methods have been proposed in the literature. Lamberti et al. presented an optoelectrochemical sensor applying modified graphene³, fluorescence and electrochemical impedance spectroscopies were combined to monitor insulin levels. Narakathu et al. built a system with a dual detection of heavy metals⁴; the electrochemical measurement was performed with electrochemical impedance spectroscopy with the use of gold interdigitated electrodes, and the optical readout was based on Raman spectroscopy. Sobaszek et al. described a setup for in situ monitoring of electropolymerization processes occurring at boron-doped diamond electrode with the use of an optical Mach–Zehnder interferometer⁵; the authors report a spectral shift resulting from surface electrode modification with melamine. Janczuk-Richet et al. constructed a setup for electrochemical reactions investigations using fiber Bragg gratings coated with ITO (indium tin oxide)^{6,7}; ITO plays the role of a working electrode in an electrochemical system and the coating increases the sensitivity of Bragg gratings to refractive index changes in the optical subsystem. Liu et al. presented a setup joining total internal reflection ellipsometry with an electrochemical setup⁸. This solution allows for monitoring of sub-surface changes during electrochemical reactions. Cobet et al. proposed ellipsometric spectroelectrochemical system for in situ investigation of polymer doping⁹. Our research assessed the sample state during the electrochemical cycle where any perturbations in the investigated liquid's refractive index indicate changes due to the EC reactions. In our study, we monitor the liquid sample itself, not the electrode surface. We have shown that the hybrid diagnostic system allows for a great reduction of the required sample volume. The quick operation, robustness, low cost and simple construction additionally distinguish our methodology from others.

Electrochemistry (EC) is of great interest in such systems as it is an extremely useful approach in technology^{10–12}. Its important usages include the detection of organic compounds and chemicals down to very small concentrations (depending on materials used for the system construction and the targeted substance, detection limit of 1 $\mu\text{g L}^{-1}$ or lower is achievable^{13,14}), the treatment of electrode surfaces, and degradation of

¹Department of Metrology and Optoelectronics, Faculty of Electronics, Telecommunications and Informatics, Gdańsk University of Technology, 11/12 Narutowicza St, 80-233 Gdańsk, Poland. ²Department of Medical Biophysics, University of Toronto, 101 College St, Toronto, ON M5G 1L7, Canada. ³Princess Margaret Cancer Centre, University Health Network, 610 University Ave, Toronto, ON M5G 2C1, Canada. ⁴Department of Radiation Oncology, University of Toronto, Stewart building, 149 College St Suite 504, Toronto, ON M5T 1P5, Canada. ✉email: monkosow@student.pg.edu.pl; malszcsze@pg.edu.pl

dangerous substances. Among electrochemical techniques, voltammetric methods can be distinguished. They are based on the investigation of the current dependence on applied voltage¹⁵. Changing voltage causes molecules to chemically gain or lose electrons, meaning they can undergo oxidation and reduction processes. As a result, current flow is registered as a function of applied voltage creating an electrochemical curve (voltammogram). Voltammetry methods are characterized by high sensitivity and specificity towards molecules¹⁶. Portable and relatively cheap apparatus can be used for the system construction, and a large variety of electrodes can be applied to best match the desired application.

Considering now the optical characterization methods, fiber-optic sensors are characterized by small dimensions allowing their applications in difficult-to-access places. They are also immune to electromagnetic interferences. Non-contact measurements and transmission of the data over long distances are possible. Further, analysis of signals in the spectral domain, such methods are largely insensitive to changes in optical transmission (signal intensity fluctuations) occurring in the measurement path. Owing to these and many other advantages, fiber-optic sensors are widely used in science and industry, including biological, chemical and environmental applications^{17–22}. One of the methods that benefit from fiber-optic implementation is low-coherence interferometry. This method ensures high measurement dynamic and resolution while eliminating the problem of ambiguous results as absolute measurement values are provided^{23,24}. For instance, optical fibers were used to construct a tandem-type interferometer utilizing a low-coherence method to monitor a metalorganic vapor-phase epitaxy process: substrate bending and temperature were monitored as well as the layer thickness²⁵. A low-coherence interferometry was also applied to monitor growth kinetics of diamond growth during microwave plasma chemical vapor deposition process where thickness and growth rate were controlled²⁶.

Our previous research on fiber-optic sensors presented a measurement module employing boron-doped diamond (BDD) film as a mirror^{27,28}. The results demonstrate that optical spectra are modulated by changes in the refractive index of the investigated liquid inside the cavity bounded by the BDD film, and by the change in the cavity length comprised of the investigated liquid. Our finding that the BDD film can successfully serve as a reflective layer in the interferometer opened a way to construct a hybrid opto-electrochemical system. The combination of these two methods has great potential, as BDDs are widely used as working electrodes in electrochemical cells²⁹. They are popular because such electrodes are characterized by a high response reproducibility, chemical inertness, wide electrochemical potential window—broader than graphite and glassy carbon³⁰, low and stable capacitive background current, long-time response stability, and biocompatibility³¹. BDD can be found in electrodes used in biosensors for the detection of various compounds such as glucose, antibiotics, amines, proteins and DNA^{32–35}. Further, their application is not only limited to detection; they are also successfully used for the degradation of dangerous chemical compounds^{36,37} and wastewater treatment³⁸. Extraordinary properties of BDD enable its performance as a working electrode and a mirror, making it unique and crucial for integration of a Fabry–Perot interferometer with an electrochemical system.

In this paper, we present a hybrid setup for simultaneous measurements of liquid samples by interferometric and electrochemical methods. We show that such construction is possible thanks to the crucial part that links up these two techniques: a boron-doped diamond film. This material has extraordinary electrochemical and optical properties allowing its usage as a joining element playing a dual role of a working electrode and a reflective surface. The system is comprised of a Fabry–Perot fiber-optic interferometer and a potentiostat–galvanostat with a 3-electrode electrochemical cell. This approach permits the monitoring of the sample state during the electrochemical cycle by means of optical interferometry and may potentiate real-time feedback. Such an approach has not been reported before, to the best of the authors' knowledge, and will enable relatively cheap and simple configuration with the possibility of miniaturization.

Results

We performed optical and electrochemical measurements during redox reactions by means of cyclic voltammetry using 2.5 mM $K_3[Fe(CN)_6]$ in a 0.5 M Na_2SO_4 solution. During the electrochemical measurements, optical spectra were recorded simultaneously. The representative electrochemical response is shown in Fig. 1. The resulting curve is consistent with standard EC behavior^{15,39}, suggesting the proper operation of the constructed system. For example, the oxidation (point A: $E = 0.247$ V, $I = 0.0195$ mA) and reduction peaks (point B: $E = -0.027$ V, $I = -0.0194$ mA) peaks, for a scan rate of 10 mV/s, correspond to the presence of $Fe(CN)_6^{3-}$ and $Fe(CN)_6^{4-}$ ions, respectively. Such visible peaks for oxidation (A—peak anodic current) and reduction (B—peak cathodic current) are typical for a reaction that is rate-dependent on the diffusion of the analyte to and from the planar working electrode surface³⁹. Achieving the correct current–voltage voltammetry response in presence of the optical system suggests that the two sub-systems do not interfere with each other, and can be used successfully for opto-electrochemical measurements.

Simultaneously with the cyclic voltammetry measurements, optical spectra were recorded, before and after the electrochemical cycle. The procedure was repeated five times. The measurements were taken with the use of a 1550 nm light source and recorded with an optical spectrum analyser. The resultant spectra are shown in Fig. 2.

With the Fabry–Perot interferometer we can detect changes of absorption and refractive index of the investigated liquid as a result of the electrochemical reaction. Potential adsorption of a newly formed chemical compound to a BDD will also influence the optical spectra. It can be noted that optical responses registered before and after the full electrochemical cycle are overlapping as expected; this holds true for every repeated measurement pair for the ~1-min duration of the experiment. This means that no significant change in the investigated sample occurred—if the refractive index of the liquid would change during the process, the spectra will be modified. Visible change of the spectra will also appear if reaction products are adsorbed onto the BDD film surface. The constancy of the optical response before and after EC and across repeated measurements implies that the sample was not damaged and optically confirms the reversibility of the electrochemical process.

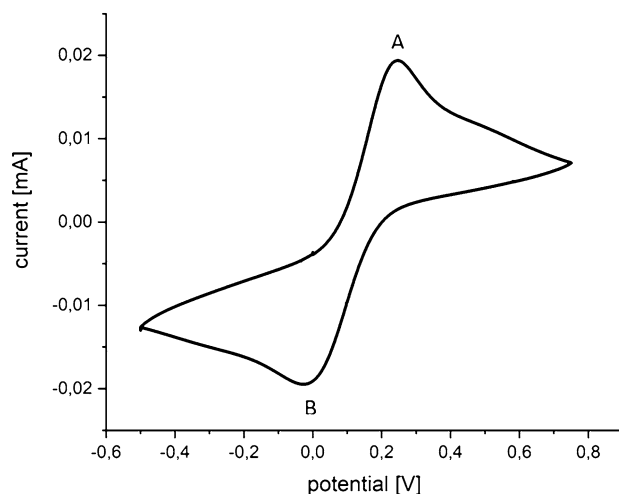


Figure 1. Representative cyclic voltammetry response recorded with a BDD film as a working electrode. Redox reactions were carried out using $K_3[Fe(CN)_6]$ in a Na_2SO_4 solution. Expected oxidation and reduction peaks are seen (points A and B, respectively), suggesting proper EC functionality of the hybrid EC-optical system (see text for details).

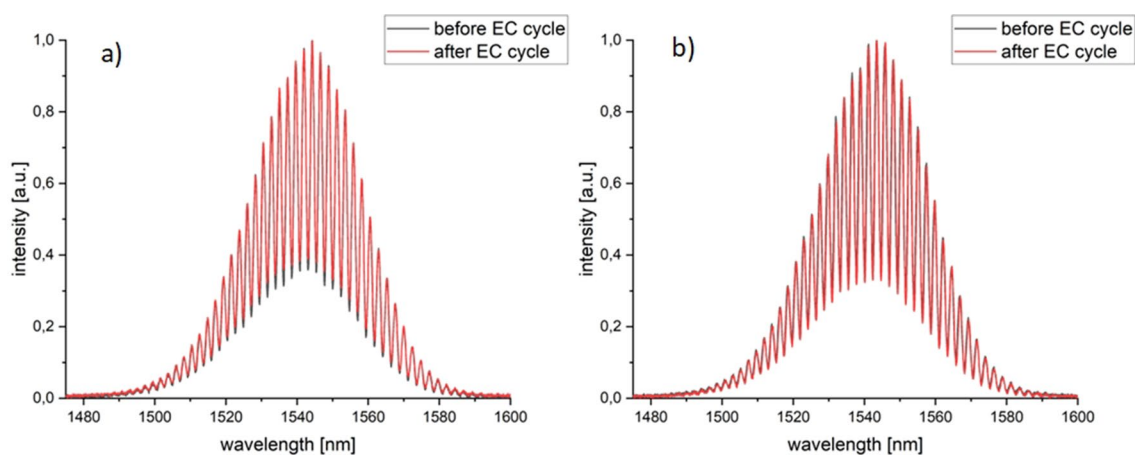


Figure 2. Optical spectra obtained before and after full electrochemical cycle. Spectra (a) and (b) show two out of five consecutive voltammetric cycles. Note the excellent overlap for the pairs, and the similarity of spectral pairs to each other across the longitudinal measurements, indicating that no significant perturbation appeared during measurements and the investigated sample (2.5 mM $K_3[Fe(CN)_6]$ in a 0.5 M Na_2SO_4) was not damaged. The results indicate the successful performance of the BDD film in its dual role of a EC working electrode and an optically reflective layer.

To quantify this constancy further, the signal fringe visibility as well as spectral shift between spectra recorded before and after the EC cycle were calculated and are shown in Fig. 3. In interferometry, fringe visibility V describes the contrast of the obtained signal, and can be calculated using the maximal I_{max} and minimal I_{min} intensity values as follows: $V = (I_{max} - I_{min}) / (I_{max} + I_{min})$. For the optimal cavity length in air, values approaching unity can be obtained for the BDD film²⁷. In our experiment, with the cavity containing 2.5 mM $K_3[Fe(CN)_6]$ in a 0.5 M Na_2SO_4 solution, a median value of $V = 0.48$ was obtained. This is due to the presence of the liquid inside the cavity and resulting absorption loss lowering the visibility value. From Fig. 3b. it can be noted that a small (<0.5 nm) spectral shift occurs, likely stemming from the small instability of the light source.

Figure 4 presents all spectra obtained for five repeated-measurement electrochemical cycles, divided into two groups: starting spectra registered before each EC cycle, and ending spectra registered after completing each EC cycle. As seen, no additional modulation occurs in optical signals for later measurements compared to the earlier ones, and the signal envelopes remain the same. These results confirm the repeatability of the measurements in the constructed opto-electrochemical system during the reversible redox reactions.

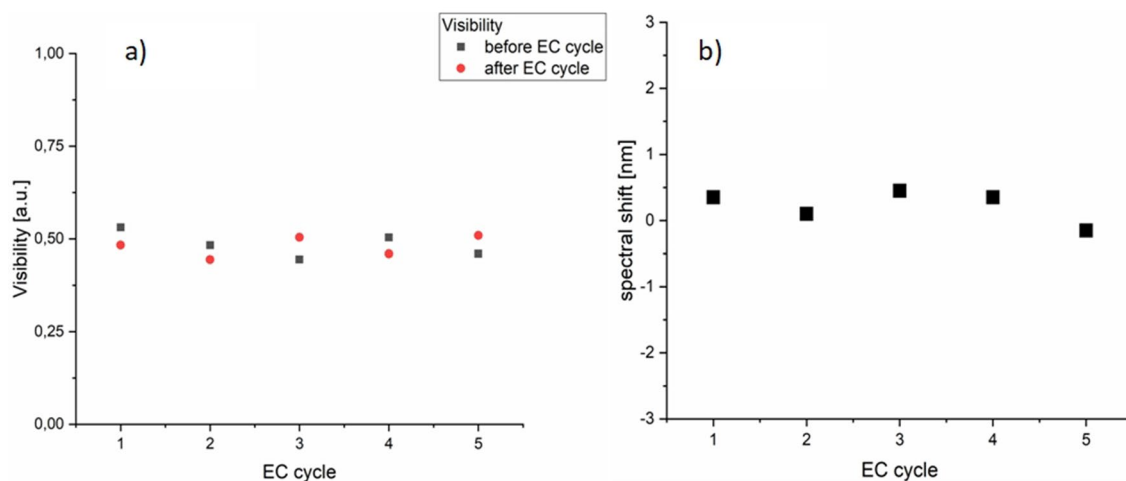


Figure 3. The analysis of the optical spectra of Fig. 2 recorded before and after each electrochemical cycle. (a) Fringe visibility values cluster around ~ 0.5 value due to the presence of the liquid inside the Fabry–Perot cavity. (b) Spectral shift between spectra recorded before and after each EC cycle. Minor changes in (a) and (b) are due to instability of the light source over time.

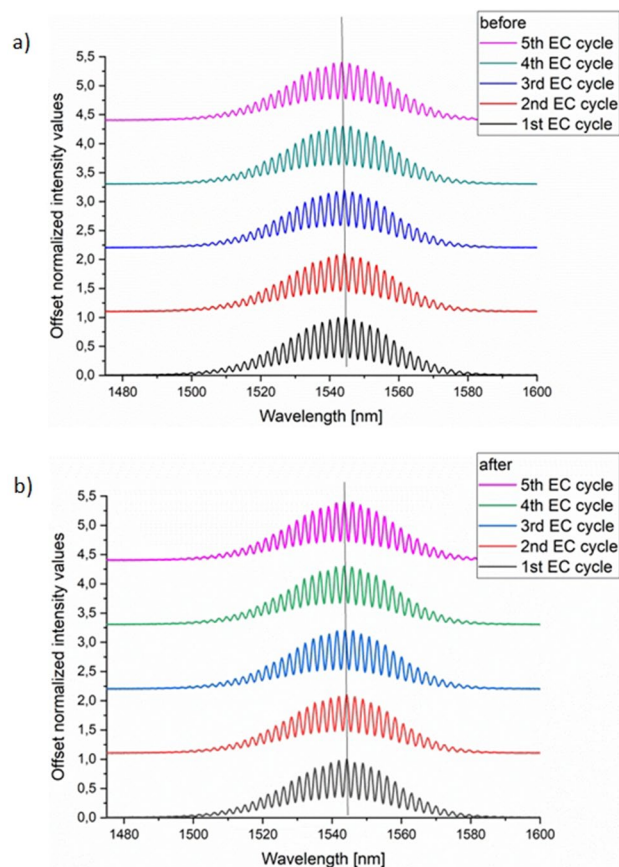


Figure 4. Stacked spectra split into *before* and *after* according EC cycles groups. The results allow for comparison of signals obtained in the time series of repeated measurements. As seen, the signals' envelopes remain approximately the same, suggesting no measurement-induced alterations were introduced to the electrochemical reactions. Vertical lines are to guide an eye to spot slight spectral shifts, if any (likely due to the light source instability).

Discussion

We have shown that it is possible to perform optical *and* electrochemical measurements in the proposed hybrid system. The obtained optical spectra remain stable during the measurements, implying that the electrochemical redox processes were carried out without any hysteresis or other irreversible alterations. Indeed, if the refractive index change of the investigated liquid was induced by the hybrid measurement process, the spectra would be altered. As the reversible process is presented, no visible spectrum modulation was observed, at least within the resolving power of our measurement system, we conclude that our hybrid system indeed operates in a true non-destructive evaluation (NDE) mode. This ensures us that the entire process was successful and that the sample was not damaged, which saves resources: sample (small volumes) and time (rapid monitoring and feedback). We can further optimize the process while maintaining low cost. For reversible reactions, we achieve the lowest measurements cost and we can optimize them as liquid and the working electrode can be used many times, since the substance quality is continuously monitored. For irreversible EC processes, we cannot use the same sample multiple times: the liquid properties change and the electrode can be covered with a new compound adsorbed to its surface. In such case, we would detect its presence through the measured refractive index changes.

The described research emphasized integration of interferometry and electrochemistry in one setup, utilizing a boron-doped diamond film as a link between two subsystems. Such BDD element working as an electrode and reflective surface replaces costly high-quality mirrors used in many photonics applications. The significant cost savings on the optical part also stem from the need of only a light source, detector and optical fibers. The use of so few optical components and the lack of additional micromechanical elements with precise alignment requirements drastically reduces the cost of construction. The use of fibers in optical process control is possible due to their dielectric nature: they do not impact the electrochemical process. Further, as we analyzed the optical data in spectral domain, robustness with respect to possible optical transmission changes was achieved. Such an approach decreases the costs of the optical part and simplifies the construction, enabling the miniaturization. This may enable monitoring of electrochemical reactions in small volumes (e.g., a drop), reducing the sample amount needed to perform the experiment. On the other hand, performing separate measurements is time-consuming, requires more material for testing and people who can operate both systems. The proposed opto-electrochemical approach will simplify the measurement procedures and also reduce the amount of material needed to carry out the measurement. The possibilities of data analysis and insight into the interrogated material will be enhanced by examining possible correlations between the measured optical and EC parameters. Such hybrid NDE systems may prove particularly useful in examining electrode surfaces, in biomedical research, and in environmental analyzes (e.g., detecting the presence, and determining the level of a given substance in a liquid sample). As we offer the continuous measurements that utilize only one dual-role element, we open up a way to construct a lab-on-chip device.

Summary and conclusion

We report a novel hybrid opto-electrochemical measurement system consisting of a 3-electrode electrochemical cell and a Fabry–Perot fiber-optic interferometer. The subsystems share a BDD film playing a dual role of a working electrode and a reflective layer. Simultaneous measurements were conducted during redox reactions in 2.5 mM $K_3[Fe(CN)_6]/0.5$ M Na_2SO_4 solutions. We obtained expected responses from both systems, confirming their proper NDE-mode operation without any sample alterations and no interference from one sub-setup to another. The simultaneous use of the BDD film as a reflecting layer in the interferometer and as a working electrode in an EC system has not been reported before. This novelty is advantageous in comparison to existing system architecture because of its simplified structure, reduced cost of construction, robust operation and system miniaturization possibilities for hybrid assessment of small droplet-sized sample volumes.

Materials and methods

Measurement setup. The measurement setup presented in Fig. 5 consists of two main parts which have a boron-doped diamond film as a common element. Those two parts are a fiber-optic Fabry–Perot interferometer and a three-electrode electrochemical system.

Due to the water-based nature of the chemical solution, the optical measurements were performed with the use of the light source operating at 1550 nm. Hence, the Fabry–Perot part was build of a super luminescence diode working at a central wavelength of 1550 nm. For recording the optical spectra an optical spectrum analyzer was used. The single-mode standard communication optical fibers and a 2×1 fiber coupler were used to connect all the parts. The fiber that played the role of an optical measurement head was stripped and cleaved to fit the measurement field. The Fabry–Perot interferometer works in a reflective mode. Here, the incident beam is guided through the optical fiber and spitted onto a reference beam and a measurement beam. They are reflected from fiber end-face/medium inside the cavity interface and medium/BDD film interface, respectively. Changes in optical path difference affecting the phase difference between those two interfering beams depend on the refractive index of the medium and a geometrical path length. Their perturbations will modulate the measurement signal.

The electrochemical system was built in a standard three-electrode configuration: working electrode which was a boron-doped diamond deposited on a silica substrate, a silver wire with deposited silver chloride onto its surface as reference electrode and a counter electrode—Pt wire. The electrodes were connected to a potentiostat that controlled the potential and recorded voltammetric curves, which were observed on the PC. The close-up of the measurement head is shown in Fig. 6.

An electrochemical cell was placed over the boron-doped diamond with a fitted laser-cut gasket. The active area of the BDD electrode was 0.2 cm². All the electrodes as well as the prepared optical fiber were immobilized on the laboratory stand and put inside the cell with special caution to assure their proper placement. It was

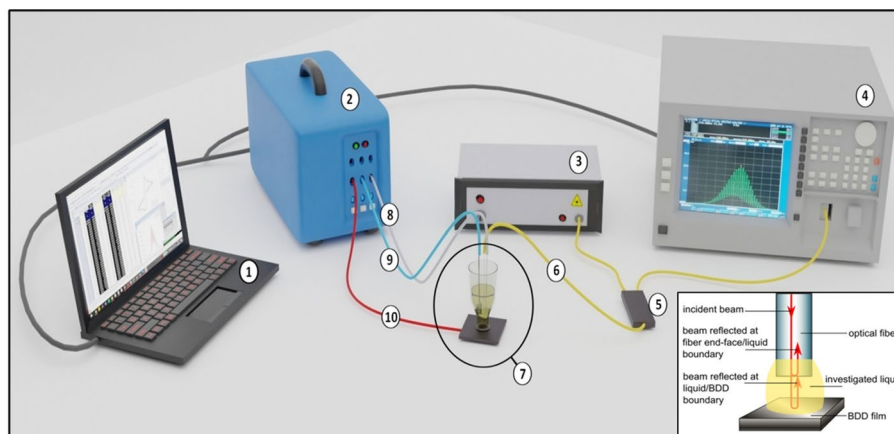


Figure 5. Measurement setup scheme (not to scale): 1—PC for storing and processing measurement data, 2—potentiostat–galvanostat, 3—light source, 4—optical spectrum analyser (OSA), 5— 2×1 fiber coupler, 6—optical fiber, 7—measurement head, 8—connection to a reference electrode, 9—connection to a counter electrode, 10—connection to a working electrode. The inset figure shows a Fabry–Perot interferometer operation principle that was utilized in an optical part of the system. Reflected beams interfere with each other giving us a signal register by OSA.

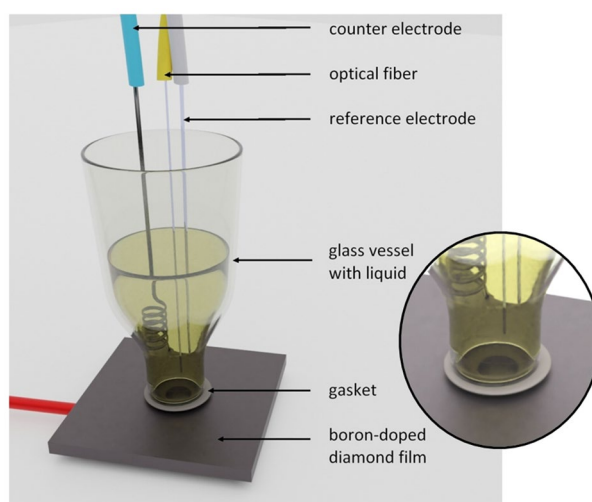


Figure 6. Measurement head scheme (not to scale). The counter, reference, and working electrodes are connected (blue, white, red wire, respectively) to the potentiostat–galvanostat, creating the electrochemical part of the measurement head. The optical fiber (yellow wire) is placed together with the electrodes in the glass vessel. The fiber and the boron-doped diamond film constitute the Fabry–Perot interferometer inside the electrochemical cell, with the cavity fulfilled by the investigated liquid. Close-up shows placement of the connections: all end above the BDD, they do not touch each other, and the optical fiber end-face is perpendicular to the BDD.

crucial for the electrodes not to touch each other and for the fiber end-face to be placed parallel to the boron-doped diamond film.

Chemicals. All reagents were of analytical grade and used without further purification. The Sodium sulfate (ACS reagent, purity $\geq 99\%$, Aldrich) and potassium hexacyanoferrate(III) (Pure p. a., Chempur) aqueous solutions were prepared using demineralised water. The Potassium nitrate (pure p.a.) and sulfuric acid (purity $\geq 95\%$) were obtained from Chempur. The synthesis gases: methane, hydrogen, and diborane were collected from Linde and were of the highest purity class.

Boron-doped diamond film deposition. A 2.45 GHz microwave plasma-assisted chemical vapor deposition system (Seki Technotron AX5400S, Japan) was used for deposition of boron-doped diamond on $1 \text{ cm} \times 1 \text{ cm}$ p-type silicon substrate with (100) orientation. All substrates were cleaned using the RCA method

before deposition, followed by seeding using slurry consisting of undoped nanodiamonds with sizes ~4–7 nm. The reactor pressure, microwave power, gas flow rate were 50 Torr, 1300 W, 300 sccm, respectively. Diborane was used as a dopant precursor and the [B]/[C] ratio was maintained at 10,000 ppm. During the growth, the temperature of the graphite stage was kept at 700 °C. A deposition time was 12 h.

After the chemical vapor deposition process, the samples were cleaned in a solution of H₂SO₄ and KNO₃ with a 2:1 weight ratio. First, the solution was heated until it reached its boiling point. Then the electrodes were placed in the boiling solution for 30 min and subsequently placed in the boiling deionized water. Next, the electrodes were ultra-sonicated in isopropyl alcohol and deionized water for 10 min. Finally, boron-doped diamond was hydrogenated in the previously mentioned system (1100 W, 50 Torr, 15 min).

Received: 18 February 2021; Accepted: 2 June 2021

Published online: 15 June 2021

References

- Potamitis, I., Rigakis, I., Vidakis, N., Petousis, M. & Weber, M. Affordable bimodal optical sensors to spread the use of automated insect monitoring. *J. Sensors* **2018**, 3949415 (2018).
- Grieshaber, D., MacKenzie, R., Vörös, J. & Reimhult, E. Electrochemical biosensors—Sensor principles and architectures. *Sensors (Basel)* **8**, 1400–1458 (2008).
- Lamberti, F. *et al.* Optoelectrochemical biorecognition by optically transparent highly conductive graphene-modified fluorine-doped tin oxide substrates. *ACS Appl. Mater. Interfaces* **6**, 22769–22777 (2014).
- Narakathu, B. B., Reddy, A. S. G., Eshkeiti, A., Bazuin, B. J. & Atashbar, M. Z. Opto-electrochemical based dual detection of heavy metal compounds using a novel flow cell, in *Sensors 2013 IEEE*, pp. 1–4 (2013). <https://doi.org/10.1109/ICSENS.2013.6688337>.
- Sobaszek, M. *et al.* In-situ monitoring of electropolymerization processes at boron-doped diamond electrodes by Mach–Zehnder interferometer. *Sensors Actuators B Chem.* **304**, 127315 (2020).
- Janczuk-Richter, M. *et al.* Optical investigations of electrochemical processes using a long-period fiber grating functionalized by indium tin oxide. *Sens. Actuators B Chem.* **279**, 223–229 (2018).
- Janczuk-Richter, M. *et al.* Optical monitoring of electrochemical processes with ITO-coated long-period fiber grating, in *26th International Conference on Optical Fiber Sensors ThE54 ThE54*, OSA Technical Digest - Optical Society of America (2018).
- Liu, W., Li, M., Luo, Z. & Jin, G. Using electrochemistry—Total internal reflection ellipsometry technique to observe the dissolved oxygen reduction on Clark electrode. *Electrochim. Acta* **142**, 371–377 (2014).
- Cobet, C. *et al.* Ellipsometric spectroelectrochemistry: An in situ insight in the doping of conjugated polymers. *J. Phys. Chem. C* **122**, 24309–24320 (2018).
- Janssen, L. J. J. & Koene, L. The role of electrochemistry and electrochemical technology in environmental protection. *Chem. Eng. J.* **85**, 137–146 (2002).
- Petro, R. & Schlesinger, M. Applications of electrochemistry in medicine. In *Applications of Electrochemistry in Medicine* (ed. Schlesinger, M.) 1–33 (Springer US, 2013). https://doi.org/10.1007/978-1-4614-6148-7_1.
- Schlesinger, M. Modern applications of electrochemical technology. In *Modern Aspects of Electrochemistry* (eds Vayenas, C. G. *et al.*) 369–416 (Springer, 2008). https://doi.org/10.1007/978-0-387-49489-0_6.
- Qian, L., Durairaj, S., Prins, S. & Chen, A. Nanomaterial-based electrochemical sensors and biosensors for the detection of pharmaceutical compounds. *Biosensors Bioelectron.* **175**, 112836 (2021).
- Gumpu, M. B., Sethuraman, S., Krishnan, U. M. & Rayappan, J. B. B. A review on detection of heavy metal ions in water—An electrochemical approach. *Sensors Actuators B Chem.* **213**, 515–533 (2015).
- Rezaei, B. & Irannejad, N. Electrochemical detection techniques in biosensor applications. *Electrochem. Biosensors* <https://doi.org/10.1016/B978-0-12-816491-4.00002-4> (2019).
- Park, C. *et al.* Fast cyclic square-wave voltammetry to enhance neurotransmitter selectivity and sensitivity. *Anal. Chem.* **90**, 13348–13355 (2018).
- Okazaki, T. *et al.* Investigation of the effects of electromagnetic field treatment of hot spring water for scale inhibition using a fibre optic sensor. *Sci. Rep.* **9**, 10719 (2019).
- Okazaki, T., Orii, T., Ueda, A., Ozawa, A. & Kuramitsu, H. Fiber optic sensor for real-time sensing of silica scale formation in geothermal water. *Sci. Rep.* **7**, 3387 (2017).
- Agayn, V. I. & Walt, D. R. Fiber-optic sensor for continuous monitoring of fermentation pH. *Bio/Technology* **11**, 726–729 (1993).
- Lao, J. *et al.* In situ plasmonic optical fiber detection of the state of charge of supercapacitors for renewable energy storage. *Light Sci. Appl.* **7**, 34 (2018).
- Wang, W. *et al.* A label-free fiber optic SPR biosensor for specific detection of C-reactive protein. *Sci. Rep.* **7**, 16904 (2017).
- Kosowska, M. *et al.* Microscale diamond protection for a ZnO coated fiber optic sensor. *Sci. Rep.* **10**, 19141 (2020).
- Clement, J., Maestre, H., Torregrosa, G. & Fernández-Pousa, C. R. Phase sensitive low-coherence interferometry using microwave photonics. *Opt. Express OE.* **28**, 30432–30446 (2020).
- Cusato, L. J., Cerrotta, S., Torga, J. R. & Morel, E. N. Extending low-coherence interferometry dynamic range using heterodyne detection. *Optics Lasers Eng.* **131**, 106106 (2020).
- Volkov, P. V. *et al.* Novel technique for monitoring of MOVPE processes. *J. Cryst. Growth* **310**, 4724–4726 (2008).
- Bushuev, E. V. *et al.* Synthesis of single crystal diamond by microwave plasma assisted chemical vapor deposition with in situ low-coherence interferometric control of growth rate. *Diam. Relat. Mater.* **66**, 83–89 (2016).
- Kosowska, M. *et al.* Doped nanocrystalline diamond films as reflective layers for fiber-optic sensors of refractive index of liquids. *Materials* **12**(13), 2124 (2019). <https://doi.org/10.3390/ma12132124>
- Majchrowicz, D., Kosowska, M., Struk, P. & Jędrzejewska-Szczerska, M. Tailoring the optical parameters of optical fiber interferometer with dedicated boron-doped nanocrystalline diamond thin film. *Physica Status Solidi (a)* **214**, 1700222 (2017).
- Niedziałkowski, P. *et al.* Comparison of the paracetamol electrochemical determination using boron-doped diamond electrode and boron-doped carbon nanowalls. *Biosens. Bioelectron.* **126**, 308–314 (2019).
- Pierpaoli, M. *et al.* Carbon nanoarchitectures as high-performance electrodes for the electrochemical oxidation of landfill leachate. *J. Hazardous Mater.* **401**, 123407 (2021).
- Zhou, Y. & Zhi, J. The application of boron-doped diamond electrodes in amperometric biosensors. *Talanta* **79**, 1189–1196 (2009).
- Niedziałkowski, P. *et al.* Melamine-modified boron-doped diamond towards enhanced detection of adenine, guanine and caffeine. *Electroanalysis* **28**, 211–221 (2016).
- Feier, B., Gui, A., Cristea, C. & Săndulescu, R. Electrochemical determination of cephalosporins using a bare boron-doped diamond electrode. *Anal. Chim. Acta* **976**, 25–34 (2017).
- Suzuki, A. *et al.* Fabrication, characterization, and application of boron-doped diamond microelectrodes for in vivo dopamine detection. *Anal. Chem.* **79**, 8608–8615 (2007).

35. Zhao, W., Xu, J.-J., Qiu, Q.-Q. & Chen, H.-Y. Nanocrystalline diamond modified gold electrode for glucose biosensing. *Biosens. Bioelectron.* **22**, 649–655 (2006).
36. Bai, H. *et al.* Boron-doped diamond electrode: Preparation, characterization and application for electrocatalytic degradation of m-dinitrobenzene. *J. Colloid Interface Sci.* **497**, 422–428 (2017).
37. Montanaro, D., Lavecchia, R., Petrucci, E. & Zuorro, A. UV-assisted electrochemical degradation of coumarin on boron-doped diamond electrodes. *Chem. Eng. J.* **323**, 512–519 (2017).
38. Panizza, M. & Cerisola, G. Application of diamond electrodes to electrochemical processes. *Electrochim. Acta* **51**, 191–199 (2005).
39. Elgrishi, N. *et al.* A practical beginner's guide to cyclic voltammetry. *J. Chem. Educ.* **95**, 197–206 (2018).

Acknowledgements

This research was funded by the Polish National Agency for Academic Exchange under Iwanowska Programme PPN/IWA/2018/1/00058/U/0001, the Gdańsk University of Technology by the DEC-034876 Grant under the Technetium Talent Management Grants—'Excellence Initiative—Research University' and the DS funds of the Faculty of Electronics, Telecommunications, and Informatics of the Gdańsk University of Technology.

Author contributions

M.K., P.J. and M.S. conceived and designed the experiments; M.K. and P.J. performed the experiments; M.K., P.J. and M.S. analyzed the data; M.R. contributed boron-doped diamond samples; M.K., P.J. and M.R. wrote the main manuscript text; M.K. prepared figures; A.V. and M.S. checked, edited and reviewed the paper.

Competing interests

The authors declare no competing interests.

Additional information

Correspondence and requests for materials should be addressed to M.K. or M.S.

Reprints and permissions information is available at www.nature.com/reprints.

Publisher's note Springer Nature remains neutral with regard to jurisdictional claims in published maps and institutional affiliations.



Open Access This article is licensed under a Creative Commons Attribution 4.0 International License, which permits use, sharing, adaptation, distribution and reproduction in any medium or format, as long as you give appropriate credit to the original author(s) and the source, provide a link to the Creative Commons licence, and indicate if changes were made. The images or other third party material in this article are included in the article's Creative Commons licence, unless indicated otherwise in a credit line to the material. If material is not included in the article's Creative Commons licence and your intended use is not permitted by statutory regulation or exceeds the permitted use, you will need to obtain permission directly from the copyright holder. To view a copy of this licence, visit <http://creativecommons.org/licenses/by/4.0/>.

© The Author(s) 2021

[MK5] Microscale Diamond Protection for a ZnO Coated Fiber Optic Sensor.

Kosowska, M.; Listewnik, P.; Majchrowicz, D.; Rycewicz, M.; Bechelany, M.; Fleger, Y.; Chen, M.; Fixler, D.; Dholakia, K.; Szczerska, M.

Scientific Reports 2020, 10, 19141, doi:10.1038/s41598-020-76253-5.

The author's contributions were:

designing and performing the experiments, optical data analysis, selected figures preparation and writing the original manuscript draft.



OPEN

Microscale diamond protection for a ZnO coated fiber optic sensor

Monika Kosowska^{1✉}, Paulina Listewnik¹, Daria Majchrowicz^{1,2✉}, Michał Ryciewicz¹, Mikhael Bechelany³, Yafit Fleger⁴, Mingzhou Chen², Dror Fixler^{4,5}, Kishan Dholakia² & Małgorzata Szczerska^{1✉}

Fiber optic sensors are widely used in environmental, biological and chemical sensing. Due to the demanding environmental conditions in which they can be used, there is a risk of damaging the sensor measurement head placed in the measuring field. Sensors using nanolayers deposited upon the fiber structure are particularly vulnerable to damage. A thin film placed on the surface of the fiber end-face can be prone to mechanical damage or deteriorate due to unwanted chemical reactions with the surrounding agent. In this paper, we investigated a sensor structure formed with a Zinc Oxide (ZnO) coating, deposited by Atomic Layer Deposition (ALD) on the tip of a single-mode fiber. A nanocrystalline diamond sheet (NDS) attached over the ZnO is described. The diamond structure was synthesized in a Microwave Plasma Assisted Chemical Vapor Deposition System. The deposition processes of the nanomaterials, the procedure of attaching NDS to the fiber end-face covered with ZnO, and the results of optical measurements are presented.

Fiber-optic sensors are widely used in environmental, biological and chemical sensing^{1–6}. That is due to their well-known advantages that allow for their use in demanding applications – they have the ability to perform real-time and remote measurements, have immunity to electromagnetic interferences and are of compact size, amongst other attributes^{7–9}. As new technologies become available, the structures of fiber-optic sensors are growing more elaborate, with integrated thin films, nanoparticles, microstructured fibers, which aim to offer increased sensing abilities. One such group are thin film-based sensors that use nanolayers deposited on the fiber surface^{10–12}. These are used to design and create structures that can be applied on the measuring heads of fiber-optic sensors, for example thin (tens of nanometers) dielectric layers made of materials characterized by high refractive index, e.g. ZnO ($n = 2.1$ at 500 nm)^{13,14}.

Using ZnO as a coating for the fiber-optic sensor has many advantages. It allows to broaden the measuring range, improves sensitivity of measured parameter, in comparison to the sensor without a coating. It also enables to perform measurements in a medium, which refractive index is close to this of optical fiber core ($n = 1.4$). Furthermore, deposition techniques of ZnO are highly developed, especially Atomic Layer Deposition (ALD) method, which ensures uniformity of the coating. However, there are several instances, in which ZnO can adversely affect the surrounding medium, therefore CVD nanocrystalline diamond sheet attached over the ZnO, is required to protect both the sensor head and the measured medium from damage in case of an unwanted reaction.

In addition, fiber-optic sensors are often used in remote places, where other devices cannot be utilized due to their physical dimensions or mechanical properties. By using CVD layer, the sensor can withstand more severe conditions and it can be utilized for longer periods of time, which in turn minimizes involvement of an operator and the cost of maintenance.

Among many extraordinary properties of synthesized diamond, several of those are of particular interest from an optical point of view. It has a very high refractive index ($n = 2.4$ at a wavelength of 500 nm), and it is transparent in the broad wavelength range. It can also work as a reflective layer when doped with other materials, e.g. boron, nitrogen^{15–17}. Diamond is also characterized by its excellent mechanical and chemical properties, as well as biocompatibility. The properties of the diamond can be also tuned by changing the parameters of the

¹Department of Metrology and Optoelectronics, Faculty of Electronics, Telecommunications and Informatics, Gdańsk University of Technology, 11/12 Narutowicza Street, 80-233 Gdańsk, Poland. ²SUPA, School of Physics and Astronomy, University of St Andrews, North Haugh, St Andrews KY16 9SS, UK. ³Institut Européen Des Membranes, IEM UMR 5635, University of Montpellier, ENSCM, CNRS, Place Eugène Bataillon, 34095 Montpellier, France. ⁴Institute for Nanotechnology and Advanced Materials, Bar-Ilan University, 52900 Ramat-Gan, Israel. ⁵Faculty of Engineering, Bar-Ilan University, 52900 Ramat-Gan, Israel. ✉email: monkosow@student.pg.edu.pl; darmajch@pg.edu.pl; malszcze@pg.edu.pl

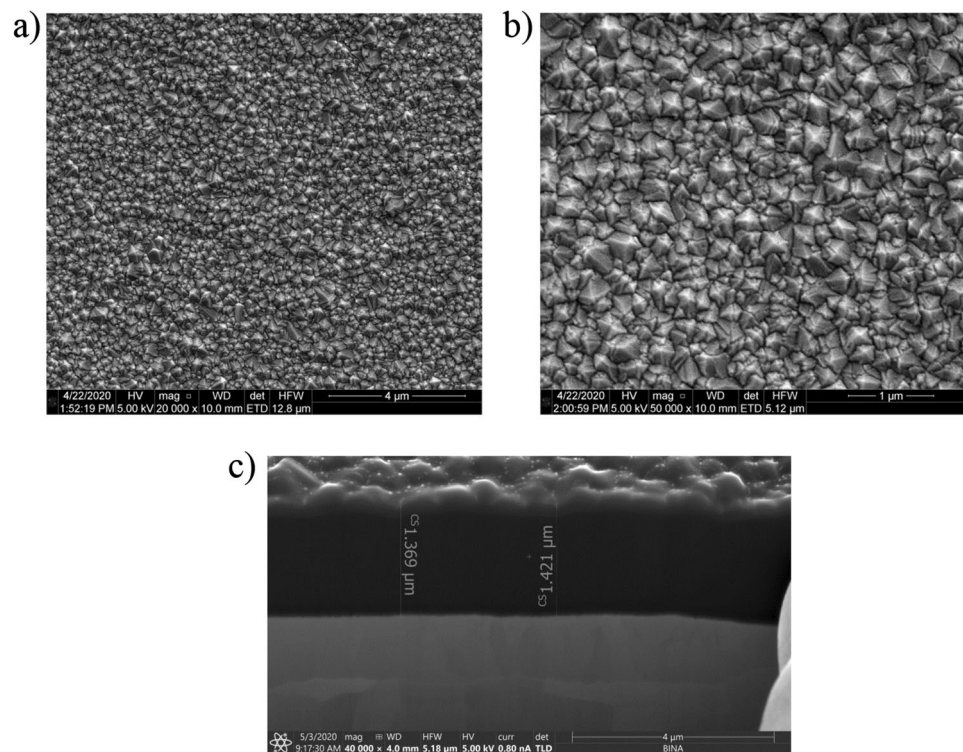


Figure 1. SEM images of nanocrystalline diamond sheet (a) magnification 20,000× (b) magnification 50,000× (c) cross-section magnification 40,000×.

deposition process e.g. temperature, time, working gas mixture composition. A set of such outstanding properties resulted in lots of applications of diamond in numerous fields of science, biomedicine and technology^{18–21}.

In this work, we investigate an undoped nanocrystalline diamond sheet attached to the ZnO-coated fiber-optic sensor head. The diamond structure was synthesized in the Microwave Plasma Assisted Chemical Vapor Deposition (MW PA CVD) system. The construction of the measurement setup with the focus on the measurement head and the results of the optical measurements are presented. The sensing abilities of the fiber-optic sensor with a ZnO coating deposited by the Atomic Layer Deposition (ALD) method, investigated for temperature change as well as refractive index, are presented elsewhere^{10,22}.

Material characterization—nanocrystalline diamond sheet. The obtained nanocrystalline diamond sheet surface morphology was investigated with the use of an Environmental Scanning Electron Microscope (E-SEM, Quanta FEG 250, FEI, Hillsboro, Oregon, USA). Figure 1 shows SEM images of the NDS attached to the tantalum substrate for two system magnifications, 20,000× and 50,000×, and for a cross-section magnification of 40,000×.

Figure 1a shows that the diamond had covered the substrate evenly, and over sufficient areas that are large enough for use in the construction of fiber-optic measurement head (with the fiber core dimensions of 8 μm). The obtained structure is uniform and continuous. No damage or other visible abnormalities of the surface were noted during the investigation. Figure 1b proves the crystalline character of the sample, with a grain size smaller than 500 nm. The nanocrystalline diamond sheet was investigated in terms of its thickness, and therefore, cross-section measurements were also taken.

Microscope photographs of the sample were taken with a (C-5060, Olympus, Japan) camera and a (LAB 40 POL, OPTA-TECH, Poland) microscope.

Camera and microscope pictures of a diamond sheet (1 cm × 1 cm in size) are presented in Fig. 2. The rough nanodiamond surface is caused by the delamination process, which facilitates the fabrication of freestanding diamond sheets.

The Raman spectra of the diamond films were measured by using a home-made wavelength modulated Raman system. The details of this system may be found in our previous works^{23,24}.

The strong fluorescence background makes it impossible to locate the Raman peaks from a standard Raman spectrum as seen in Fig. 3a. However, our approach of using wavelength modulated Raman system enabled by a tunable narrow linewidth laser can remove the strong fluorescent background efficiently and reveal the underlying Raman features. To achieve this, the wavelength of the laser is tuned in five steps over a range of 1.5 nm from 785 nm. At each step, a Raman spectrum with an integration time of 1 s is recorded. As the fluorescence background does not change over this small wavelength interval, it can be removed with a post-processing algorithm, namely principal component analysis (PCA). This way, the characteristic Raman peak for nanocrystalline diamond sheet at room temperature can be recovered^{25,26}, visualized as a zero-crossing, at 1331 cm⁻¹, as shown

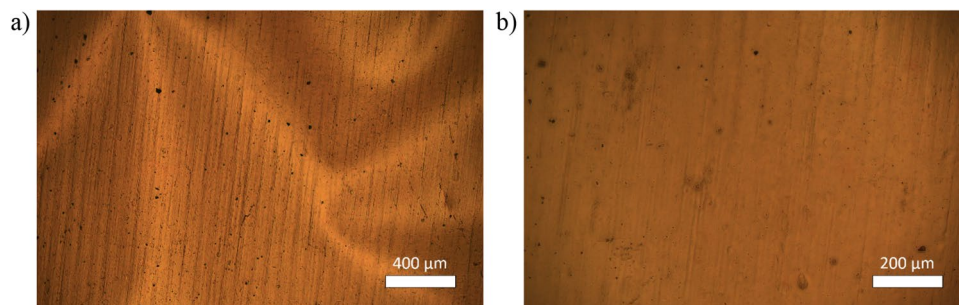


Figure 2. Optical microscope photographs of the diamond sheet (a) magnification 50×, (b) magnification 100×.

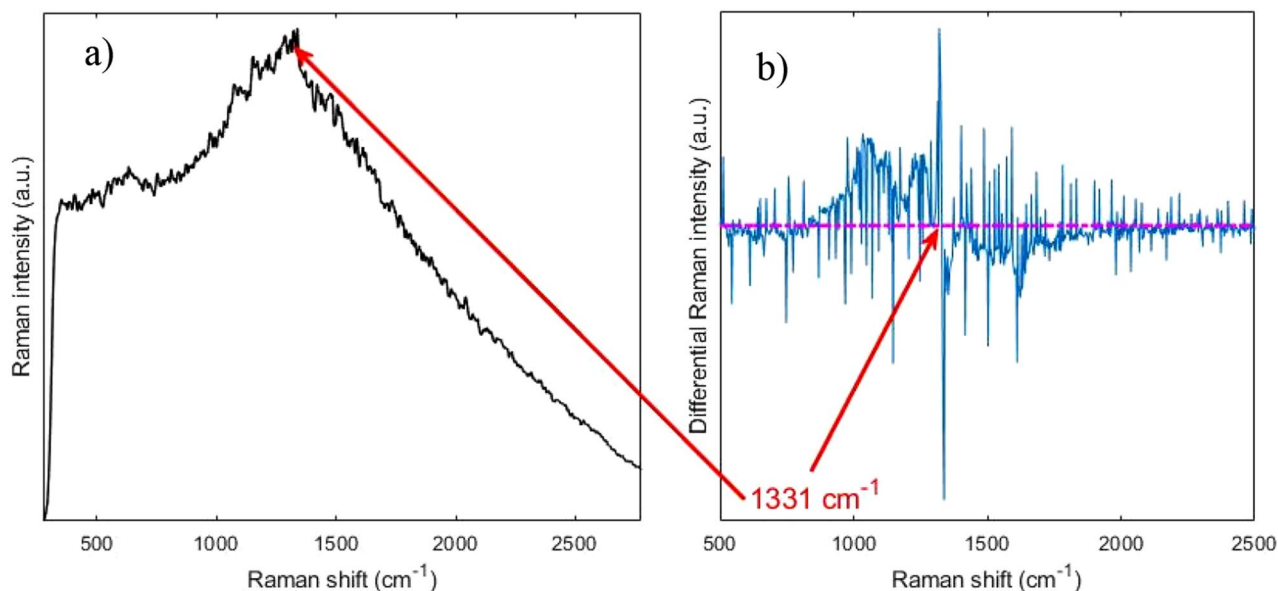


Figure 3. Raman spectra acquired from the nanocrystalline diamond sheet. (a) Shows a standard Raman spectrum with a very strong fluorescence background. (b) Shows the wavelength modulated Raman spectrum with the 1331 cm^{-1} peak. Arrows point at the zero crossings where the peak is and its possible location in the standard Raman spectrum.

in Fig. 3b. As this dominant band is assigned to the diamond at room temperature, the investigation proved the successful deposition process resulting in the diamond structure.

Results

This section contains the experimental measurements, which were performed to evaluate the influence of nanocrystalline diamond sheet attached over ALD ZnO coating. The series of measurements were executed by increasing the distance between the sensor head and the silver mirror by a fixed increment over $500\text{ }\mu\text{m}$. The measurements were performed using the sensor in two configurations: firstly, with only ZnO coating deposited on the end-face of the fiber, followed by attachment of the NDS and repeating the measurements. The results for both configurations are presented including comparison between them. Figure 4 shows the representative spectra, where the intensity of the obtained signal was normalized. The Fabry–Perot cavity length was set to $50\text{ }\mu\text{m}$, $100\text{ }\mu\text{m}$, $150\text{ }\mu\text{m}$ and $200\text{ }\mu\text{m}$, respectively.

It can be noted from representative spectra that there is a visible signal modulation while changing the cavity length—the longer the cavity, the greater number of maxima in the investigated wavelength range. This behavior agrees with our previous findings²⁷. Figure 5 shows the representative spectra, where the obtained signals for the measurement head with ZnO coating, as well as ZnO coating and nanocrystalline diamond sheet were compared. It can be noted that the intensity of the signal is decreasing while applying the nanocrystalline diamond sheet, which can be observed in Fig. 5. The decrease in the signal intensity does not impact the number of maxima in the spectrum. This demonstrates that NDS provides protection for the fiber end-face covered with a ZnO coating.

The application of the nanodiamond sheets decreases the signal intensity, but the signal visibility is not significantly changed.

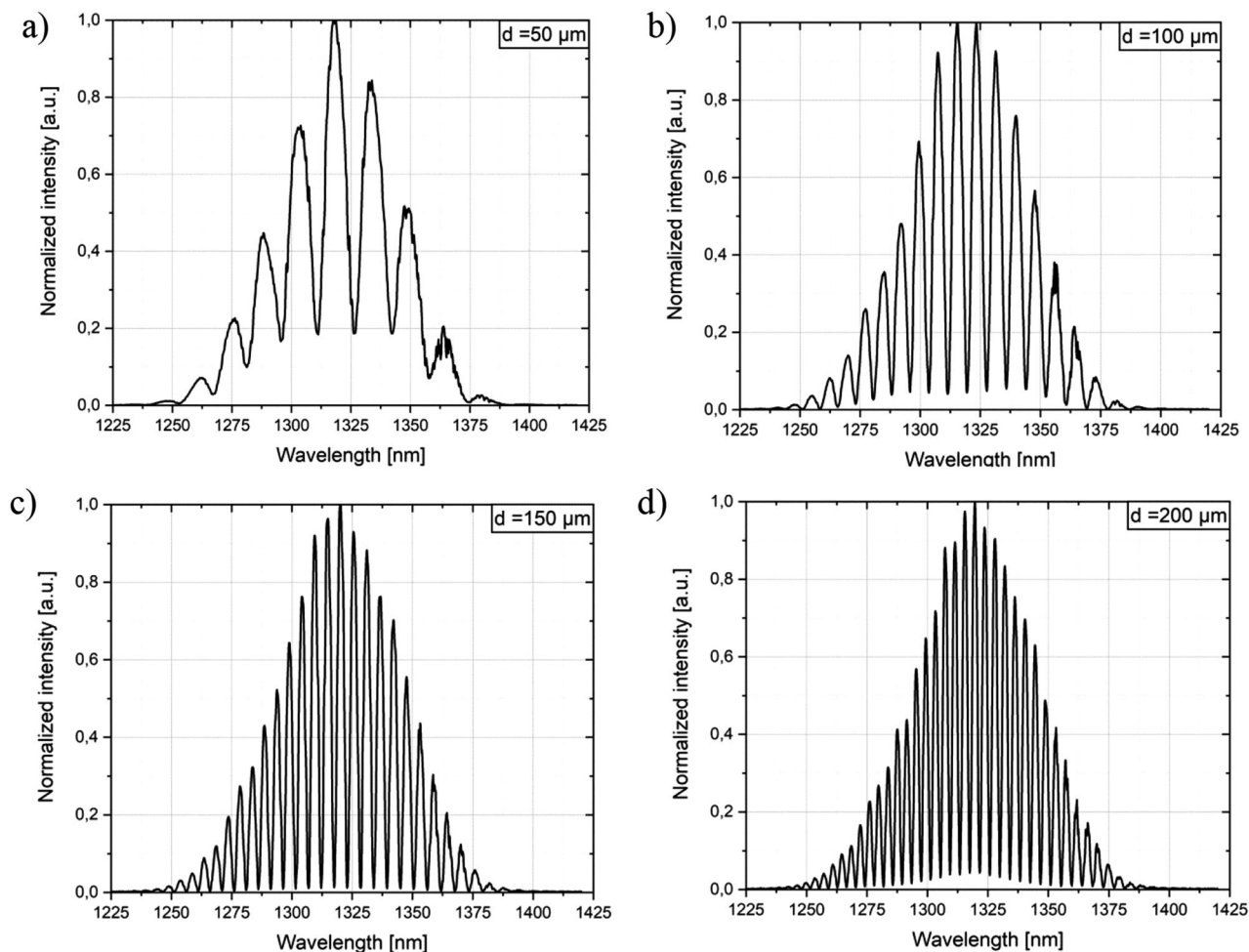


Figure 4. Signal obtained for the measurement head with ZnO layer and nanocrystalline diamond sheet. The Fabry-Perot cavity length was set to: (a) 50 μm , (b) 100 μm , (c) 150 μm , (d) 200 μm .

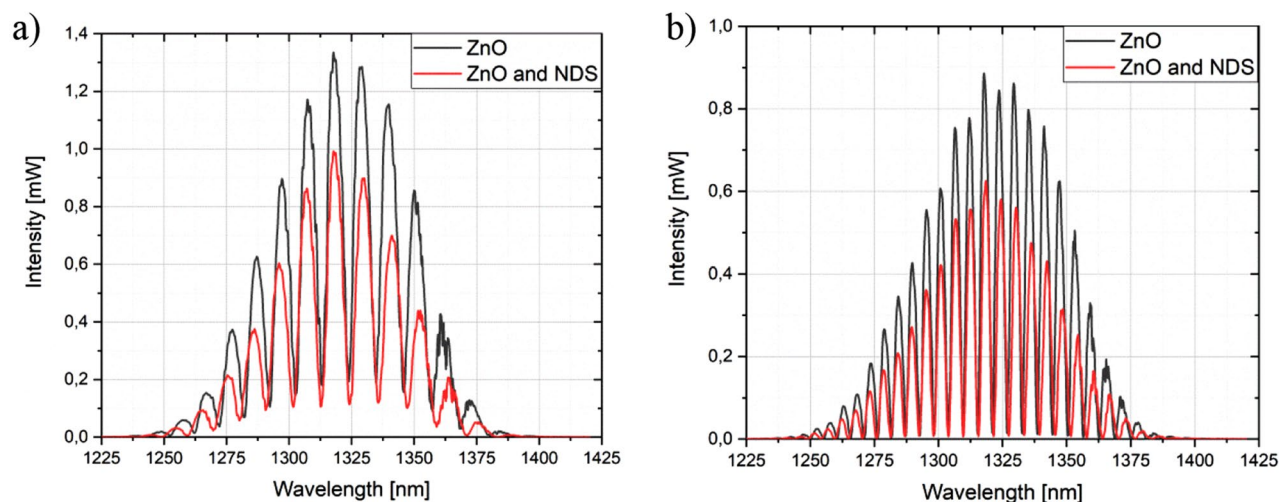


Figure 5. Measurement signals obtained for the measurement head with ZnO coating, and ZnO coating and nanocrystalline diamond sheet. The Fabry-Perot cavity length was set to: (a) 70 μm , (b) 140 μm .

Cavity length (μm)	Visibility for measurement head with ZnO layer and NDS
50	0.690
80	0.844
110	0.947
140	0.979
200	0.921
300	0.767

Table 1. Representative values of visibility for different Fabry–Perot cavity lengths.

The important parameter indicating the contrast of the measurement signal is the visibility value. It can be described with the following formula (1)^{28,29}:

$$V = \frac{I_{\text{max}} - I_{\text{min}}}{I_{\text{max}} + I_{\text{min}}} \quad (1)$$

where I_{max} —maximum value of the signal intensity and I_{min} —minimum value of the signal intensity.

Table 1 presents values of visibility for measurement head with ZnO layer and nanodiamond sheets for different Fabry–Perot cavity lengths.

Discussion

To date, only several research groups work on the nanocrystalline diamond sheets, focusing on deposition process, characterization of such structure and methods to transfer the resulting material onto the target surface^{30–32}. However, example applications are scarce so far. Bogdanowicz et al. presented the deposition process of a large area NDS, characterization of its properties and demonstration of potential application. This leads to the development of a prototypical, low-temperature diamond-on-graphene transistor²⁷. Seshan et al. showed the fabrication process and development of a transfer technique of the obtained diamond sheets with the use of a visco-elastic stamp. The NDS sheets were then used in the fabrication of mechanical resonators³³.

To the best of author's knowledge, only our research group reports the application of the NDS in the fiber-optic sensors. The main goal of this study was to investigate the possibility of elaborating a fiber-optic measurement head applying a ZnO coating and the nanocrystalline diamond sheet attached over it as a protection. We showed that such integration can be performed in a simple way, assuring the correct operation of the interferometric sensor. Addition of the NDS provides a protective cover while maintaining the sensing abilities and metrological parameters. Such configuration can extend the lifespan of the sensor and prevent the coating underneath from degradation in challenging environments.

Further investigation regarding the usage of NDS for fiber-optic measurement heads in chemically aggressive media is planned. The comparison of measurement head (with and without NDS) metrological parameters after such experiments, as well as specifying the lifespan difference between them, would be the next step to directly show the benefits of NDS protection.

Conclusions

In this paper, the fiber-optic measurement head comprising of a single-mode optical fiber, ZnO coating deposited on its end-face, and with an attached nanocrystalline diamond sheet was performed. The results of the optical measurements were described. The study proves that a NDS can be applied as a protection of the fiber-optic end-face. The attachment of the NDS did not influence the sensing abilities of the fiber sensor. This provided protection for the measurement head, which can be exposed to demanding environmental conditions. Furthermore, such protection does not influence meteorological parameters of the fiber-optic sensors because even with the NDS it was able to obtain the visibility of measured signal at the value of 0.979.

On the other hand, maximum visibility can be achieved with a small cavity length at 140 μm , which guarantees the possibility of using very small samples, which is extremely important for example during biological measurement and with the use of biological samples.

Methods

Chemical vapor deposition. Nanocrystalline diamond sheets were synthesized in a Microwave Plasma Enhanced Chemical Vapor Deposition (MW PECVD) reactor with a frequency of 2.45 GHz (SEKI Technotron AX5400S, Japan) on mirror-polished tantalum substrates (Sigma-Aldrich Chemie, thickness 0.025 mm, 99.9% metal base) and attached to the sensor head by employing the Van der Waals force. Prior to growth, the substrates were ultrasonically abraded for 30 min in a water suspension consisting of nanodiamond particles of 4–7 nm in diameter, followed by ultrasonic cleaning in acetone and 2-propanol. The temperature of the graphite stage, on which the substrates rested, was kept at 500 °C with a deposition time of 3 h. The microwave power, gas flow rate, and $\text{CH}_4:\text{H}_2$ molar ratio were 1.1 kW, 300 sccm, and 1%, respectively. The chemical vapor deposition process pressure was maintained at 50 Torr. The detailed description of the deposition process may be found elsewhere^{26,27}.

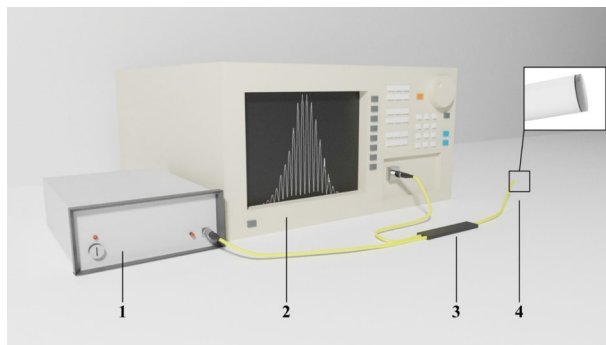


Figure 6. Schematic of the experimental setup, where: 1—light source, 2—Optical Spectrum Analyzer, 3—optical coupler, 4—measurement head.



Figure 7. The nanodiamonds structure deposition on the tantalum substrate.

Fiber-optic interferometer. To verify the sensing parameters of each layer, they were examined in an experimental setup, presented in Fig. 6.

The configuration of the setup was that of Fabry–Perot operated in a reflective mode. A light source with a wavelength of 1310 ± 10 nm—superluminescent diode (SLD-1310-18-W, FiberLabs Inc., Japan) was chosen to perform experimental measurements. The light propagated through the optical coupler and the end-face of the measuring head, and it was reflected of the silver mirror, which was placed directly under the sensor head. The signal reflected from fiber end-face (in configuration ZnO coating and a diamond sheet) and the mirror superpose, resulting in an interference, which can be observed on an Optical Spectrum Analyzer (OSA, AndoAQ6319, Japan). Obtained interferograms can be then analyzed.

The attachment of the nanocrystalline diamond sheet. To assess the impact of the nanocrystalline diamond sheet on the obtained signal, NDS was attached over fiber end-face with deposited ZnO. Figure 7 shows the structure of the nanodiamond deposited on the tantalum substrate.

The procedure of the application of the NDS starts with its delamination from the tantalum substrate. The deposition process of the diamond structure was designed in such a way, that the resulting NDS shows low adhesion to the substrate, to ease the process of its release. A scalpel was used to induce stress in the structure in order to achieve a free-standing diamond sheet. Due to this, a part of the sheet detached from the tantalum in the form of an irregular flake which can be transferred onto the desired surface. The NDS was placed on a table of a micromechanical setup, where the fiber-optic measurement head was mounted. The diamond structure was then positioned centrally beneath the fiber. To attach the diamond structure to the measurement head, the van der Waals force was employed by slowly decreasing the distance between the structures, using micrometer screw. The bond was then strengthened by a slight press against the NDS.

Received: 7 August 2020; Accepted: 26 October 2020

Published online: 05 November 2020

References

- Jiao, L. *et al.* Recent advances in fiber-optic evanescent wave sensors for monitoring organic and inorganic pollutants in water. *TrAC Trends Anal. Chem.* **127**, 115892 (2020).
- Calcerrada, M., García-Ruiz, C. & González-Herráez, M. Chemical and biochemical sensing applications of microstructured optical fiber-based systems. *Laser Photon. Rev.* **9**, 604–627 (2015).

3. Pospíšilová, M., Kuncová, G. & Trögl, J. Fiber-optic chemical sensors and fiber-optic bio. *Sensors* **15**, 25208–25259 (2015).
4. Wang, X. & Wolfbeis, O. S. Fiber-optic chemical sensors and biosensors (2015–2019). *Anal. Chem.* **92**, 397–430 (2020).
5. Wencel, D. *et al.* Optical sensor for real-time pH monitoring in human tissue. *Small* **14**, 1803627 (2018).
6. Wang, J. *et al.* Diaphragm-based optical fiber sensor for pulse wave monitoring and cardiovascular diseases diagnosis. *J. Biophoton.* **12**, e201900084 (2019).
7. Huang, Y. W., Tao, J. & Huang, X. G. Research progress on F-P interference—based fiber-optic sensors. *Sensors* **16**, 1424 (2016).
8. Castellon-Urbe, J. Optical fiber sensors: an overview. *Fiber Opt. Sens.* <https://doi.org/10.5772/28529> (2012).
9. Roriz, P., Frazão, O., Lobo-Ribeiro, A. B., Santos, J. L. & Simoes, J. A. Review of fiber-optic pressure sensors for biomedical and biomechanical applications. *JBO* **18**, 050903 (2013).
10. Hirsch, M. *et al.* ZnO coated fiber optic microsphere sensor for the enhanced refractive index sensing. *Sens. Actuators A* **298**, 111594 (2019).
11. Yin, M. *et al.* Recent development of fiber-optic chemical sensors and biosensors: mechanisms, materials, micro/nano-fabrications and applications. *Coord. Chem. Rev.* **376**, 348–392 (2018).
12. Yang, M. & Dai, J. Review on optical fiber sensors with sensitive thin films. *Photon. Sens.* **2**, 14–28 (2012).
13. Bond, W. L. Refractive index of ZnO (Zinc monoxide): Bond-o. <https://refractiveindex.info/?shelf=main&book=ZnO&page=Bond-o> (2020).
14. Coelho, L., Viegas, D., Santos, J. L. & de Almeida, J. M. M. Characterization of zinc oxide coated optical fiber long period gratings with improved refractive index sensing properties. *Sens. Actuators B* **223**, 45–51 (2016).
15. Coe, S. E. & Sussmann, R. S. Optical, thermal and mechanical properties of CVD diamond. *Diam. Relat. Mater.* **9**, 1726–1729 (2000).
16. Phillip, H. R. & Taft, E. A. Refractive index of C (Carbon, diamond, graphite, graphene). <https://doi.org/10.1103/PhysRev.136.A1445> (2020).
17. Kosowska, M. *et al.* Doped nanocrystalline diamond films as reflective layers for fiber-optic sensors of refractive index of liquids. *Materials* **12**, 1–12 (2019).
18. Yang, N. *et al.* Conductive diamond: synthesis, properties, and electrochemical applications. *Chem. Soc. Rev.* **48**, 157–204 (2019).
19. Rifai, A. *et al.* Polycrystalline diamond coating of additively manufactured titanium for biomedical applications. *ACS Appl. Mater. Interfaces* **10**, 8474–8484 (2018).
20. Koizumi, S., Nebel, C. & Nesladek, M. *Physics and Applications of CVD Diamond* (Wiley, Hoboken, 2008).
21. *CVD Diamond for Electronic Devices and Sensors*. (Wiley, Hoboken, 2009). <https://doi.org/10.1002/9780470740392.fmatter>.
22. Jędrzejewska-Szczerska, M. *et al.* Chapter 14 - Nanolayers in Fiber-Optic Biosensing. in *Nanotechnology and Biosensors* (eds. Nikolelis, D. P. & Nikoleli, G.-P.) 395–426 (Elsevier, Amsterdam, 2018). <https://doi.org/10.1016/B978-0-12-813855-7.00014-3>.
23. Baron, V. O. *et al.* Real-time monitoring of live mycobacteria with a microfluidic acoustic-Raman platform. *Commun. Biol.* **3**, 1–8 (2020).
24. Woolford, L., Chen, M., Dholakia, K. & Herrington, C. S. Towards automated cancer screening: label-free classification of fixed cell samples using wavelength modulated Raman spectroscopy. *J. Biophoton.* **11**, e201700244 (2018).
25. Ficek, M. *et al.* Optical and electrical properties of boron doped diamond thin conductive films deposited on fused silica glass substrates. *Appl. Surf. Sci.* **387**, 846–856 (2016).
26. Bogdanowicz, R. *et al.* Growth and isolation of large area boron-doped nanocrystalline diamond sheets: a route toward diamond-on-graphene heterojunction. *Adv. Func. Mater.* **29**, 1805242 (2019).
27. Kosowska, M. *et al.* Nanocrystalline diamond sheets as protective coatings for fiber-optic measurement head. *Carbon* **156**, 104–109 (2020).
28. Born, M. & Wolf, E. *Principles of Optics* (Pergamon, New York, 1980).
29. Majchrowicz, D. *et al.* Application of thin ZnO ALD layers in fiber-optic Fabry–Pérot sensing interferometers. *Sensors* **16**, 416 (2016).
30. Behroudj, A. & Strehle, S. *Transfer of Nanocrystalline Diamond Films Grown by Chemical Vapor Deposition for Sensors and Other Applications*. (VDE, 2016).
31. Lodes, M. A., Kachold, F. S. & Rosiwal, S. M. Mechanical properties of micro- and nanocrystalline diamond foils. *Philos. Trans. R. Soc. A* **373**, 20140136 (2015).
32. Engenhorst, M. *et al.* Thermoelectric transport properties of boron-doped nanocrystalline diamond foils. *Carbon* **81**, 650–662 (2015).
33. Seshan, V. *et al.* Pick-up and drop transfer of diamond nanosheets. *Nanotechnology* **26**, 125706 (2015).

Acknowledgements

The authors want to acknowledge the financial support of the Polish National Science Centre under Grant No. 2017/25/N/ST7/01610, the Polish National Agency for Academic Exchange NAWA under Bilateral exchange of scientists between France and Poland PHC Polonium PPN/BFR/2019/1/00005/U/00001, Polish National Agency for Academic Exchange under Iwanowska Programme PPN/IWA/2018/1/00026/U/00001, Polish National Agency for Academic Exchange under Iwanowska Programme PPN/IWA/2018/1/00058/U/00001, and DS Programs of Faculty of Electronics, Telecommunications and Informatics of Gdańsk University of Technology. KD thanks the UK Engineering and Physical Sciences Research Council for funding (Grant EP/P030017/1).

Author contributions

M.K., P.L. D.M. and M.S. conceived and designed the experiments. M.K., D.M., M.R., Y.F. and M.C. performed the experiments; M.K., P.L., D.M. and M.S. analyzed the data of optical spectrum analyzer; M.K. and Y.F. performed images with SEM; D.M. and M.C. performed and analyzed data from Raman System; M.R. contributed NDS; M.R. prepared the images from optical microscope; M.B. contributed the ZnO coating on the optical fibers. M.K., P.L., D.M., M.R., Y.F. and M.C. wrote the main manuscript text; M.K., P.L., M.R., Y.F., D.M., M.C. prepared figures. M.B., D.F. K.D and M.S. checked, reviewed; M.S. edited the paper.

Competing interests

The authors declare no competing interests.

Additional information

Correspondence and requests for materials should be addressed to M.K., D.M. or M.S.

Reprints and permissions information is available at www.nature.com/reprints.

Publisher's note Springer Nature remains neutral with regard to jurisdictional claims in published maps and institutional affiliations.



Open Access This article is licensed under a Creative Commons Attribution 4.0 International License, which permits use, sharing, adaptation, distribution and reproduction in any medium or format, as long as you give appropriate credit to the original author(s) and the source, provide a link to the Creative Commons licence, and indicate if changes were made. The images or other third party material in this article are included in the article's Creative Commons licence, unless indicated otherwise in a credit line to the material. If material is not included in the article's Creative Commons licence and your intended use is not permitted by statutory regulation or exceeds the permitted use, you will need to obtain permission directly from the copyright holder. To view a copy of this licence, visit <http://creativecommons.org/licenses/by/4.0/>.

© The Author(s) 2020

CONTRIBUTIONS

Gdańsk, 28/06/21

Place and date

Mateusz Ficek, PhD EE
Department of Metrology and Optoelectronics
Faculty of Electronics, Telecommunications and Informatics
Gdansk University of Technology
Poland

Statement on my contribution to joint publications with Monika Kosowska

Referencing to the below publications:

1. M. Kosowska, D. Majchrowicz, M. Ficek, P. Wierzba, Y. Fleger, D. Fixler, M. Szczerska, Nanocrystalline diamond sheets as protective coatings for fiber-optic measurement head, Carbon. 156 (2020) 104–109. <https://doi.org/10.1016/j.carbon.2019.09.042>.
2. M. Kosowska, D. Majchrowicz, K.J. Sankaran, M. Ficek, K. Haenen, M. Szczerska, Doped Nanocrystalline Diamond Films as Reflective Layers for Fiber-Optic Sensors of Refractive Index of Liquids, Materials. 12 (2019) 2124. <https://doi.org/10.3390/ma12132124>.

I declare, that my contribution to the publication is:

- synthesis of the boron-doped diamond films and nanocrystalline diamond sheets with specific optical and morphological parameters,
- writing selected parts of the manuscripts.



Signature

Delft, 04.08.21

Place and date

Michał Rycewicz, MSc EE
Department of Metrology and Optoelectronics
Faculty of Electronics, Telecommunications and Informatics
Gdansk University of Technology
Poland

Statement on my contribution to joint publications with Monika Kosowska

Referencing to the below publications:

1. M. Kosowska, P. Jakóbczyk, M. Rycewicz, A. Vitkin, M. Szczerska, Low-coherence photonic method of electrochemical processes monitoring, Sci Rep. 11 (2021) 12600. <https://doi.org/10.1038/s41598-021-91883-z>.
2. M. Kosowska, P. Listewnik, D. Majchrowicz, M. Rycewicz, M. Bechelany, Y. Flegler, M. Chen, D. Fixler, K. Dholakia, M. Szczerska, Microscale diamond protection for a ZnO coated fiber optic sensor, Scientific Reports. 10 (2020) 19141. <https://doi.org/10.1038/s41598-020-76253-5>.

I declare, that my contribution to the publication is:

- synthesis of the nanocrystalline diamond sheets with specific optical, morphological, and electrical parameters,
- preparing selected figures (Figures 2 and 7 in [2]),
- writing selected parts of the manuscripts.


Signature

10.08.2021
Odisha, India

K. J. Sankaran, PhD
Institute of Minerals and Materials Technology
Council of Scientific and Industrial Research (CSIR)
India

Statement on my contribution to joint publications with Monika Kosowska

Referencing to the below publications:

1. Kosowska, S. Pawłowska, K.J. Sankaran, D. Majchrowicz, K. Haenen, K. Dholakia, M. Szczerska, Incorporation of nitrogen in diamond films – A new way of tuning parameters for optical passive elements, *Diamond and Related Materials*. 111 (2021) 108221. <https://doi.org/10.1016/j.diamond.2020.108221>.
2. M. Kosowska, D. Majchrowicz, K.J. Sankaran, M. Ficek, K. Haenen, M. Szczerska, Doped Nanocrystalline Diamond Films as Reflective Layers for Fiber-Optic Sensors of Refractive Index of Liquids, *Materials*. 12 (2019) 2124. <https://doi.org/10.3390/ma12132124>.

I declare, that my contribution to these publications are:

Manuscript 1.

- conceptualization, methodology and validation of the materials science part,
- synthesis of nitrogen-doped diamond films,
- investigation using SEM, AFM, microRaman, EELS systems and data analysis,
- preparing selected figures (Fig.2, Fig.3, Fig.4, Fig.5)
- writing selected parts of the manuscript.

Manuscript 2.

- synthesis of nitrogen-doped diamond films,
- writing selected parts of the manuscript.



Signature

Gdańsk, 23/06/21

Place and date

Sandra Pawłowska, MSc EE
Department of Metrology and Optoelectronics
Faculty of Electronics, Telecommunications and Informatics
Gdansk University of Technology
Poland

Statement on my contribution to joint publication with Monika Kosowska

Referencing to the below publication:

1. Kosowska, M.; Pawłowska, S.; Sankaran, K.J.; Majchrowicz, D.; Haenen, K.; Dholakia, K.; Szczerska, M. Incorporation of Nitrogen in Diamond Films – a New Way of Tuning Parameters for Optical Passive Elements. *Diamond and Related Materials* 2021, 111, 108221, doi:10.1016/j.diamond.2020.108221.

I declare, that my contribution to the publication is:

- performing the measurements,
- analyzing the data of the optical spectrum analyzer,
- writing selected parts of the manuscript.

Sandra Pawłowska

Signature

St Andrews, Scotland, UK
02 August 2021
Place and date

Mingzhou Chen
SUPA, School of Physics and Astronomy
University of St Andrews
United Kingdom

Statement on my contribution to joint publication with Monika Kosowska

Referencing to the below publication:

1. Kosowska, M.; Listewnik, P.; Majchrowicz, D.; Rycewicz, M.; Bechelany, M.; Flegler, Y.; Chen, M.; Fixler, D.; Dholakia, K.; Szczerska, M. Microscale diamond protection for a ZnO coated fiber optic sensor. Sci. Rep. 2020, 10, doi:10.1038/s41598-020-76253-5.

I declare, that my contribution to the publication is:

- performing the experiments with Raman Spectrometer and analyzing the data,
- preparing Figure 3,
- writing selected parts of the manuscript.


.....
Signature

Gdańsk, 28.06.2021

Place and date

Paweł Jakóbczyk, PhD
Department of Metrology and Optoelectronics
Faculty of Electronics, Telecommunications and Informatics
Gdansk University of Technology
Poland

Statement on my contribution to joint publication with Monika Kosowska

Referencing to the below publication:

1. M. Kosowska, P. Jakóbczyk, M. Ryciewicz, A. Vitkin, M. Szczerska, Low-coherence photonic method of electrochemical processes monitoring, Sci Rep. 11 (2021) 12600. <https://doi.org/10.1038/s41598-021-91883-z>.

I declare, that my contribution to the publication is:

- conceiving and designing experiments,
- performing experiments,
- analyzing the data from electrochemical system,
- writing selected parts of the manuscript.


Signature

28.06.2021 Gdańsk

Place and date

Paulina Listewnik, MSc EE
Department of Metrology and Optoelectronics
Faculty of Electronics, Telecommunications and Informatics
Gdansk University of Technology
Poland

Statement on my contribution to joint publication with Monika Kosowska

Referencing to the below publication:

1. Kosowska, M.; Listewnik, P.; Majchrowicz, D.; Rycewicz, M.; Bechelany, M.; Flegler, Y.; Chen, M.; Fixler, D.; Dholakia, K.; Szczerska, M. Microscale diamond protection for a ZnO coated fiber optic sensor. Sci. Rep. 2020, 10, doi:10.1038/s41598-020-76253-5.

I declare, that my contribution to the publication is:

- analyzing the data of the optical spectrum analyzer,
- preparing figure (Fig. 6)
- writing selected parts of the manuscript.



Signature

Gdańsk, June 28th 2021
.....
Place and date

Paweł Wierzba, Phd DSc EE
Department of Metrology and Optoelectronics
Faculty of Electronics, Telecommunications and Informatics
Gdansk University of Technology
Poland

Statement on my contribution to joint publication with Monika Kosowska

Referencing to the below publication:

1. M. Kosowska, D. Majchrowicz, M. Ficek, P. Wierzba, Y. Fleger, D. Fixler, M. Szczerska, Nanocrystalline diamond sheets as protective coatings for fiber-optic measurement head, Carbon. 156 (2020) 104–109. <https://doi.org/10.1016/j.carbon.2019.09.042>.

I declare, that my contribution to the publication is:

- numerical modeling of the reflectance of the nanocrystalline diamond sheet (NDS),
- numerical modeling of the reflectance spectra for the interferometer with NDS and silver mirror,
- preparing figure 2,
- writing selected parts of the manuscript.


.....
Signature

2/8/2021

Yafit Fleger, PhD
Institute for Nanotechnology and Advanced Materials
Bar-Ilan University
Israel

Statement on my contribution to joint publications with Monika Kosowska

Referencing to the below publications:

1. M. Kosowska, D. Majchrowicz, M. Ficek, P. Wierzba, Y. Fleger, D. Fixler, M. Szczerska, Nanocrystalline diamond sheets as protective coatings for fiber-optic measurement head, Carbon. 156 (2020) 104–109. <https://doi.org/10.1016/j.carbon.2019.09.042>.
2. M. Kosowska, P. Listewnik, D. Majchrowicz, M. Rycewicz, M. Bechelany, Y. Fleger, M. Chen, D. Fixler, K. Dholakia, M. Szczerska, Microscale diamond protection for a ZnO coated fiber optic sensor, Scientific Reports. 10 (2020) 19141. <https://doi.org/10.1038/s41598-020-76253-5>.

I declare, that my contribution to the publication is:

- performing the experiments,
- performing SEM imaging,
- preparing selected figures (paper 1 – Fig. 3, paper 2 – Fig 1c).



.....
Signature

Israel, August 2021

.....
Place and date

Prof. Dror Fixler
Faculty of Engineering and
Institute for Nanotechnology and Advanced Materials
Bar-Ilan University
Israel


Statement on my contribution to joint publications with Monika Kosowska

Referencing to the below publications:

1. M. Kosowska, D. Majchrowicz, M. Ficek, P. Wierzba, Y. Fleger, D. Fixler, M. Szczerska, Nanocrystalline diamond sheets as protective coatings for fiber-optic measurement head, Carbon. 156 (2020) 104–109. <https://doi.org/10.1016/j.carbon.2019.09.042>.
2. M. Kosowska, P. Listewnik, D. Majchrowicz, M. Rycewicz, M. Bechelany, Y. Fleger, M. Chen, D. Fixler, K. Dholakia, M. Szczerska, Microscale diamond protection for a ZnO coated fiber optic sensor, Scientific Reports. 10 (2020) 19141. <https://doi.org/10.1038/s41598-020-76253-5>.

I declare, that my contribution to the publications is:

- checking, editing and reviewing the manuscript.


.....
Signature

....Toronto, Canada; August 3, 2021....

Place and date

Prof. I. Alex Vitkin
Department of Medical Biophysics
University of Toronto
University Health Network
Princess Margaret Cancer Centre
Canada

Statement on my contribution to joint publication with Monika Kosowska

Referencing to the below publication:

1. M. Kosowska, P. Jakóbczyk, M. Rycewicz, A. Vitkin, M. Szczerska, Low-coherence photonic method of electrochemical processes monitoring, Sci Rep. 11 (2021) 12600. <https://doi.org/10.1038/s41598-021-91883-z>.

I declare that my contribution to the publication is:

- checking, editing and reviewing the manuscript and its revisions.



.....

Signature

.....

Montpellier, August 2nd 2022

**Statement on my contribution to joint publication
with Monika Kosowska**

Referencing to the below publication:

1. Kosowska, M.; Listewnik, P.; Majchrowicz, D.; Rycewicz, M.; Bechelany, M.; Fleger, Y.; Chen, M.; Fixler, D.; Dholakia, K.; Szczerska, M. Microscale diamond protection for a ZnO coated fiber optic sensor. Sci. Rep. 2020, 10, doi:10.1038/s41598-020-76253-5.

I declare, that my contribution to the publication is:

- depositing the ZnO coating on the fiber samples,
- checking and reviewing the manuscript.

Yours sincerely,

Mikhael BECHELANY

Chargé de recherches CNRS

Institut Européen des Membranes (IEMM, ENSCM UM CNRS UMR5635)

Place Eugène Bataillon

34095 MONTPELLIER Cedex 5

Email: mikhael.bechelany@umontpellier.fr



Adelaide, 03 August 2021.....

Place and date

Prof. Kishan Dholakia
SUPA, School of Physics and Astronomy
University of St Andrews
United Kingdom

Statement on my contribution to joint publications with Monika Kosowska

Referencing to the below publications:

1. M. Kosowska, P. Listewnik, D. Majchrowicz, M. Rycewicz, M. Bechelany, Y. Fleger, M. Chen, D. Fixler, K. Dholakia, M. Szczerska, Microscale diamond protection for a ZnO coated fiber optic sensor, Scientific Reports. 10 (2020) 19141. <https://doi.org/10.1038/s41598-020-76253-5>.
2. M. Kosowska, S. Pawłowska, K.J. Sankaran, D. Majchrowicz, K. Haenen, K. Dholakia, M. Szczerska, Incorporation of nitrogen in diamond films – A new way of tuning parameters for optical passive elements, Diamond and Related Materials. 111 (2021) 108221. <https://doi.org/10.1016/j.diamond.2020.108221>.

I declare, that my contribution to the publications is:

- checking, reviewing and editing the manuscript.



.....
Signature

Gdańsk 28.06.21

Place and date

Daria Majchrowicz, PhD EE
Department of Metrology and Optoelectronics
Faculty of Electronics, Telecommunications and Informatics
Gdansk University of Technology
Poland

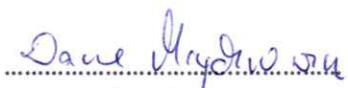
Statement on my contribution to joint publications with Monika Kosowska

Referencing to the below publications:

1. Kosowska, M.; Pawłowska, S.; Sankaran, K.J.; Majchrowicz, D.; Haenen, K.; Dholakia, K.; Szczerska, M. Incorporation of Nitrogen in Diamond Films – a New Way of Tuning Parameters for Optical Passive Elements. *Diamond and Related Materials* 2021, 111, 108221, doi:10.1016/j.diamond.2020.108221.
2. Kosowska, M.; Majchrowicz, D.; Sankaran, K.J.; Ficek, M.; Haenen, K.; Szczerska, M. Doped Nanocrystalline Diamond Films as Reflective Layers for Fiber-Optic Sensors of Refractive Index of Liquids. *Materials* 2019, 12, 2124, doi:10.3390/ma12132124.
3. Kosowska, M.; Majchrowicz, D.; Ficek, M.; Wierzba, P.; Fleger, Y.; Fixler, D.; Szczerska, M. Nanocrystalline Diamond Sheets as Protective Coatings for Fiber-Optic Measurement Head. *Carbon* 2020, 156, 104–109, doi:10.1016/j.carbon.2019.09.042.
4. Kosowska, M.; Listewnik, P.; Majchrowicz, D.; Rycewicz, M.; Bechelany, M.; Fleger, Y.; Chen, M.; Fixler, D.; Dholakia, K.; Szczerska, M. Microscale Diamond Protection for a ZnO Coated Fiber Optic Sensor. *Sci Rep* 2020, 10, 19141, doi:10.1038/s41598-020-76253-5.

I declare, that my contribution to the publication is:

- conceiving and designing the experiments [1-4],
- performing experiments with Raman Spectrometer and analyzing the data [4]
- analyzing the data of the optical spectrum analyzer [2,4],
- preparing figure 3 [4],
- writing selected parts of the manuscript [1-4].


Signature



Gdańsk 28/06/2021

Place and date

Prof. Małgorzata Szczerska
Department of Metrology and Optoelectronics
Faculty of Electronics, Telecommunications and Informatics
Gdansk University of Technology
Poland

Statement on my contribution to joint publications with Monika Kosowska

Referencing to the below publications:

1. M. Kosowska, S. Pawłowska, K.J. Sankaran, D. Majchrowicz, K. Haenen, K. Dholakia, M. Szczerska, Incorporation of nitrogen in diamond films – A new way of tuning parameters for optical passive elements, *Diamond and Related Materials*. 111 (2021) 108221. <https://doi.org/10.1016/j.diamond.2020.108221>.
2. M. Kosowska, P. Jakóbczyk, M. Ryciewicz, A. Vitkin, M. Szczerska, Low-coherence photonic method of electrochemical processes monitoring, *Sci Rep.* 11 (2021) 12600. <https://doi.org/10.1038/s41598-021-91883-z>.
3. M. Kosowska, D. Majchrowicz, M. Ficek, P. Wierzba, Y. Flegler, D. Fixler, M. Szczerska, Nanocrystalline diamond sheets as protective coatings for fiber-optic measurement head, *Carbon*. 156 (2020) 104–109. <https://doi.org/10.1016/j.carbon.2019.09.042>.
4. M. Kosowska, P. Listewnik, D. Majchrowicz, M. Ryciewicz, M. Bechelany, Y. Flegler, M. Chen, D. Fixler, K. Dholakia, M. Szczerska, Microscale diamond protection for a ZnO coated fiber optic sensor, *Scientific Reports*. 10 (2020) 19141. <https://doi.org/10.1038/s41598-020-76253-5>.
5. M. Kosowska, D. Majchrowicz, K.J. Sankaran, M. Ficek, K. Haenen, M. Szczerska, Doped Nanocrystalline Diamond Films as Reflective Layers for Fiber-Optic Sensors of Refractive Index of Liquids, *Materials*. 12 (2019) 2124. <https://doi.org/10.3390/ma12132124>.

I declare, that my contribution to the publications is:

- conceiving and designing experiments,
- analysing and interpreting the data from optical spectrum analyser,
- checking, reviewing and editing the manuscripts.

M. Szczerska

Signature